# Influence of alkali-silica reaction on the physical, mechanical, and structural behaviour of reinforced concrete

Ricardo Antonio Barbosa

PhD Thesis

Department of Civil Engineering
2017

DTU Civil Engineering Report R-363

PhD Thesis

Influence of alkali-silica reaction on the physical, mechanical, and structural behaviour of reinforced concrete

Ricardo Antonio Barbosa

2017

Cover photo: Part of a fluorescence impregnated ASR-damaged concrete core seen under ultraviolet light. Photo by Ricardo Antonio Barbosa.

Supervisors:
Associate Professor Kurt Kielsgaard Hansen, Technical University of Denmark
MSc Bent Grelk, Technical University of Denmark
Professor Linh Cao Hoang, Technical University of Denmark
MSc PhD Claus Pedersen, Rambøll Denmark
MSc PhD Erik Stoklund Larsen, Danish Road Directorate

Assessment Committee:
Associate Professor Marianne Tange Hasholt, Technical University of Denmark
Professor Benoît Fournier, Université Laval
Professor Børge Johannes Wigum, Norwegian University of Science and Technology

This thesis is submitted in partial fulfillment of the requirements for the degree of Doctor of Philosophy in Civil Engineering at the Technical University of Denmark.

Preface

This PhD thesis is submitted in partial fulfillment of the requirements for the PhD degree in Civil Engineering at the Technical University of Denmark.

This PhD project was carried out at the Department of Civil Engineering with Associate Professor Kurt Kielsgaard Hansen as the main supervisor and MSc Bent Grelk, Professor Linh Cao Hoang, MSc PhD Claus Pedersen and MSc PhD Erik Stoklund Larsen as co-supervisors.

Ricardo Antonio Barbosa
Kgs. Lyngby, Denmark, January 2017

Acknowledgements

I would like to thank my main supervisor, Associate Professor Kurt Kielsgaard Hansen, for his endless commitment and believe in the project during the last years. Thank you for your knowledge, support, inspiration, and your always-open door for discussions.

Great thanks are due to my co-supervisors, MSc Bent Grelk, Professor Linh Cao Hoang, MSc PhD Claus Pedersen, MSc PhD Erik Stoklund Larsen for their profound knowledge, ideas, and support.

Great thanks to all of the laboratory technicians at the Department of Civil Engineering. This work would not have been possible without your interest in the project and willingness to help me.

Thanks to my colleagues from the Building Materials research group and PhD colleagues for your inspiration and friendship. Especially, I would like to thank PhD candidate Søren Gustenhoff Hansen for years of challenging discussions, analyzes, and writing hours. Special thanks to MSc PhD Mia Schou Møller Lund for her great help with the completion of this thesis and the friendship we have established.

Great thanks to the Danish Road Directorate for their financial support and the opportunity to conduct tests on specimens from ASR-damaged slab bridges. The support and interest from Iben Maag is gratefully acknowledged.

Finally, I would like to thank my family for their great support. Especially, I would like to apologize to my wife and children for all the canceled weekends, partially canceled vacations, and many inattentive hours at home. Thank you for your endurance.

Abstract

Alkali-silica reaction (ASR) is one of the major concrete deterioration mechanisms in the world. Cracking in concrete structures due to ASR has been observed worldwide. In Denmark numerous concrete structures have been built with a critical amount of ASR-reactive aggregate, mostly as porous opaline and porous calcareous opaline flint in the fine aggregate fraction. During the last few decades, an increasing number of bridges in Denmark have been severely damaged due to ASR. In the most severe cases, the ASR-damaged bridges have been demolished and reconstructed due to uncertainty about their residual load-carrying capacity. The decisions to demolish and reconstruct these bridges have been based on visual appearance of drilled concrete cores and rough estimates of their residual load-carrying capacity. Research into the mechanical properties of drilled cores and the residual load-carrying capacity of ASR-damaged flat slab bridges in service is very limited.

This PhD thesis contributes to the documentation and better understanding of the influence of ASR on the physical and mechanical properties of ASR-damaged concrete, and on the residual load-carrying capacity of an actual ASR-damaged flat slab bridge. The ASR-damaged concrete originated from ASR-damaged flat slab bridges in service and from laboratory-casted and laboratory-accelerated reinforced slabs. In this study, slab segments from three ASR-damaged slab bridges without shear reinforcement were examined. All the examined slabs had following features in common: (a) significant amount of ASR cracks were observed on and inside the slabs, (b) the ASR cracks were oriented parallel to the plane of the slabs, and (c) ASR occurred in the fine aggregate fraction.

In this PhD study, both the compressive strength and tensile strength of drilled cores, from all slabs, were found to be negatively influenced by ASR. However, the compressive and tensile strength depended on the orientation of the ASR cracks inside the cores. It was found that the compressive strength in the direction perpendicular to ASR cracks can be significantly smaller than the strength in the direction parallel to ASR cracks. Consequently, evaluation of compressive strength based on vertically drilled cores (ASR cracks oriented perpendicular to the load direction) can be rather conservative. It is argued that the difference in compressive strength for the two crack orientations (perpendicular or parallel to the load direction) will decrease as the amount of ASR cracks in the concrete increases. An explanation of the effect of ASR cracks and their orientation on the compressive strength is proposed. The tensile strength of concrete specimens depended on the test method applied. Both direct and indirect tensile strength test methods showed shortcomings when testing ASR-damaged specimens.

The residual load-carrying capacity was determined on 18 beams cut from six reinforced slab segments from a severely ASR-damaged flat slab bridge. Nine beams were tested in a three-point bending setup and nine beams were tested in an asymmetrical four-point bending setup. The ASR cracks had a significant influence on the propagation of load-induced cracks in the beams. Additionally, the test setups had different influence on the failure mechanism and measured load-carrying capacities. Most of the beams tested in the three-point setup suffered ductile rotational failure in diagonal cracks and most of the beams tested in the four-point setup suffered ductile shear failure. It was found that the measured load-carrying capacities were at least equivalent to the calculated load-carrying capacities based on the compressive strength of vertically and horizontally drilled cores. It was measured that the ASR-induced expansions resulted in significant tensile strains and stresses (pre-stress effect) in the reinforcing bars. The measured tensile strains were not proportional to the extent of ASR cracks in the beams or to the compressive strengths.

This PhD study also contributes to better understanding of the time-dependent effect of ASR on the physical and mechanical properties of laboratory-casted and laboratory-accelerated reinforced slabs. The sources of alkali to the concrete were found to have a significant influence on the development and orientation of the ASR cracks inside the slabs. The external supply of saturated NaCl solution from the upper slab surfaces was found to be crucial to develop ASR cracks with orientations comparable to those observed on actual bridge slabs, while the slabs with high initial Na_2O eq. content developed random map-cracks. The development of ASR cracks inside the slabs exposed to NaCl solution had a negative and rapid influence on the compressive strength of vertically drilled cores. Although accelerated at high temperature and high RH, it was found that the rate of the downwards penetration and development of ASR cracks inside the slabs was very fast. In this study it is argued that the correlation between vertical expansion and surface expansion of the slabs can be divided into three phases, which may lead to challenges in the interpretation of internal ASR cracking based on the surface expansion measurements.

Resumé

Alkalikiselreaktioner (AKR) er en af de større nedbrydningsmekanismer i beton. Revnedannelser i betonbygværker som følge af AKR er blevet observeret i hele verden. I Danmark er mange bygværker opført med et kritisk indhold af AKR-reaktivt tilslagsmateriale, mest som porøs opalflint og porøs kalcedonflint i sandfraktionen. I Danmark er et stigende antal broer blevet svært AKR-skadede i de seneste årtier. I de mest alvorlige tilfælde er de beskadigede broer blevet revet ned og genopbygget på grund af usikkerheden om deres restbæreevne. Beslutningen om at nedrive og genopbygge disse AKR-skadede broer har været baseret på det visuelle udseende af udborede betonkerner samt grove skøn af broernes restbæreevne. Forskning i de mekaniske egenskaber af udborede kerner og restbæreevne af AKR-skadede broer er meget begrænset.

Denne ph.d.-afhandling bidrager til dokumentation og bedre forståelse for indflydelsen af AKR på dels de fysiske og mekaniske egenskaber af AKR-skadet beton, dels restbæreevnen af en eksisterende AKR-skadet slapt armeret broplade. Den AKR-skadede beton stammede dels fra AKR-skadede brodæk, dels fra laboratoriestøbte og laboratorieaccelererede armerede plader. I dette studie er AKR-skadede bropladeelementer uden forskydningsarmering udtaget fra tre broer blevet undersøgt. Alle de undersøgte broplader havde følgende egenskaber til fælles: (a) der var betydelige revnedannelser som følge af AKR, (b) AKR revnerne var overfladeparallelle og (c) AKR forekom i sandfraktionen.

I dette ph.d.-studie viste både tryk- og trækstyrken af de udborede kerner at være negativt påvirket af AKR. Imidlertid var tryk- og trækstyrken afhængig af orienteringen af AKR revner i kernerne. Trykstyrken vinkelret på AKR revner var betydelig mindre end styrken parallelt med AKR revner. Bestemmelsen af betonens trykstyrke baseret på lodret udborede kerner (AKR revner orienteret vinkelret på trykretningen) kan være temmelig konservativ i forhold til trykstyrke baseret på vandret udborede kerner (AKR revner orienteret parallelt med trykretningen). Der er argumenteret for, at forskellen i trykstyrke for de to revneorienteringer (vinkelret på eller parallelt med trykretningen) vil falde med et stigende omfang af AKR revner i betonen. En forklaring på indvirkningen af AKR revnerne og deres orientering på trykstyrken er foreslået. Betonprøveemnernes trækstyrke afhang hovedsageligt af den anvendte testmetode. Både direkte og indirekte testmetoder udviste væsentlige mangler ved test af AKR-skadet beton.

Restbærevnen blev bestemt på baggrund af 18 bjælker udsavet fra seks pladeelementer udtaget fra en eksisterende svært AKR-skadet slapt armeret broplade. Ni bjælker blev testet i en tre-punkts bøjningsopstilling, og de resterende ni bjælker blev testet i en asymmetrisk fire-punkts bøjningsopstilling. Det blev konstateret, at

AKR-revnerne havde en betydelig indflydelse på udbredelsen af de lastfremkaldte revner i bjælkerne. Derudover havde de anvendte testopstillinger forskellig indflydelse på brudmekanismen og restbæreevnen. De fleste bjælker testet i tre-punkts opstillingen havde et sejt rotationsbrud i diagonalrevner, og de fleste bjælker testet i fire-punkts opstillingen havde et sejt forskydningsbrud. Det blev fundet, at de målte bæreevner mindst svarede til bæreevneberegninger baseret på trykstyrken fra lodret og vandret udborede kerner. Det blev målt, at AKR ekspansionen resulterede i betydelige trækspændinger og trætøjninger (forspændingseffekt) i armeringsjernene. De målte trætøjninger var ikke proportionale med omfanget af AKR revner i bjælkerne eller med trykstyrkerne.

Dette ph.d.-studie bidrager også til en bedre forståelse for den tidsafhængige indflydelse af AKR på de fysiske og mekaniske egenskaber af laboratoriestøbte og laboratorieaccelerede armerede plader. Kilden til alkali i betonen viste sig at have en betydelig indflydelse på udviklingen og orienteringen af AKR revnerne inde i pladerne. Det blev konstateret, at den eksterne tilførelse af mættet NaCl opløsning fra pladernes overside førte til revneorienteringer tilsvarende revnerne, der er observeret på eksisterende broplader, mens NaOH tilført blandevandet førte til netrevner. Udviklingen af AKR revner ned igennem pladerne havde en betydelig negativ og hurtig indflydelse på trykstyrken af de lodret udborede kerner. Selv om pladerne er accelereret ved høj temperatur og høj RF, viste revnernes indtrængningshastighed sig at være overraskende hurtig. I dette ph.d.-projekt er det argumenteret, at korrelationen mellem pladernes lodrette ekspansion og overfladeekspansion kan opdeles i tre faser. Dette skaber udfordringer i fortolkningen af interne AKR revnedannelser baseret på målinger af pladernes overfladeekspansion.

Table of contents

Introduction

This PhD project investigates the physical, mechanical, and structural influence of alkali-silica reaction (ASR) on concrete cores and reinforced concrete beams acquired from actual ASR-damaged slab bridges in Denmark. Furthermore, this PhD project investigates the time-dependent influence of ASR deterioration on the physical and mechanical properties of 1.5 x 1.5 x 0.25 m^3 reinforced concrete slabs accelerated in a laboratory at 40°C and high relative humidity.

To understand the relevance of this PhD project, this chapter gives an historical background of ASR research in Denmark. The motivation for initiating the PhD project is described, and the aim and objectives of this PhD project are defined. Finally, this chapter outlines the structure of the thesis.

1.1 Alkali-Silica Reaction

Distresses in actual concrete structures due to alkali-silica reaction (ASR) have been observed worldwide, in some cases causing uncertainties about the structural integrity of the affected concrete structures (Swamy, 1992).

ASR is a complex physical and chemical reaction between the alkali hydroxides in the pore solution of concrete and certain forms of silica minerals in aggregates (Hobbs, 1988). Although the mechanism of the reaction is not completely understood, it is generally agreed upon among researchers that the chemical reaction occurs as a result of increased solubility of certain types of silica minerals in high-pH solutions (Wigum *et al.*, 2006). The nature of the reaction creates a hygroscopic reaction product, alkali-silica gel, which imbibes water and swells (see Figure 1.1). The physical nature of the reaction is characterized as expansive. With sufficient quantities of reactive aggregate particles in the concrete, the expansive reaction may exert considerable tensile stresses on the concrete leading to premature deterioration visualized as cracking of aggregates and cement paste (see Figure 1.2). For the expansive reaction to occur, high moisture content in the concrete, sufficient concentration of alkalis (Na^+, K^+) in the concrete pore solution, $Ca(OH)_2$ and

sufficient amounts of reactive particles in the aggregates must be present at the same time in the concrete (Chatterji *et al.*, 1988). An absence of any of the above components will reduce or prevent the expansion.
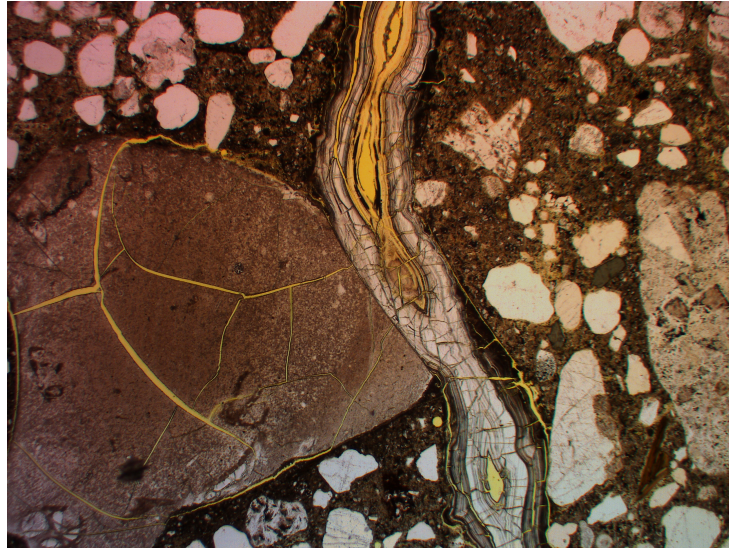
Figure 1.1: Microphotograph of a specific part of a thin section. Width of field 4.8 mm. Plane polarized light: Deposits of alkali-silica gel partially filling an ASR induced crack.
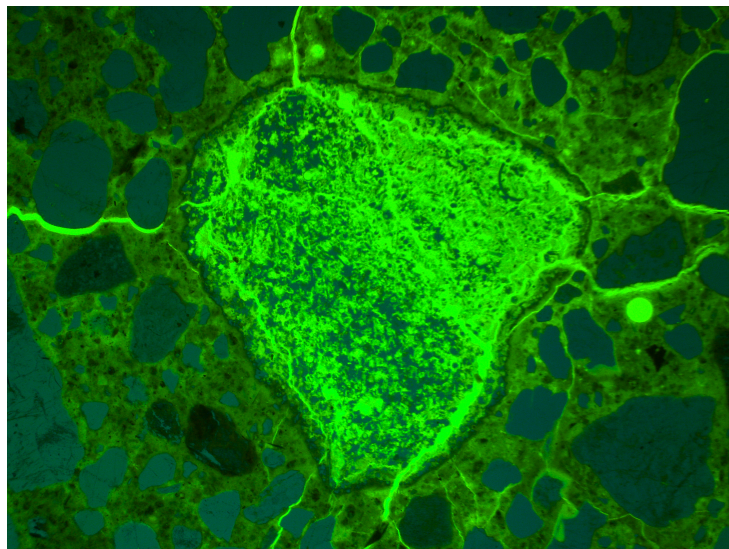
Figure 1.2: Microphotograph of a specific part of a thin section. Width of field 4.8 mm. Fluorescent light: Massive cracking in reactive sand particle and in cement paste due to ASR.

1.2   Alkali-Silica Reaction in Denmark

In Denmark, ASR is, to a certain extent, a well-known deterioration mechanism. The awareness and acceptance of ASR in Danish concrete structures can be traced back to the early 1950s.

In Denmark, long before the ASR discovery by Thomas Stanton in America, one of the first publications concerning durability of concrete structures that might be related to ASR cracking was published by the Danish engineer Poulsen in 1914 (Poulsen, 1914). At that time the cracking observed in concrete structures was believed to be caused by other deterioration mechanisms, mainly freeze-thaw deterioration, and no systematic research on the cause of cracking was conducted.

The Danish concrete researcher Poul Nerenst became aware of the ASR discovery from Thomas Stanton by participating in a conference held by the American Association of State Highway Officials in Miami, Florida in December 1950 (Nerenst, 1952). In 1951, based on the report from Nerenst (Nerenst, 1952), The Danish National Institute of Building Research (DNIBR) started a series of studies of concrete structures in Denmark (see Figure 1.3), in order to identify if the cracking observed on the structures could be related to the reactions between alkali hydroxides and reactive silica minerals in aggregates.

Figure 1.3: Crackling in a Danish concrete bridge. Photo adapted from (Nerenst 1952), taken in the early 1950s.

As a consequence of the preliminary investigations and acceptance of ASR in Danish concrete structures in 1951, systematic research on ASR was initiated in 1954 by the Academy of Technical Sciences (ATV) and DNIBR. A joint committee on alkali-reactions in concrete was appointed by ATV and DNIBR (Nerenst, 1957).

At that time, research on ASR was divided into three major subcommittees: 1) field investigations, 2) investigations of aggregates, and 3) laboratory investigations (Plum *et al.*, 1957). Results of the comprehensive research conducted by the Danish Committee on alkali-reactions in concrete were published in 23 reports (Swamy, 1992). The most important contribution to the research was the classification of reactive aggregate types. Denmark is a small and homogeneous country with regard to geology and only a few aggregate types are found to be reactive. In Denmark, the aggregate sources contain reactive silica minerals, both in the fine aggregate fraction (see Figure 1.4) and in the coarse aggregate fraction (see Figure 1.5) (Plum, 1961). Porous opaline and porous calcareous opaline flint were found to be the main reactive aggregate types. Both reactive aggregate types are characterized as fast-reactive and even in very small amounts they can cause deleterious ASR cracking in concrete structures within 2 to 5 years of field exposure under specific conditions. In many other countries, Norway for example, the reactive aggregates are characterized as slowly reactive, causing deleterious cracking in concrete structures after 15 or 20 years of field exposure (Lindgård, 2013).

Another considerable contribution by the Danish Committee on alkali-reactions in concrete was the recommendation of preventive measures; the use of fine aggregates containing less than 2 vol.% reactive particles of porous opaline and/or calcareous opaline flint prevents the risk of deleterious expansion and cracking of the concrete (Plum, 1961). Most cases of ASR damages in Danish concrete structures are caused by reaction in the fine aggregate fraction, sand fraction.

A different phase of the Danish research on ASR was conducted from the 1970s to the mid-1980s. Until the 1970s, the assumption was that the only source of alkalis in the concrete was from the cement which was expected to remain constant and uniformly distributed through the service life of the structure (Swamy, 1992). However, severe ASR cracking in actual concrete structures with alkali content below 0.6% Na_2O eq. occurring just a few years after their inauguration, changed that assumption. External supplies of alkalis from sources such as de-icing salts, sea water and salt water were investigated as possible sources of alkali to the concrete. This research phase led to the development of the TI-B 51 mortar-bar expansion method, where some mortar bars are immersed in a saturated sodium chloride solution at 50°C, and others are exposed to 100% RH at 50°C (TI-B 51, 1985). The mortar bars were exposed to the accelerated conditions for up to 20 weeks, and the mortar bars' expansion was measured periodically. In Denmark, the critical expansion in length of mortar bars with fine aggregates is set to 0.1% (DS Standard, 2011). The TI-B 51 mortar-bar expansion method has proven to be very effective in verification of Danish reactive aggregate types, especially for porous opaline flint. For porous calcareous opaline flint, the expansion is slower than for the porous opaline flint, and the 20 weeks of exposure in the TI-B 51 mortar-bar test is probably not always sufficient to verify the reactivity of the porous calcareous opaline flint.
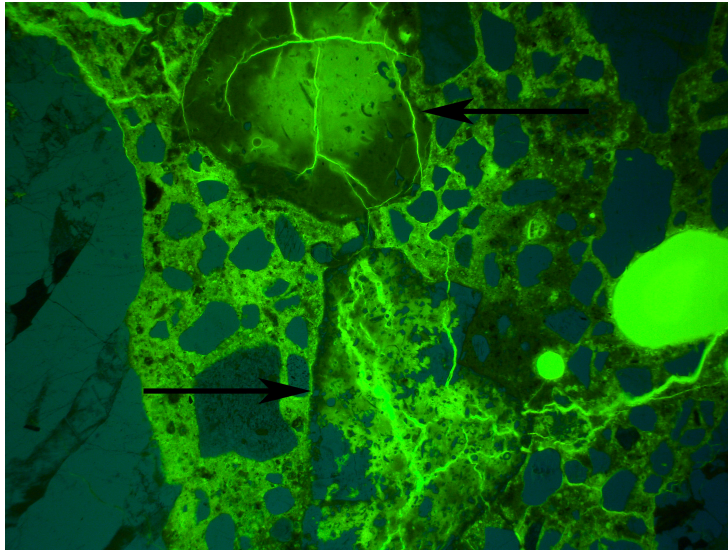
Figure 1.4: Microphotograph of a specific part of a thin section. Width of field 4.8 mm. Fluorescent light: Two reactive fine aggregate particles.
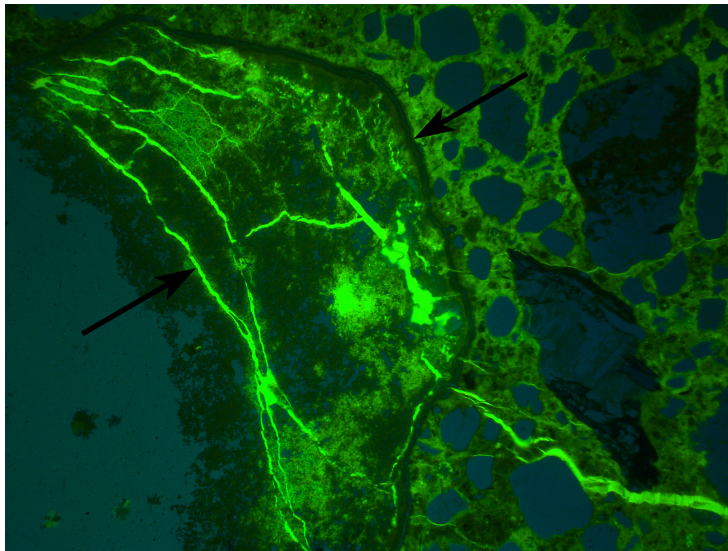
Figure 1.5: Microphotograph of a specific part of a thin section. Width of field 4.8 mm. Fluorescent light: Reactive porous opaline flint skin in a coarse aggregate particle.

1.3   ASR deterioration in older Danish bridges

One would expect that the early comprehensive Danish research on ASR conducted in the 1950s and 1960s would have a preventive influence on the quantity of older concrete bridges with the potential to develop ASR. However, that seems not to be the case in Denmark.

Many of today's potential ASR-reactive concrete bridges were built during the fast development of the Danish road infrastructure system in the 1960s and 1970s.

During that time frame the Danish parliament approved the idea of a unified Danish highway network in the shape of a large H (see Figure 1.6), and construction of large road systems in Zealand and in Jutland was launched (Larsen, 2014).
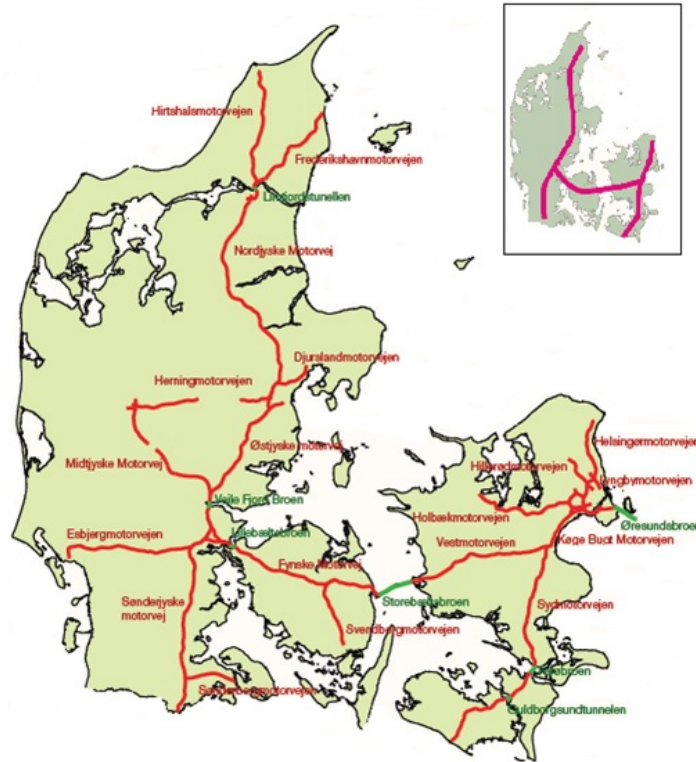
Figure 1.6: Illustration of the Danish highway network in 2013. The Danish highway network is unified in the shape of a large H. Illustration adapted from (Larsen 2014).

Even though preliminary preventive measures for ASR were published and available to the concrete industry in 1961 (Plum, 1961) no official regulation or requirements concerning the amount of ASR-reactive particles in aggregates were mandatory at that time. Apparently, the main reason for that was the lack of support from some of the leading researchers behind the Danish Committee on alkali-reactions in concrete. Some of the leading researchers argued that implementation of such requirements would have a negative socioeconomic effect on the concrete and aggregate industry (Grelk, 2014).

In 1986, after intense debate, a code of practice was adopted, which specifies specific requirements for the critical amount of reactive aggregates that can be used in the concrete for all public and governmental constructions. The code of practice was published in 1987 (Byggestyrelsen, 1987). Preventive measures from 1961 concerning specific requirements for the critical amount of ASR-reactive particles in Danish aggregates are used today and were implemented in the code of practice from 1987, 26 years after its first publication.

Consequently, local ASR-reactive aggregates characterized as fast-potential reactive were used in the numerous bridge constructions as part of the development

of the Danish road infrastructure system. In Denmark, 15 percent of the concrete road bridges, which correspond to approximately 600 road bridges, and an unknown amount of municipal and railway bridges, have potential to develop ASR damages (Østergaard, 2012).

The fact that more than 600 Danish concrete bridges are "only" potentially ASR reactive is a consequence of the Danish construction tradition, where a waterproofing membrane is used between the upper surface of the concrete bridge deck and a high-quality asphalt pavement (Wegan, 2000). The waterproofing membrane can protect the upper concrete deck surface from external supply of water and de-icing salts. In Denmark, the supply of de-icing salts for road bridges is crucial for the ASR deterioration process. The alkali content, Na_2O eq. content, in the most commonly used Danish types of cement varied at that time between 0.5% to 0.8% by weight of cement (Swamy, 1992). Consequently, the alkali content from the cement in the vast majority of Danish concrete bridges built in the 1960s and 1970s is estimated to be well below the alkali threshold value of 3.0 kg Na_2O eq. content per m^3 of concrete (Nielsen *et al.*, 2004).

Traditionally, the lifespan of the waterproofing membrane in Denmark is approximately 40 to 50 years (Stoltzner *et al.*, 2005). However, a 40 to 50 year lifespan is only an average estimate. Several types of waterproofing membrane have been used and their durability may vary due to several factors, such as, the construction on top of the waterproofing membrane, load actions, and possible execution errors. In the near future, major economic investments will be needed in replacement of existing waterproofing membrane on bridges constructed in the 1960s and 1970s, to prevent ingress of water and de-icing salts to the concrete and prevent the initiation of deleterious ASR. However, in practice it will not be possible to avoid exposure of all the potential ASR-reactive bridge slabs to external supply of water and de-icing salts during their service life, and as a consequence, in the future we may expect new cases of ASR deterioration in Danish bridges.

Today, to the author's knowledge, 20 to 25 Danish bridges are severely damaged due to ASR. The existing cases of severe ASR deterioration in Danish bridges are related to defects in and leakage of the waterproofing membranes.

1.4 Assessment of Danish ASR-damaged bridges

The current approach to diagnosing ASR in bridges can be traced back to Idorn's dissertation (Idorn, 1967), where a systematic approach to the assessment of field concrete deterioration was proposed.

For the concrete bridges managed by the Danish Road Directorate and Rail Net Denmark, regular routine inspections are usually conducted in a period of 1 to 6 years (Road Directorate, 1994). For the municipality-managed bridges, the routine inspections are often governed by the accessible financial latitude. Routine inspections for municipality-managed bridges may not be as periodic and systematic.

Routine inspections are typically the first step in which the premature signs of ASR deterioration can be detected by trained engineers. In Denmark, routine inspections are normally conducted by engineers trained for evaluation of different

distress mechanisms in field structures. Routine inspections are visual inspections mostly conducted on visual parts of the bridge without any evaluation of possible interior cracking. Interior parts inside the bridge slabs or just below the waterproofing membrane may present signs of ASR cracks, but these may not be detected during routine inspections. If no visual signs of cracking are observed, further actions on the inspected bridge are typically postponed until the next routine inspection, or until evaluation reveals that the waterproofing membrane is no longer intact as a consequence of its estimated lifespan.

If cracking is observed on parts of the bridge structure, special inspections are the second step in the condition survey of potential ASR-deteriorated bridges. Based on the routine inspections, concrete cores may be drilled from selected parts of the bridge deck (see Figure 1.7a). Petrographic examinations, macroscopic and microscopic, will be conducted on drilled cores. Thin-section examinations by optical microscope are conducted to verify the presence of ASR and/or other deterioration mechanisms. Additionally, impregnation of cores by epoxy containing fluorescent dye can complement the thin-section examinations and visualize the quantity and orientation of the cracking (see Figure 1.7b). The evaluation of the quantity and orientation of cracking in the cores is a subjective evaluation. In Denmark the only tool used to assess the future possibility for ASR is the residual expansion test of cores. Residual expansion will occasionally be tested by exposing small specimens cut from the cores to conditions similar to that of the TI-B 51 mortar-bar test method. The expansion in length of specimens will be measured periodically within a 20-week period. The residual expansion test will only provide a pessimistic possibility for the aggregates to react under certain accelerated conditions and will not correspond to future expansion in the examined bridge.

During the special inspections, the condition of the waterproofing membrane and possible reason for moisture and de-icing salt supply to the bridge deck may be evaluated. Based on the special inspections, remedial actions will be planned. In Denmark, the remedial actions will mostly consist of replacing the defective or obsolete waterproofing membrane on top of the bridge decks, thus preventing additional supply of water and de-icing salts to the deck. Optionally, coating of edge beams and additional structural elements is conducted. It must be acknowledged that the above-mentioned remedial actions are idealized. Cost-benefit analyses might result in strategies other than replacing the waterproofing membrane. Waterproofing membrane systems are relatively expensive and time-consuming repair techniques which often lead to significant traffic disturbances (Stoltzner *et al.*, 2005).

1.5 Structural integrity of Danish ASR-damaged bridges

If special inspections reveal severe ASR cracking in large parts of the bridge deck, structural engineers might perform calculations to assess the residual load-carrying capacity of the affected bridge. However, evaluation of structural integrity of severely ASR-damaged concrete bridges is a complex process.

Figure 1.7: Railway bridge slab. (a) Typical ASR cracks seen from underneath a railway bridge slab. (b) Typical ASR crack orientation on a fluorescence impregnated vertically drilled concrete core seen under ultraviolet (UV) light.

In Denmark and in many countries, there is no commonly accepted regulation, calculation methods or models to predict the residual load-carrying capacity of severely ASR-damaged concrete bridges. Rarely, the in-situ drilled cores are in a condition and size to be used for mechanical testing. If mechanical testing is possible, potential differences in the extent of ASR cracking in parts of the bridge deck may create challenges in the interpretation and evaluation of mechanical testing. Furthermore, in-situ drilling is often only possible from beneath or above the bridge deck. The in-situ drilled cores will in most cases have a very specific crack orientation depending on the type of the structure.

The structural integrity of actual ASR-damaged bridges may be evaluated from the limited studies of laboratory-prepared and -accelerated small-scale specimens. However, the configurations of the simplified small-scale specimens may not be representative of the actual damaged concrete bridge. The reinforcement configuration, test setup, type of ASR-reactive aggregate and conditioning of the small-scale specimens might vary in all studies and may not be compatible with the ASR-damaged bridges. Additionally, the limited studies on the effect of ASR on the load-carrying capacity of small-scale laboratory-prepared and -exposed specimens are contradictory. Both increases and decreases in the load-carrying capacity due to ASR deterioration and cracking are reported (Bach *et al.*, 1993; Road Directorate, 1990; Ahmed *et al.*, 1984; Deschenes *et al.*, 2009; Chana and Korobokis, 1991; Bilodeau *et al.*, 2016; Inoue, 1980; Okada *et al.*, 1989; Fujii *et al.*, 1986). The laboratory studies are not irrelevant, but a great risk is to believe that laboratory

studies of small-scale laboratory-conditioned specimens are the basis for in-situ performance of ASR-damaged bridges in service. This means that Danish consultant engineers are often left without any objective tools or realistic and reliable data to evaluate the residual load-carrying capacity of the ASR-damaged bridges in service.

To the author's knowledge four severely ASR-damaged road bridges have in recent time been demolished and reconstructed in Denmark due to uncertainties about their residual load-carrying capacity. The decision to demolish these bridges has in general been based on lack of knowledge, with the decision to demolish these bridges based on subjective evaluations built on visual appearance, petrographic examinations of drilled cores and rough estimates of the residual load-carrying capacity of the ASR-damaged bridges.

1.6   Scope and objectives

Presently and in the future it will not be economically possible to demolish and reconstruct existing and possible future ASR-damaged bridges in Denmark. Instead, testing of materials acquired from these bridges will be essential to objectively evaluate their residual load-carrying capacity.

Therefore, the scope of this PhD project is to experimentally provide realistic and reliable data on the influence of ASR cracking on the mechanical properties of ASR-damaged concrete, and on the residual load-carrying capacity of an actual ASR-damaged flat slab bridge. The ASR-damaged concrete originate from ASR-damaged flat slab bridges in service. In this study, slab segments from three ASR-damaged slab bridges without shear reinforcement will be examined. However, recognizing that tests on segments sawn from slab bridges in service only provide a snapshot of the condition at one point in the ASR deterioration process, large-scale reinforced slabs will be casted and accelerated under laboratory conditions at high temperature and high relatively humidity. This approach is performed in order to provide and improve the knowledge about the time-dependent physical and mechanical effect of ASR on reinforced slabs.

The overall objectives of the PhD project are to:

- Test the influence of ASR on the uniaxial compressive strength and tensile strength of drilled concrete cores from ASR-damaged bridge slabs in service

- Identify and understand the influence of the ASR crack orientation on the uniaxial compressive strength, tensile strength and Young's modulus of cores drilled from the ASR damaged bridge slabs

- Test the residual shear strength of ASR-damaged reinforced beams acquired from a severely ASR-damaged flat slab bridge, and

- Investigate the time-dependent influence of ASR on the physical and mechanical properties on large-scale laboratory-casted and laboratory-accelerated reinforced concrete slabs.

On the basis of realistic and reliable tests and better understanding of the challenges related to ASR in actual bridge slabs, it might in the near future be possible to establish new methods, methodologies and/or calculation models that can be applied to assess the residual load-carrying capacity of severely ASR-damaged bridge slabs in service.

1.7 Thesis outline

The structure of this PhD thesis is in accordance with the "paper based model". This means that journal papers constitute three of the chapters. However, one of the main research areas of this PhD project concerns research on the time-dependent influence of ASR on the physical and mechanical properties of laboratory-casted and laboratory-accelerated reinforced slabs. In this PhD thesis the research on laboratory-accelerated reinforced slabs is reported as one chapter. This is due to the development of ASR and related ASR-induced cracks in some of the accelerated reinforced slabs, which have not reached a stationary level.

This PhD project includes two main research areas:

1. Influence of ASR on the mechanical properties of ASR-damaged concrete and on the residual shear strength of a severely ASR-damaged flat slab bridge (Chapter 2, Chapter 3 and Chapter 4)

2. Research on the time-dependent influence of ASR development on the physical and mechanical properties of laboratory-casted and laboratory-accelerated reinforced slabs (Chapter 5)

Chapter 2 consists of one journal paper (Paper I) that experimentally investigates the influence of ASR and ASR crack orientation on the compressive strength of drilled concrete cores. The cores were drilled from slab segments sawn from three ASR-damaged slab bridges. The paper provides an explanation of the effects of ASR crack orientation on the failure mechanism and compressive strength of the cores. Additionally, the influence of ASR cracks on the Young's modulus of the cores is discussed.

Chapter 3 consists of one journal paper (Paper II) which investigates the influence of ASR cracks and ASR crack orientation on the tensile strength of specimens from the same three ASR-damaged slab bridges as the cores tested in compression (Paper I). Indirect and direct tensile strength test methods were investigated. An evaluation of each tensile strength test method and its applicability are discussed.

Chapter 4 consists of one journal paper (Paper III) that investigates the residual shear strength of beams sawn from a severely ASR-damaged flat slab bridge. In total 18 beams were tested; 9 beams were tested in an asymmetrical four-point bending setup and 9 beams were tested in a three-point bending setup. The paper discusses the effect of shear span-to-effective depth ratio on the shear strength of the beams. Additionally, the influence of ASR cracks on the failure mechanism of the beams is discussed. The tested shear strengths are compared to shear strength

calculations by Eurocode 2. The ASR-induced tensile strain in reinforcing bars is measured and discussed.

Chapter 5 concerns the time-dependent influence of ASR development on the physical and mechanical properties of six large laboratory-casted and laboratory-accelerated reinforced slabs. Some of the reinforced slabs have high initial alkali content and other slabs are externally exposed to saturated NaCl solution. The influence of ASR crack penetration depth on the compressive strength of drilled cores and the rate of downwards ASR crack penetration are discussed. Ultrasonic pulse velocity measurements were conducted and correlated to the crack penetration depth and core compressive strength. The applicability of exposure conditions in this laboratory-accelerated research is evaluated and compared to ASR-damaged bridge slabs in service.

Chapter 6 summarizes the main findings of this PhD study.

1.8   Publications arising from thesis

Four ISI journal papers were written and submitted based on the work concerning the mechanical properties and the residual shear strength of ASR-damaged bridge slabs in service. Three of the journal papers are a part of this thesis. Moreover six conference papers were published in conference proceedings and presented at international conferences.

Journal papers arising from thesis

Paper I **Barbosa RA**, Hansen SG, Hansen KK, Hoang LC, Grelk B. Influence of alkali-silica reaction and crack orientation on the uniaxial compressive strength of concrete cores from slab bridges. Submitted to Cement and Concrete Research in 2017.

Paper II **Barbosa RA**, Hansen KK, Hoang LC, Grelk B. Influence of alkali-silica reaction and crack orientation on the tensile strength of concrete specimens from severely ASR-damaged slab bridges. Submitted to Cement and Concrete Research in 2017.

Paper III **Barbosa RA**, Hansen SG, Hansen KK, Hoang LC. Residual shear strength of a severely ASR-damaged flat slab bridge. Submitted to Engineering Structures in 2017.

Journal papers arising from thesis (not included)

Paper IV Schmidt JW, Hansen SG, **Barbosa RA**, Henriksen A. Novel shear capacity testing of ASR damaged full scale concrete bridge. Eng. Struct. 79. (2014) p. 365-374.

Conference papers arising from thesis (not included)

- **Barbosa RA**, Hansen KK The influence of Alkali-Silica Reaction and Crack Orientation of the Mechanical Properties of Concrete. In: Bastien J, Rouleau N, Fiset M, Thomassin M, editors. Procedings of the 10th fib International PhD Symposium in Civil Engineering; 2014 Jul 21-23; Québec, Canada. Québec: Research Center on Concrete Infrastructure (CRIB), Université Laval; 2014. p. 111-116

- **Barbosa RA**, Hansen KK, Hoang LC, Larsen ES. Alkali-Silica Reaction in Reinforced Concrete Structures, Part I: Material Properties and Crack Orientation. In: The Nordic Concrete Federation, editors. Proceedings of XXII Nordic Concrete Research Symposium; 2014 Aug 13-15; Reykjavik. Norsk Betongforening; 2014. p. 65-68.

- **Barbosa RA**, Hansen KK, Hoang LC, Maag I. Alkali-Silica Reaction in Reinforced Concrete Structures, Part II: Shear Strength of severe ASR Damaged Concrete Beams. In: The Nordic Concrete Federation, editors. Proceedings of XXII Nordic Concrete Research Symposium; 2014 Aug 13-15; Reykjavik. Island; Oslo: Norsk Betongforening; 2014. p. 69-72.

- **Barbosa RA**, Hansen SG, Hansen KK, Hoang LC, Grelk B , Maag I. Assessment of Severely ASR Damaged Bridges: From Diagnosis to Structural Effects. In: Bernardes H.D., Hasparyk N.P., editors Proceedings of the 15th International Conference on Alkali-Aggregate Reaction in Concrete, 2016 Jul 03-07, São Paulo.

- Hansen SG, **Barbosa RA**, Hoang LC. Shear Capacity of ASR Damaged Structures - In-depth analysis of some in-situ shear tests on bridge slabs. In: Bernardes H.D., Hasparyk N.P., editors Proceedings of the 15th International Conference on Alkali-Aggregate Reaction in Concrete, 2016 Jul 03-07, São Paulo.

- Hansen SG, **Barbosa RA**, Hoang LC. Prestressing of reinforcing bars in concrete slabs due to concrete expansion induced by Alkali-Silica Reaction. In: Proceedings of the fib Symposium 2016:Performance-based approaches for concrete structures, 2016 Nov 21-23, Cape Town.

Influence of alkali-silica reaction and crack orientation on the uniaxial compressive strength of concrete cores from slab bridges

Paper I

"Influence of alkali-silica reaction and crack orientation on the uniaxial compressive strength of concrete cores from slab bridges"

R.A. Barbosa, S.G. Hansen, K.K. Hansen, L.C. Hoang and B.Grelk

Influence of alkali-silica reaction and crack orientation on the uniaxial compressive strength of concrete cores from slab bridges

Ricardo Antonio Barbosa[a], Søren Gustenhoff Hansen[b], Kurt Kielsgaard Hansen[a], Linh Cao Hoang[a], Bent Grelk[a]

[a] *Technical University of Denmark, Brovej, Building 118, 2800 Kgs. Lyngby, Denmark*
[b] *University of Southern Denmark, Campusvej 55, 5230, Odense M, Denmark*

Abstract

For a reliable structural analysis and risk assessment of concrete structures damaged by alkali-silica reaction (ASR), knowledge of the concrete compressive strength is essential. Existing studies have shown that ASR-induced cracks only slightly affect the concrete compressive strength. Most of these studies are based on experiments with laboratory-casted and laboratory-accelerated specimens. The specimens are accelerated without any realistic restraint conditions, as would be for reinforced concrete bridge slabs in service. The ASR-induced crack pattern within these laboratory specimens varies significantly from the crack pattern observed on reinforced bridge slabs in service. In general, there is a lack of knowledge about the effects of ASR cracking on the concrete compressive strength of severely ASR-damaged bridge slabs.

This study investigates the residual compressive strength of concrete cores drilled from three severely ASR-damaged flat slab bridges in service. Furthermore, the influence of the ASR-induced crack orientation on the compressive strength is investigated. Uniaxial compression tests, visual observations, and thin section examinations were performed on more than 100 cores drilled from the three severely ASR-damaged flat slab bridges. It was found that the orientation of ASR-induced cracks has a significant influence on the uniaxial compressive strength and the stress-strain relationship of the tested cores. The compressive strength in a direction parallel to ASR cracks is significantly higher than the strength in the direction perpendicular to ASR cracks. In the latter case, more than 60% reduction from the original strength was observed.

Alkali-Silica Reaction, Slab bridges, Uniaxial compressive strength, Young's modulus, Crack orientation, Thin section examination, Failure mechanism

1. Introduction

Numerous concrete structures around the world are either damaged or have the potential to develop damage and cracking due to alkali-silica reaction (ASR) [1]. ASR is a complex

physical and chemical reaction between alkalis (Na^+, K^+) present in the concrete pore solution, usually originating from the cement but also supplied from outside sources such as de-icing salts, certain types of reactive aggregates containing reactive silica minerals, and moisture [2]. The reaction produces an alkali-silica gel which can absorb water and expand. With sufficient amounts of reactive aggregates in the concrete, the reaction can generate expansion and internal pressure that causes serious cracking in concrete structures [1].

To the authors' knowledge, four slab bridges in Denmark have in recent time been demolished due to ASR cracking and uncertainties regarding their structural integrity. The decision to demolish these bridges has, to the authors' knowledge, been based on a subjective evaluation built on in-situ visual inspections and petrographic examinations of drilled cores. Rarely, the in-situ drilled cores will be in a condition and size to perform compressive strength tests.

In order to conduct a reliable structural analysis and risk assessment of real-life ASR-damaged concrete structures, determining the compressive strength of the ASR-cracked concrete is essential.

Several experimental studies on the effect of ASR damages on the compressive strength of concrete have been published [3–17]. The experimental studies, as regards to the boundary conditions of the specimens, can be divided into two categories: unrestrained concrete specimens and restrained concrete specimens. Usually the experimental studies are based on small-scale laboratory-casted and accelerated cylinders, prisms, and cubes, under free expansion, and unrestrained. Many studies of unrestrained specimens conclude that the compressive strength of ASR-damaged concrete is only slightly affected by the ASR cracking. However, from these laboratory experimental studies it is difficult to generalize the influence of ASR cracking on the compressive strength of concrete because the expansion at time of the destructive tests, the used reactive aggregate types, exposure conditions, and several additional parameters vary from study to study. As a consequence, the experimental results are contradictory. Most importantly, it is difficult to generalize the laboratory experimental studies of unrestrained specimens to actual reinforced concrete structures.

In actual reinforced concrete structures in service, the development and orientation of the ASR-induced cracks are influenced by the structural boundary conditions and the reinforcement configuration. ASR-induced cracking in unrestrained concrete is typically

oriented randomly, because the expansion is not restricted in any direction. This random crack patterning is often referred to as *map cracking* [18]. In the presence of reinforcement the expansion is elastically restrained in the reinforcement direction, leading to tensile stresses in the reinforcement bars and suppression of the concrete expansion in the main reinforcement direction. Consequently, the ASR-induced cracks form parallel to the main reinforcement direction as seen in bridge slabs in service without shear reinforcement [19].

More realistic restraint configurations in laboratory-conditioned specimens are essential. Rigden *et al.* [9] studied the long-term development of crack patterns and mechanical properties in ASR-reactive concrete blocks subjected to different levels of uniaxial compressive stresses. Rigden *et al.* observed that the blocks subjected to compressive stresses developed ASR cracks parallel to the uniaxial compressive stresses. Unloaded concrete blocks formed random map cracking. The applied compressive stresses during ASR crack development had a significant influence on the measured compressive strength and elastic modulus of the drilled cores. Rigden *et al.* reported that the compressive strength and elastic modulus of drilled cores with ASR cracks oriented parallel to the load direction were greater than drilled cores with ASR cracks perpendicular to the load direction. Giaccio *et al.* [10] and Majlesi [13] also studied the influence of long-term compressive stresses on the crack patterns of concrete cylinders. The experimental studies by Giaccio *et al.* and Majlesi confirm the results by Rigden *et al.* Additionally, the influence of ASR-induced crack orientation on the Young's modulus was reported to be greater than the influence in compressive strength.

To the authors' knowledge, only limited studies have been based on cores drilled in different directions from reinforced ASR beams or slabs climate accelerated in the laboratory [15–17]. Jones *et al.* [11] stated that the compressive strength of the concrete in an ASR-reinforced beam is greater in the direction of largest restraint. The studies of Hiroi *et al.* [15], based on drilled cores in different directions from laboratory accelerated post-tensioned reinforced beams, supports the statement from Jones *et al.* However, the studies from Bach *et al.* [16] diverge from the results of Jones *et al.* [11] and Hiroi *et al.* [15]. Bach *et al.* [16] reported that the compressive strength of drilled cores from laboratory climate accelerated non-shear reinforced beams were greater in the direction of least restraint. This dissimilarity may be caused by differences in ASR-induced crack patterns within the drilled cores. Allard *et al.* [17] reported no statistically significant differences in the compressive strength of cores drilled vertically and horizontally from climate accelerated thick concrete beams. As shown, the influence of crack orientation on

reinforced concrete beams climate accelerated in the laboratory is contradictory. In addition, the results obtained from reinforced beams may not be comparable to slabs due to differences in reinforcement configurations and crack patterns. Hansen *et al.* [20] illustrated the differences in ASR-induced crack orientation as a result of differences in reinforcement configurations between ASR deteriorated slabs in service and accelerated beams.

To the authors' knowledge there exist no studies of the influence of ASR cracking and the orientation of ASR cracking on the uniaxial compressive strength of concrete in ASR-damaged bridge slabs in service. In order to provide such experimental evidence uniaxial compressive strength tests, visual observations and thin sections examinations were performed on cores drilled from three severely ASR-damaged flat slab bridges in service. The cores were drilled vertically and horizontally from the bridge slabs. Besides testing the residual compressive strength of the ASR-cracked concrete, the influence of the ASR-induced crack orientation on the uniaxial compressive strength was determined. Additionally, this paper provides a background on the three ASR-damaged bridge slabs and the cracking patterns observed within the slabs.

2. Materials

In Denmark, more than 600 concrete bridges have the potential to develop ASR cracking. The majority of these bridges were constructed during the 1960s and 1970s [21]. Some of these bridges are severely damaged with considerable ASR cracking. Compared to other countries, Denmark is a small and homogeneous country with regard to geology; only a few aggregate types are found to be reactive [22]. The Danish porous flint, consisting of porous opaline and calcareous flint, is found to be very fast reactive. In Denmark, the large majority of the cases with ASR-damaged concrete structures is caused by reactions in the fine aggregate (sand) fraction.

The uniaxial concrete compressive strength was determined by testing cores drilled from three severely ASR-damaged flat slab bridges in service. All the examined bridge slabs are reinforced with two layers of horizontal reinforcement nets and are not provided with shear reinforcement. Consequently, the vertical expansion is not restrained by any reinforcement.

2.1 The examined ASR-damaged flat slab bridges in service

2.1.1 Slab bridge A

Slab bridge A, also known as Vosnæsvej bridge, was built in 1976 and consists of three spans. The total bridge length is 54.5 m, and the width is 10.0 m. The bridge was constructed with two pre-stressed beams and an integrated deck (a double T structure) where the deck was constructed as a concrete slab without shear reinforcement.

In 2012, visual inspection of the bridge slab showed comprehensive fine wet longitudinal ASR cracking combined with gel exudation at the cantilevered part of the integrated deck.

For determination of the mechanical properties of the ASR-cracked concrete, 12 beams, 1.3-m-long, were cut from the cantilever part of the bridge slab; six beams were cut from the western bridge end, and six beams from the eastern bridge end. The distance between the eastern and western ends was approximately 30 m. The beams were cut during the preparation for an in-situ full-scale test of the load-carrying capacity of the bridge slab. The results of these in-situ full-scale tests were reported by Schmidt *et al.* [23] and further analysed by Hansen *et al.* [24]. The cores were drilled from the 12 beams.

2.1.2 Slab bridge B

Slab bridge B, also known as Gammelrand bridge, was built in 1976 and consisted of three spans. The width of the bridge slab was 9.1 m, and the total length was 30.5 m; the longest span was 14.0 m. The entire bridge was constructed as a concrete slab without shear reinforcement.

Visual inspections of the bridge and drilled cores showed that the entire 0.7-m-thick slab was cracked and delaminated due to ASR. In 2010, the bridge was demolished due to uncertainties regarding the residual load-carrying capacity. Beforehand, four 7.65-m-long and 0.6-m-wide beams were cut and stored until testing in 2013. Because the beams were cut from the same place on the bridge slab, the extent of ASR cracking between the beams was not visually different. Cores were drilled from two adjacent beams.

2.1.3 Slab bridge C

Slab bridge C, also known as Lindenborg Pæledæk bridge, was built in 1966-1967 as a multi-span, pile-supported slab bridge consisting of a southern and a northern bridge. The total length of the northern bridge slab is 312 m, and the total length of the southern

bridge slab is 120 m. The width of the two bridges is 10 m, and the height of the slabs is 0.3 m. The entire bridge deck was constructed as a concrete slab without shear reinforcement.

Only 10 years after the inauguration of the bridge, inspections showed major signs of ASR-induced cracks combined with gel exudation. Several additional special inspections of the bridge slab showed that the entire slab of the northern and the southern bridge were severely cracked and delaminated due to ASR.

Due to uncertainties about the residual load-carrying capacity of the bridge slab, a large, full-scale test project was initiated in 2014; six large, 2.4- to 4.2-m-long, 2.2-m-wide trapezoidal slabs were cut from the northern bridge slab. The trapezoidal slabs were transported to the laboratory, and each slab was then cut into seven beams. Cores were drilled from four of the seven beams on each trapezoidal slab. The three additional beams from each trapezoidal slab were used for bending tests.

2.2 Thin sections examinations

To verify the presence of ASR, and to disregard the possibility of other deterioration mechanisms in the bridge slabs, optical microscopy examinations of several thin sections were conducted. The thin sections were prepared from slices cut from fluorescence-impregnated drilled cores. The cores were impregnated with epoxy containing a fluorescent dye under vacuum; the fluorescent epoxy impregnates surface open cracks and voids.

The thin section examinations confirmed that ASR in all bridge slabs occurred in the sand fraction as shown in Fig 1(a). Fig. 1(a) shows a microphotograph from a part in a thin section under fluorescent light. In Fig. 1(a), the ASR-induced cracks and voids appear as a light green colour. The microphotograph shows two reactive opaline flint particles containing cracks; at the upper right, a reactive sand particle is almost dissolved and has developed considerable cracking in the surrounding cement paste, and at the lower left, a larger particle contains a few inner cracks and only a few cracks propagating into the cement paste. This larger particle has the potential to develop additional ASR cracking in the cement paste. Fig. 1(b) shows a microphotograph of the ASR gel partially filling the ASR-induced cracks in the same thin section as Fig. 1(a). In Fig. 1(b), voids appear yellow in colour, and ASR gel appears white in colour under plane polarized light. As shown in Fig. 1(b), the reaction of opaline flint sand aggregate has developed a

considerable amount of ASR gel. The thin section examinations showed that the ASR gel filling the cracks varied from 3 to 15% of the entire crack volume.
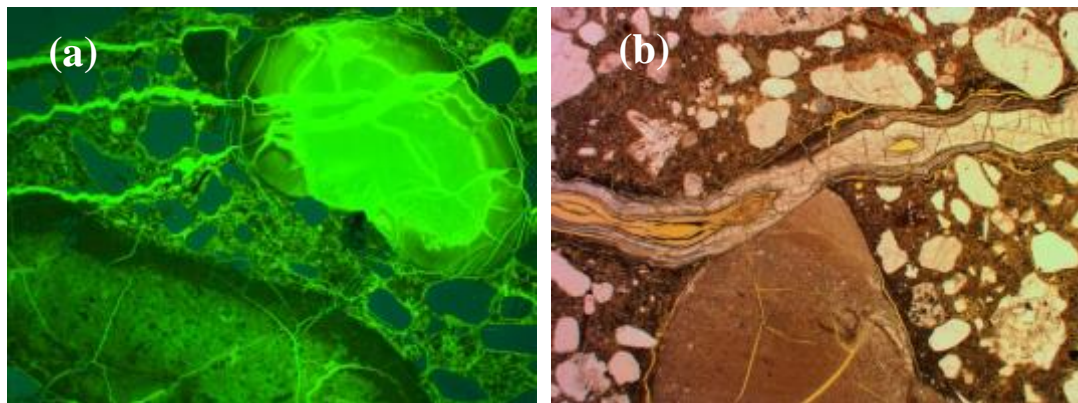

Fig. 1: Microphotograph of thin sections. Width of fields 4.8 mm. (a) Fluorescent light. Reactive aggregate particles. (b) Plane polarized light. ASR-induced crack is partially filled with ASR gel. The width of the crack is approximately 0.7 mm.

From the thin section examinations combined with visual inspections of the cores, the authors could overlook the possibilities of other contributing deterioration factors that may cause the observed cracking in the cores. There was no sign of additional cracking due to freeze-thaw cycles, reinforcement corrosion, delayed ettringite formation or fatigue by repeated traffic loading.

2.3 ASR crack orientation in the examined bridge slabs

In all the examined bridge slabs, the ASR cracks inside the concrete slabs were predominantly oriented parallel to the restraining longitudinal and transverse reinforcement bars. Fig. 2 depicts the typical ASR cracking in the bridge slabs. After drilling, the cores shown in Fig. 2 were impregnated with epoxy containing a fluorescent dye, under vacuum. Under ultraviolet (UV) light, the hardened fluorescent epoxy penetrating the cracks and voids appears as a light green colour. The ASR crack orientation is representative for all three examined bridge slabs. However, the amount of ASR cracking and the crack widths varied between the three bridge slabs and within beams and cores from the same bridge slab.

The width of the ASR cracks in the cores averaged 0.1 mm, varying from 0.05 and (locally) to 2.5 mm.
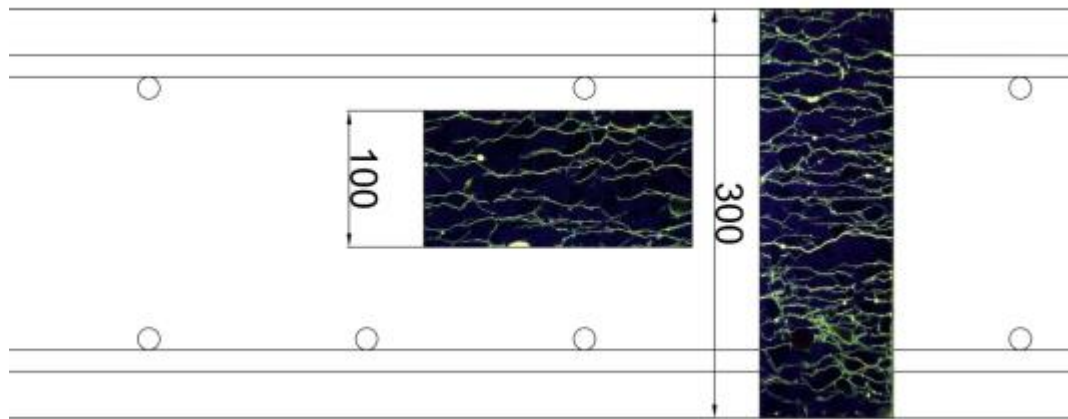
Fig. 2: Cross-section of slab bridge C. The cores were drilled vertically (perpendicular cracks) and horizontally (parallel cracks) from slab bridge C with dimensions given in mm. The concrete cores were impregnated under vacuum with epoxy containing a fluorescent dye.

3. Methods

To test the influence of the ASR-induced crack orientation on the uniaxial concrete compressive strength, more than 100 cores have been drilled from beams cut from the three bridge slabs. The cores were drilled vertically (most common in-situ drilling orientation) and horizontally. The vertically drilled cores have ASR cracks oriented predominantly perpendicular to the compressive load direction, and the horizontally drilled cores have ASR cracks oriented predominantly parallel to the compressive load direction.

3.1 Drilling and preparation of the cores

For the drilling, a circular diamond drill cooled by water circulation was used. The majority of the cores were cohesive despite the effect of drilling and ASR cracking. The Danish porous opaline and the calcareous opaline flint are known to produce a considerable amount of ASR gel. Based on the observation from the drilled cores, this ASR gel could act as a strong glue, locally binding the ASR crack walls together.

After drilling, the drilling water at the sides of the cores was wiped off with a wet cloth. The drilled core was then wrapped in cling-film to avoid desiccation, then stored in sealed plastic bags.

To ensure even stress distribution during the uniaxial compressive test the ends of the cores were sawn with a water-cooled diamond saw, and the end faces were ground plane.

Hereafter, the cores were again wrapped with cling-film and sealed in plastic bags until the uniaxial compressive strength tests were conducted. The cores were tested approximately 3 weeks after drilling.

3.2 Uniaxial compressive testing

All cores were tested in displacement-controlled hydraulic machines. The core tests were carried out with a constant displacement rate of 0.5 mm/minute, which differs from DS/EN 12390-3 [25], where the uniaxial compressive strength tests had to be performed as load controlled with a load rate of 0.6±0.2 MPa/s.

During the compressive tests the vertical deformations of the cores were logged by an LVDT on each side of the core as shown in Fig. 3. The core tests were conducted with 3-mm-thick high density wood fibre boards between the cores and steel loading platens.

Fig. 3: Test setup for the uniaxial compressive test. The deformations during loading were measured by two LVDTs placed between rigid rings closely fixed to the concrete core.

3.4 Conversion of measured compressive concrete core strength

In this paper, the tested compressive strength, $f_{c, core - strength}$, of drilled cores are converted into the "in-place" uniaxial compressive strength, f_c, for a standard cylinder (diameter/height=150/300 mm) according to Eq. (1); a method provided by the Danish Road Directorate [26].

$$f_c = k_1\, k_2\, k_3\, f_{c,\text{ core strength}} \quad (1)$$

where k_1, k_2 and k_3 are correction factors. Factor $k_1=0.2l/d+0.6$ corrects for different length to diameter ratios, factor $k_2=0.95$ for a diameter of 100 mm corrects for different diameters, and factor $k_3=1.15$ corrects for the effects of damage during core drilling. For the majority of the cores, the length to diameter ratio is 2.0, and the diameter is 100 mm. Thus, the converted in-place concrete strength is approximately 9% higher than the measured compressive strength. However, the length to diameter ratio was between 1.5 and 2.0 for cores drilled from slab bridge A. In this paper, the in-place uniaxial compressive strength is presented for all examined bridge slabs.

3.5 Estimation of original uniaxial compressive strength by means of fluorescence microscopy

To estimate the reduction of the compressive strength, the expected original compressive strength without inclusion of cracking was estimated by means of fluorescence microscopy [27]. The estimated original strength was calculated on the basis of optically determined parameters (water-cement ratio, air void content, and volume of cement paste) on thin sections.

4. Results

4.1 Uniaxial compressive strength and influence of ASR-induced crack orientation

4.1.1 Uniaxial compressive strength for slab bridge A

Fig. 4 depict a so-called box plot of the compressive strength of 33 cores from slab bridge A. In the box plot the strength results are divided into quartiles. The tops of the boxes represent the third quartile, the bottoms of the boxes represent the first quartile, and the thick horizontal lines inside the boxes represent the medians. The top and bottom of the whiskers represent the maximum and minimum strength, respectively. The red dots inside the boxes represent the average compressive strengths. 5 to 14 cores with ASR perpendicular cracks were drilled from the eastern and western bridge end, respectively. 6 to 8 cores with ASR parallel cracks were drilled from the western bridge end, respectively.

Fig. 4(a) shows the compressive strength in the direction perpendicular to ASR cracks, $f_{c,90}$, corresponding to vertical drilling. As can be seen, the average strength of the western

bridge end is, on average, 5.0 MPa higher than the average strength of the eastern bridge
end.
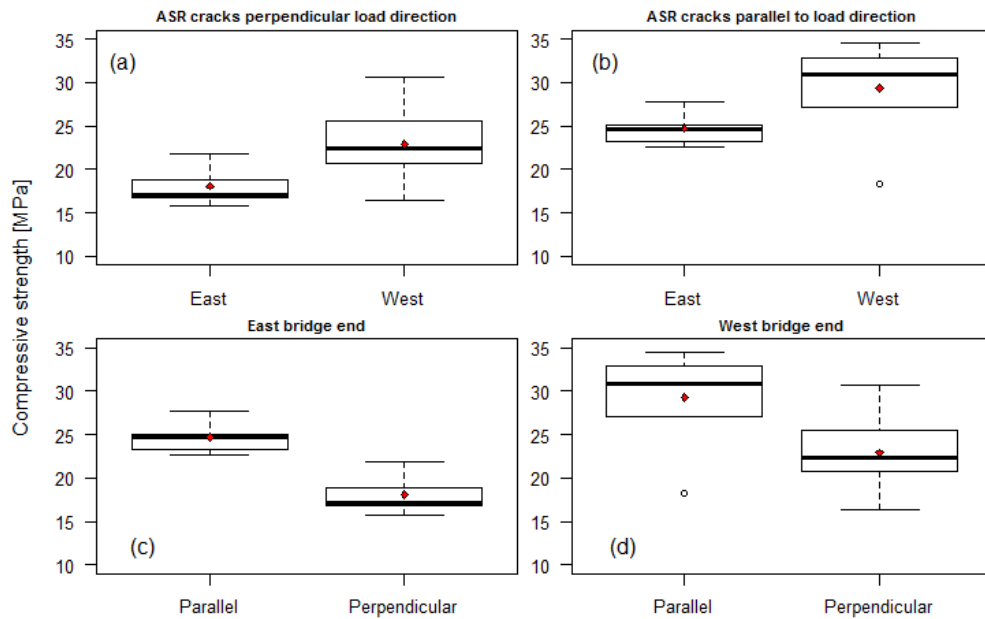
Fig. 4: Strength, $f_{c,90}$ (perpendicular cracks) and $f_{c,0}$ (parallel cracks) of cores from beams cut from
slab bridge A, eastern and western bridge ends.

Fig. 4(b) shows the strength in the direction parallel to ASR cracks, $f_{c,0}$. The results show
the same tendency as those from Fig. 4(a). The average strength of the western bridge end
is 4.7 MPa higher than the average strength of the eastern bridge end. These results
correspond to the visual appearance of the cores. Examinations of fluorescence-
impregnated cores visualized different amounts of ASR cracks between the eastern and
western bridge ends. The cores from the eastern bridge end appeared visually to be more
cracked than those from the western bridge end. However, the visual in-situ inspection
from beneath the bridge slab showed no notable differences in the amount of surface ASR
cracks between the eastern and western bridge ends.

Fig. 4(c) and 4(d) shows the strength for the eastern and western bridge end, respectively.
As can be seen, $f_{c,90}$ is considerably lower than $f_{c,0}$. This observation holds for both bridge
ends. The average $f_{c,90}$ are 36% and 22% lower for the eastern and western ends,
respectively.

The estimated average original compressive strength, $f_{c,ori}$ determined by fluorescence
microscopy is 45 MPa, varying between 42 and 48 MPa. This variation is due to
variations in the water-cement ratio and in homogeneity of the cement paste. The

11

estimated $f_{c,ori}$ is valid for both the eastern and western bridge end. Thus, strengths for the western bridge ends are reduced 35% and 49% for $f_{c,0}$ and $f_{c,90}$, respectively. At the eastern bridge end, the strength reduction is even greater, with reductions of $f_{c,ori}$ by 45% and 60% for $f_{c,0}$ and $f_{c,90}$, respectively.

4.1.2 Uniaxial compressive strength for slab bridge B

Fig. 5 shows the strength of 20 cores from slab bridge B. These cores were drilled from the same area in two of the four beams. Again, a considerable lower average

strength was found for $f_{c,90}$ than $f_{c,0}$. The average difference between the two crack orientations is 4.3 MPa. As determined by the one-way ANOVA, there are statistically significant differences between the average uniaxial compressive strength for the two ASR crack orientations ($p = 4.5 \cdot 10^{-3}$).
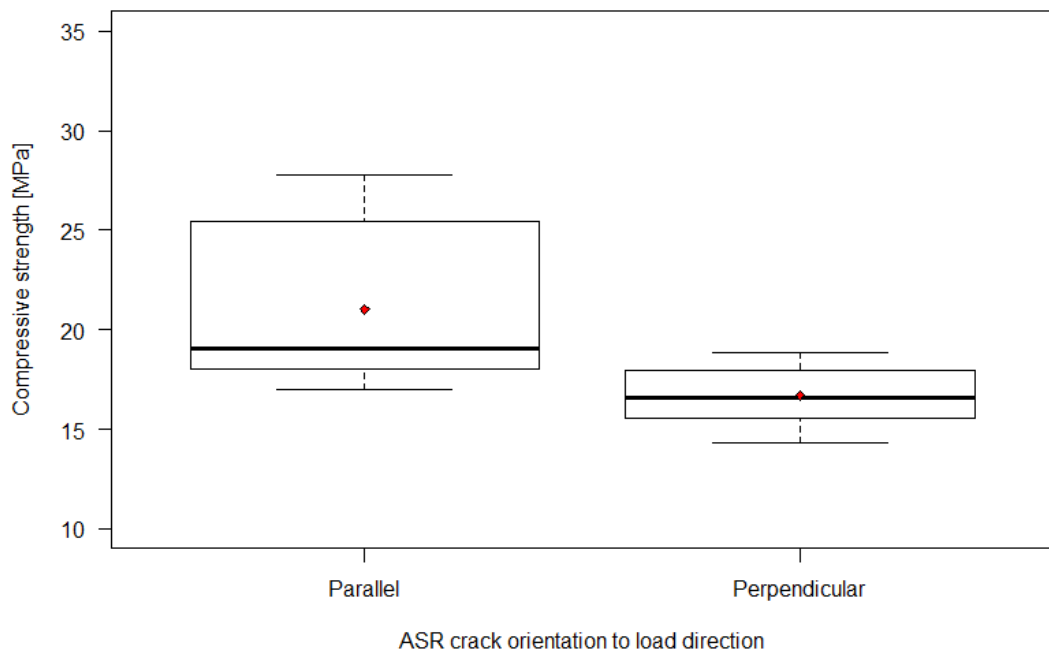

Fig. 5: Strength, $f_{c,0}$ (parallel cracks), and $f_{c,90}$ (perpendicular cracks), of cores from beams cut from slab bridge B.

The $f_{c,ori}$ varies between 40 – 45 MPa with an average of 42.5 MPa. Hence, the strength of the ASR-damaged concrete has been reduced by 51% for $f_{c,0}$ and 61% for $f_{c,90}$, respectively.

4.1.3 Uniaxial compressive strength for slab bridge C

For slab bridge C, 93 cores were drilled from beams cut from six trapezoidal concrete slab segments. Fig. 6 shows the strength $f_{c,90}$. It appears that the strength of slab element 2 is remarkably higher than the strength of the other segments. Additionally, based on the one-way ANOVA, there are no statistically significant differences between the average strength of the other five slab segments (p=0.29). These results were supported by the visual inspection of the drilled cores and segments. Visually, slab segment 2 was different from the other segments by having a considerably lower extent of ASR cracks while the remaining five slab segments were visually similar.
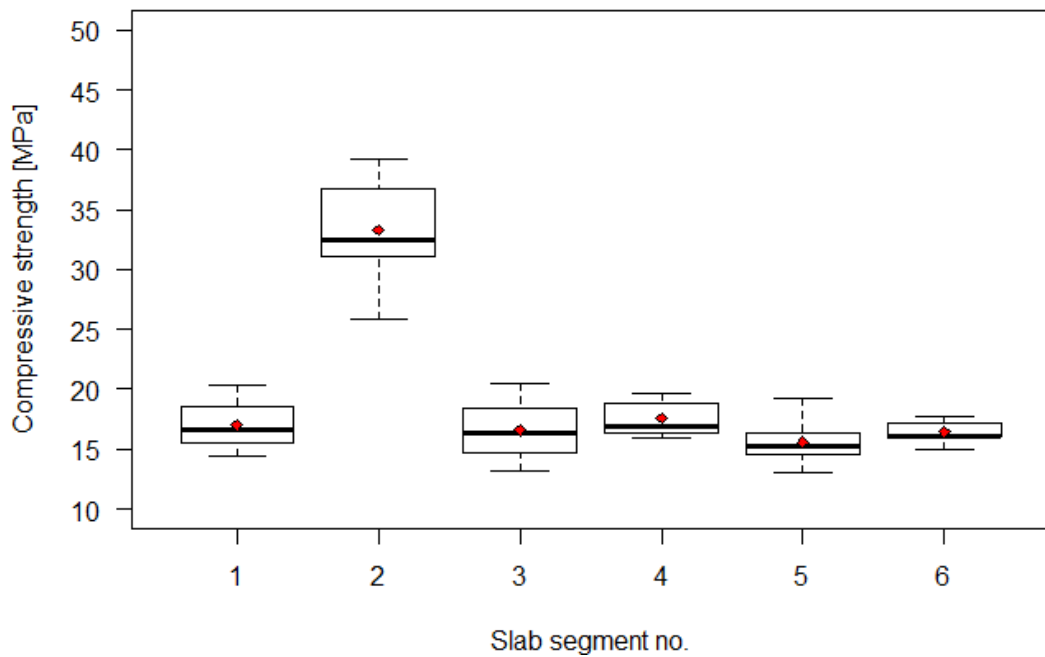
Fig. 6: Strength, $f_{c,90}$ (perpendicular cracks) of cores from beams cut from slab bridge C.

Fig. 7 shows the strength $f_{c,0}$. Similar to the tendency in Fig. 6, cores from slab segment 2 displayed a significantly higher strength. However, in contrast to the cores with perpendicular cracks, there were statistically significant differences between cores from the other five slab segments. As determined from the one-way ANOVA, there were no statistically significant differences between slab segments 1 and 3 (p=0.44). Furthermore, there were no statistically significant differences between slab segments 4, 5, and 6 (p=0.18). However, the compressive strength for slab segments 1 and 3 are statistically significantly different from slab segments 4, 5, and 6 (p = $8.98 \cdot 10^{-9}$). These differences were not supported by the visual appearance of the drilled cores and segments; we were not able to distinguish any difference between the extent of ASR cracking in the five slab segments.
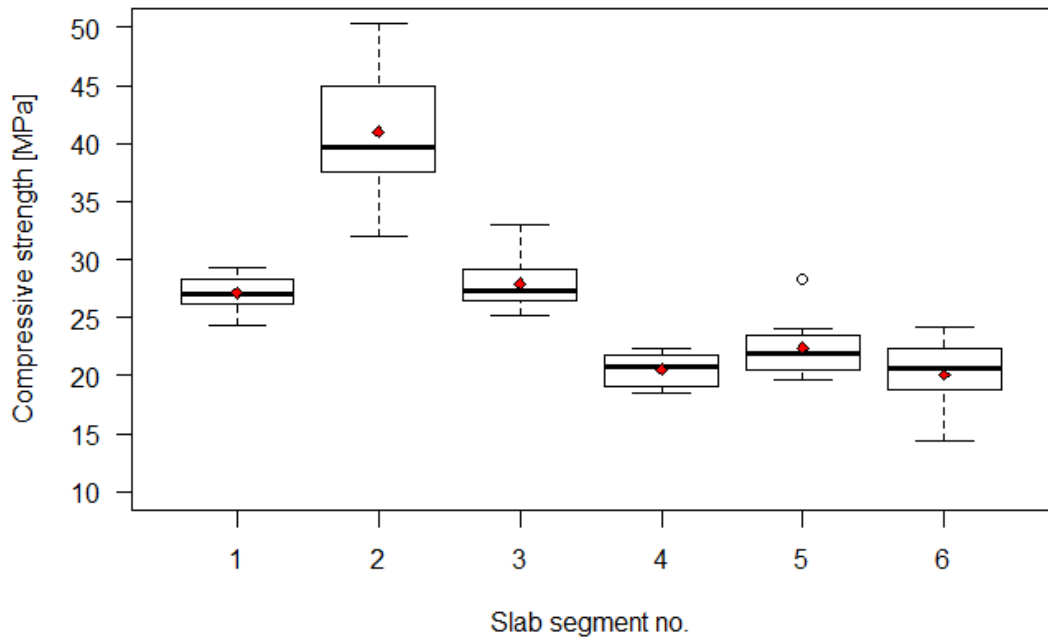
Fig. 7: Strength $f_{c,0}$ (parallel cracks) of cores from beams cut from slab bridge C.

Fig. 8 shows the average strengths, $f_{c,0}$ and $f_{c,90}$, for all the six slab segments. As can be seen, the absolute difference between the orientation dependent strengths are small for slab segments 4 and 6, while it is considerably higher for slab segments 1, 2, 3, and 5.
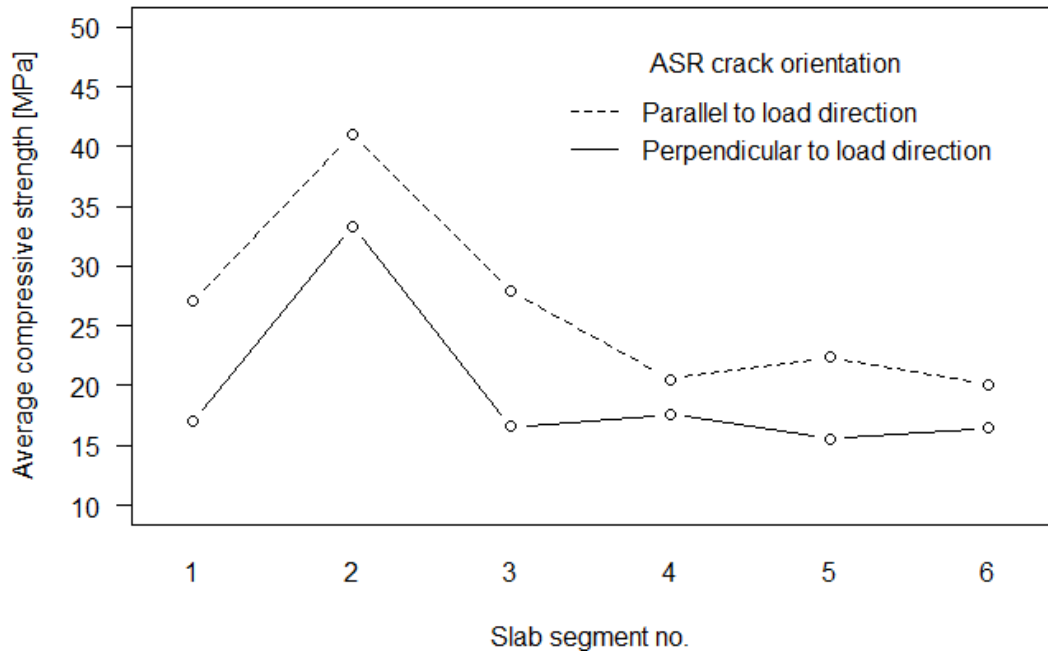
Fig. 8: Relationship between the average strength for the two crack orientations at the six slab segments.

Table 1 shows the ratios between the orientation dependent strengths as well as the relative decrease of strengths from $f_{c,ori}$.

Table 1: $f_{c,ori}$, $f_{c,0}$, $f_{c,90}$ as well as $f_{c,0}$ and $f_{c,90}$ decrease from $f_{c,ori}$. The ratios between the orientation dependent strengths are also shown.

| Slab segment no.	1	2	3	4	5	6
$f_{c,ori}$ (and variation) [MPa]	37.5 (35-40)	45 (40-50)	42.5 (40-45)	42.5 (40-45)	42.5 (40-45)	37.5 (35-40)
$f_{c,0}$ [MPa]	27.1	41.0	27.5	20.5	22.4	20.1
$f_{c,0}$ decrease from $f_{c,ori}$ [%]	28	9	35	52	47	46
$f_{c,90}$ [MPa]	17.0	33.3	16.6	17.6	15.5	16.4
$f_{c,90}$ decrease from $f_{c,ori}$ [%]	55	26	61	59	64	56
$f_{c,0}/f_{c,90}$ [-]	1.59	1.23	1.66	1.16	1.45	1.23

It is seen from Table 1 that $f_{c,0}$ is at least 16% higher than $f_{c,90}$ drilled from the same slab segment. Furthermore, it is seen that $f_{c,0}$ has decreased by up to 52%, while $f_{c,90}$ has decreased by up to 64%.

4.2 Stress-strain relationship

Fig. 9 shows two typical stress-strain relationships found from core testing. The stress-strain relationship is greatly affected by the crack orientation. In general, it was found that the shape of the stress-strain curve for cores having parallel cracks is comparable to that of uncracked concrete. In contrast, the stress-strain curve for cores having perpendicular cracks seems to be more affected by the orientation of the cracks and displays a concave as well as a convex part in the pre-peak regime. The initially flat and concave part of the curve is most probably a result of crack closure. Therefore, the cores experienced increase of stiffness as the load increased.
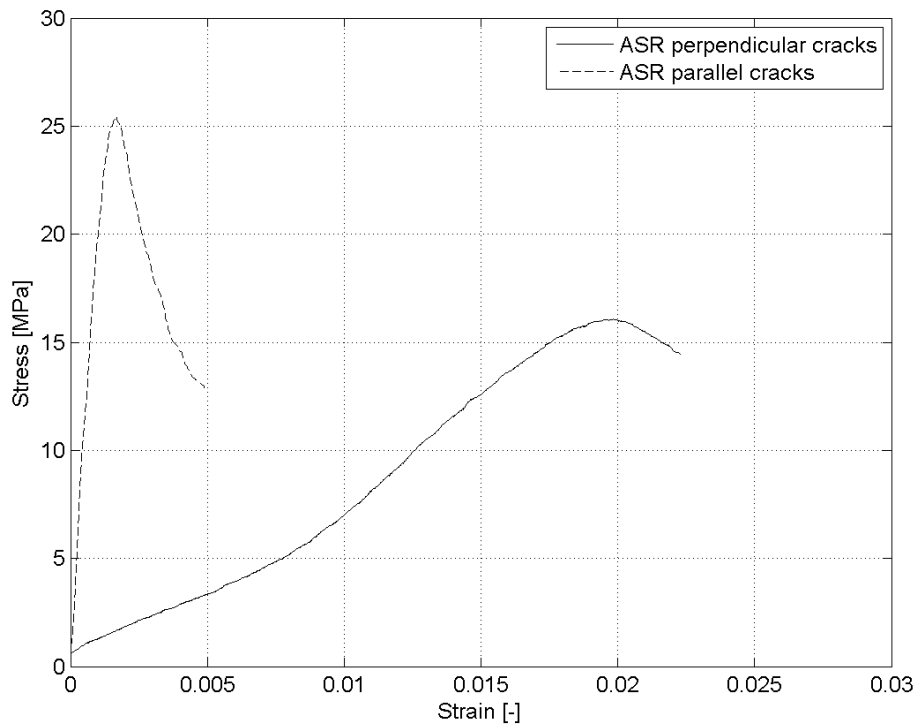
Fig. 9: Typical stress-strain curves for the cores having ASR cracks parallel or perpendicular to the load direction.

Despite the fact that the shapes of the stress-strain curves shown in Fig. 9 are representative for the two crack directions, care must be taken in the analysis of the curves based on the average strain (as calculated from two LDVT-measurements). The ASR cracks may not be uniformly distributed in the cores and could lead to eccentric deformations during loading. As seen in Fig. 10, the two LDVT measurements for a core having perpendicular cracks show similar deformations until approximately 10 MPa. Thereafter, LVDT 1 shows larger deformations than LVDT 2. At peak stress there is 60% difference between the peak strains for the two LVDTs. It is important to state that eccentric deformations of cores having perpendicular cracks may occur immediately, from the beginning of loading.

For a concrete core having parallel cracks to the load direction, the deformations during loading may also be eccentric; see Fig. 10.
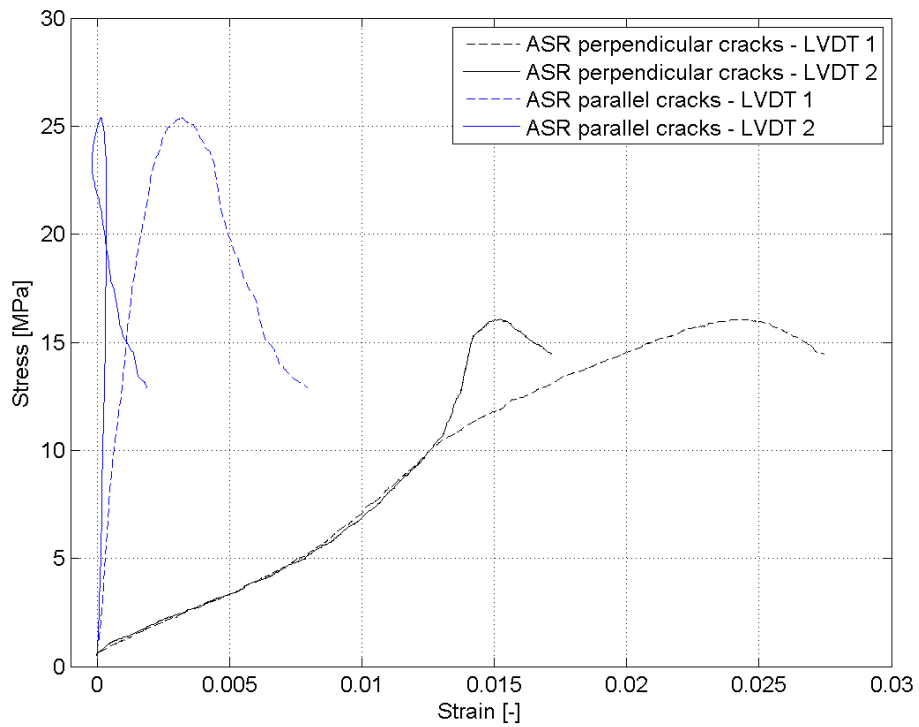
Fig. 10: Stress-strain curves for each LVDT on a core with parallel cracks or perpendicular cracks to the load direction.

4.3 Static Young's modulus

As seen in Fig. 10, determining a "true" static Young's modulus of the tested ASR-cracked cores is complicated because eccentric deformations occur during testing. Additionally, for cores having perpendicular cracks, the shape of the curve will change during testing; in the beginning, the curve will be flat due to closure of ASR cracks.

In this paper, the static Young's modulus is computed based on the stress and the average strain attained from the strength tests. The Young's modulus is computed by the secant line between 0 and $0.4f_c$ and compared to an estimated Young's modulus for undamaged concrete. The original Young's modulus is estimated in accordance with the equation provided by Eurocode 2 [28].

Fig. 11 shows the Young's modulus for the cores from slab bridge A, computed using the average strain from LVDT 1 and LVDT 2. As seen, the Young's modulus of cores having parallel cracks is less affected than that of cores having perpendicular cracks. Moreover, the results show that the Young's modulus for the ASR-cracked cores is significantly reduced compared to the estimated original Young's modulus of 34.5 GPa. The average

Young's modulus is reduced by 41% for cores having parallel cracks and by 90% for cores having perpendicular cracks.
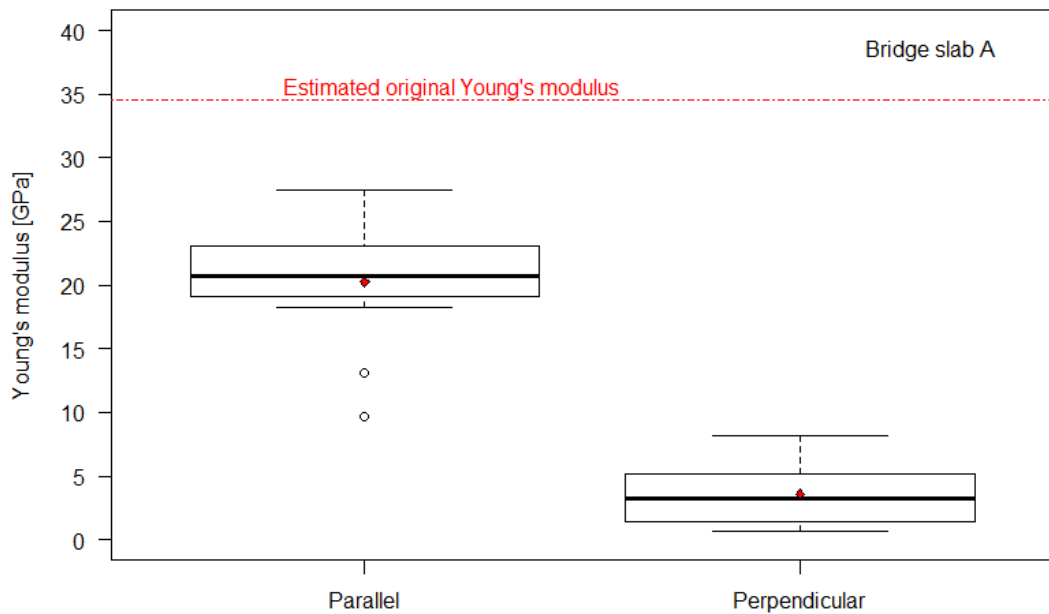
Fig. 11: Young's modulus for cores from slab bridge A. Red horizontal line refers to the estimated original Young's modulus.

Although the results presented in Fig. 11 are for slab bridge A, the same tendency for the static Young's modulus holds for slab bridge B and slab bridge C.

4.4 Visual observations of the failure

To understand the results of the strength tests, tested cores were visually examined, with observations consisting of comparisons of the cores and ASR cracks both before and after the tests. In addition, thin section examinations by optical microscopy were conducted. The thin sections were prepared from tested fluorescent epoxy-impregnated cores. The impregnation of the tested cores stabilizes the load- and ASR-induced cracks.

4.4.1 Cores with cracks parallel to the load direction

Figs. 12(a) - 12(b) show a concrete core having ASR cracks parallel to the load direction before and after loading, respectively. As seen in Fig. 12(b) the coarser, parallel ASR cracks were opened as a consequence of loading. Consequently, the core was split into small columns during loading.
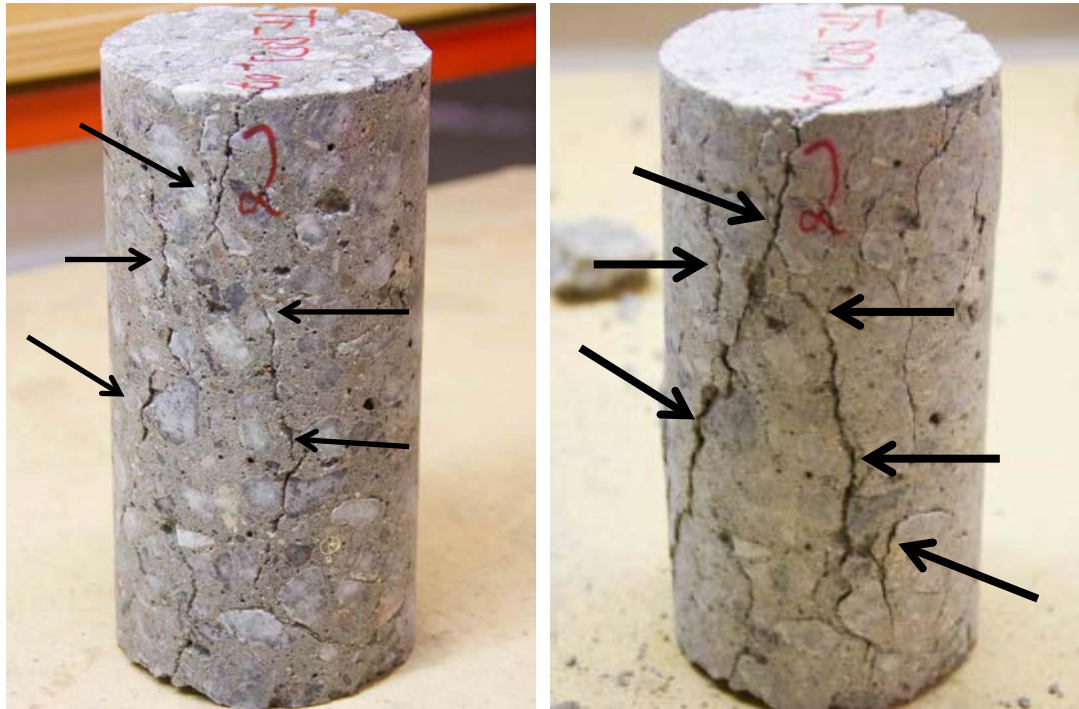
Fig. 12: Core with parallel ASR cracks (indicated by arrows) before loading (a) and after loading (b).

The fact that the parallel ASR cracks were opened further due to the load direction was confirmed by thin section examinations. Fig. 13(a) shows parts of a thin section prepared from a core having parallel cracks. As seen, a fine parallel ASR crack in the left side of the microphotograph (white arrows) is filled with unbroken ettringite crystals (brownish crystals in the yellow crack) due to many years of exposure to water. However, a coarser parallel ASR crack on the right side of the microphotograph (black arrows) was opened due to loading. This is visualized by the presence of broken ettringite crystals along the crack walls. Fig. 13(b) confirms the observations from Fig. 13(a), where debonding of ettringite crystals between crack walls was observed. In addition, some of the ettringite crystals are freely available inside the opened ASR crack without any bonding to the crack walls.
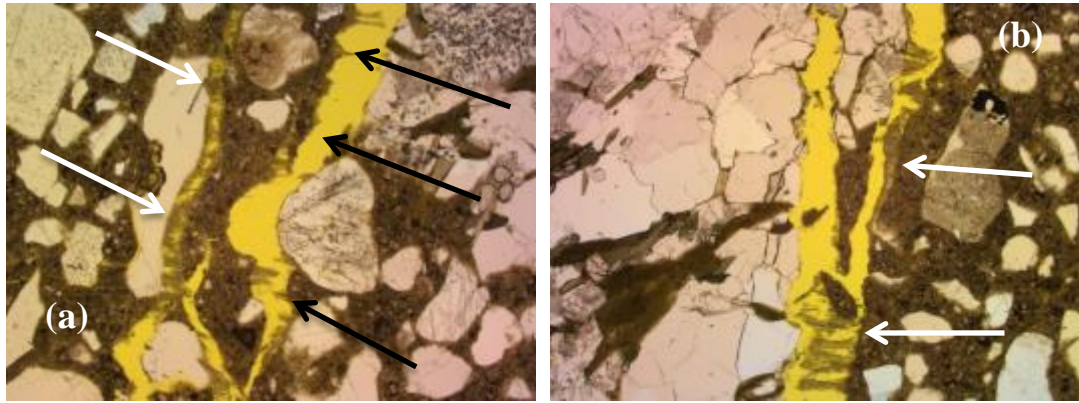
Fig. 13: Plane polarized light. Width of fields 2.4 mm. Two sections, (a) and (b), of a tested core with ASR cracks parallel to the load direction.

4.4.2 Cores with cracks perpendicular to the load direction

Figs. 14(a) - 14(b) show a concrete core with ASR cracks perpendicular to the load direction before and after loading, respectively. Fig. 14(b) shows that several vertical splitting cracks (white arrows) are formed between the perpendicular cracks. The formation of vertical splitting cracks results in significant lateral deformation of the core during loading. As shown in Fig. 14(b), some parts in the middle height of the core were spalled due to the formation of vertical splitting cracks and the lateral deformations.
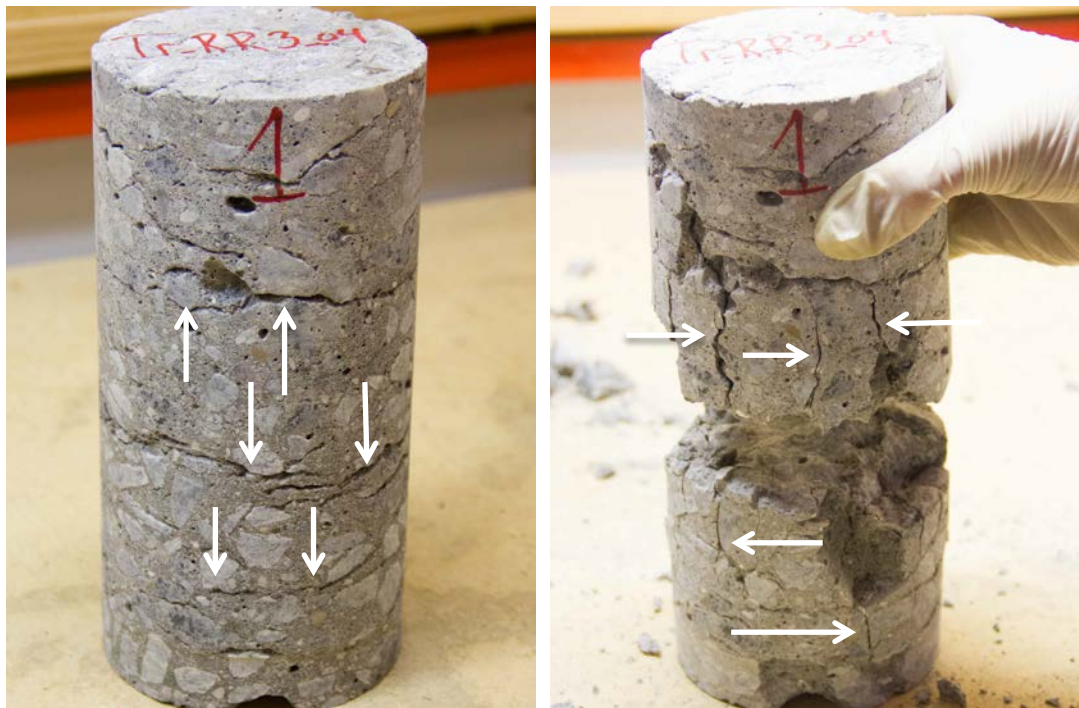
Fig. 14: Core having perpendicular ASR cracks (white arrows) before loading (a) and after loading (b).

Closure of the perpendicular cracks (the effect of which is observed on the stress-strain curve in Figs. 9 - 10) was confirmed by thin section examinations. Figs. 15(a) - 15(b)

show that the ASR cracks were closed during the loading. Fig. 15(a) shows that ettringite crystals (white arrows) inside the ASR cracks were crushed due to loading. In addition, Fig. 15(b) shows local crushing and debonding of the cement paste close to the ASR crack.
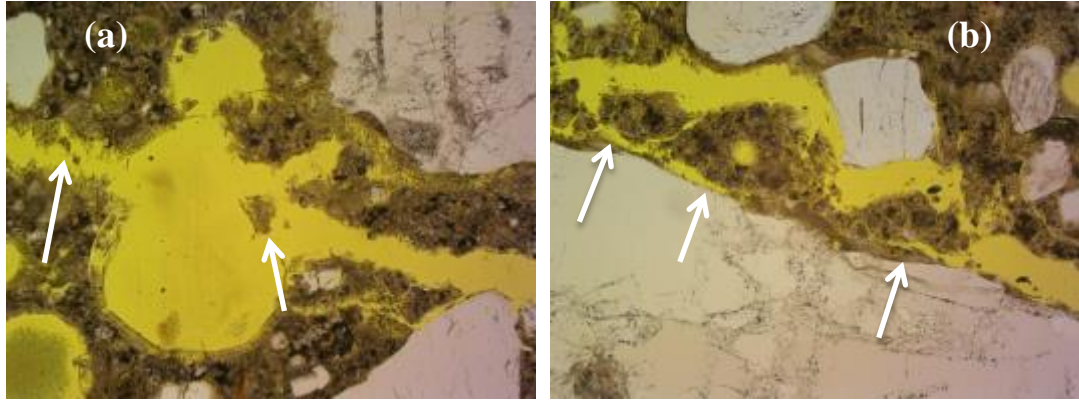

Fig. 15: Plane polarized light. Width of fields 1.2 mm. Two sections, (a) and (b), of a tested core with ASR cracks perpendicular to the load direction.

5. Discussion

5.1 Influence of ASR cracks on the uniaxial compressive strength

Several studies [12][5][3] have reported that the compressive strength of ASR-damaged concrete does not indicate the degree of ASR deterioration in cores. The strength is reported to be only sligtly influenced by the ASR cracking. Based on our results on cores from ASR-damaged bridge slabs, we may argue the opposite. In our opinion, a strength decrease up to 64% is remarkable. However, we agree with the previous studies [12][5][3], that the percentage decrease of the uniaxial tensile strength and Young's modulus will be higher than the decrease of the compressive strength. As seen from Figs. 4, 6, and 7 we may argue that an increase in ASR cracks in the cores will result in a decrease in strength. However, this reduction will depend on the ASR crack orientation within the cores.

5.2 Influence of ASR crack orientation on the uniaxial compressive strength

Compression tests of cores show that the ASR crack orientation has a significant influence on the measured strength. The strength in a direction perpendicular to ASR cracks is significantly lower than the strength in a direction parallel to ASR cracks. Based on our results, we may argue that perpendicular cracks have higher and more rapidly negative impact on the strength than parallel cracks. Additionally, we may argue that the

strength in a direction parallel to ASR cracks may be more representative for the degree of ASR deterioration or ASR crack extent in the concrete.

Considering Fig. 8, we may argue that the strength in the direction perpendicular to ASR cracks will reach a low and stable limit long before the strength in the direction parallel to ASR cracks. However, from our results, we are not able to conclude if continuing development of ASR cracks would cause further decrease in strength in the direction perpendicular to ASR cracks. As seen in Fig. 8, the strength of cores in the direction parallel to ASR cracks in slabs 4, 5, and 6 reaches values close to those measured for cores having perpendicular cracks. From these results we may propose that with an increasing amount of ASR cracking, the anisotropic concrete behaviour in compression will reduce. However, we cannot conclude that the strength in a direction parallel to ASR cracks will reach a value corresponding to the strength in a direction perpendicular to ASR cracks.

In practice, vertical core drilling corresponding to cores having ASR cracks perpendicular is the only possible in-situ drilling orientation on bridge slabs. Thus, the strength used to calculate the load-carrying capacity will be rather conservative. However, the conservatism may be reduced by increasing ASR deterioration degree or ASR cracking.

5.3 Young's modulus and stress-strain relationship

It is clear that the Young's modulus decreases due to ASR cracks. Furthermore, the Young's modulus is also greatly influenced by the orientation of ASR cracking. Our results are compatible with the results of Jones [29], who reported that the Young's modulus in restrained specimens was greater in the direction of restrain (parallel ASR cracks) than in the unrestrained direction (perpendicular ASR cracks).

The shape of the stress-strain curve for compression perpendicular to ASR cracks will be governed by the crack closure. Different widths of the ASR cracks will influence the shape of the stress-strain curve. Furthermore, an uneven distribution of ASR cracks will result in eccentric deformations during loading. The core having parallel ASR cracks may be characterized as a concrete core split into slender columns. The shape of the stress-strain curve will be governed by the failure of individual slender columns within the core. The concentration of thinner slender columns at one side of the core will result in eccentric deformation due to crushing and/or bending of the these outermost-located thin slender columns.

Although the ASR cracks have a significant impact on the Young's modulus of drilled cores, a reduction in flexural stiffness of reinforced ASR-cracked elements may be less significant or not even reduced. Several studies [30–33] on laboratory-accelerated ASR-reactive reinforced beams showed that the flexural stiffness of the damaged beams was not reduced even by severe ASR cracking. That is despite a significant decrease in Young's modulus of cores drilled from the same ASR-damaged reinforced beams. Generally, a decrease in concrete stiffness of cores is reported to be compensated for by the ASR-induced pre-stress effect in the reinforcement. In general, these studies express the difficulties in relating the properties obtained from drilled cores to the structural behaviour of ASR-damaged reinforced elements.

5.4 Explanation of failure mechanism

Visual observations of the cores during and after loading made it possible to provide a simple definition of the failure mechanisms for the tested cores. We must acknowledge that crack formation in cores is a complex, three-dimensional process, and surface cracks may not always reflect the internal cracking process. Therefore, thin sections were examined as a supplement to the visual observations, in order to reveal internal failure mechanisms in the tested cores.

Drilled cores having ASR cracks parallel to the load direction may, be characterized as a concrete core split to slender columns due to the ASR cracking. The slender columns and crack walls will locally be glued by the ASR gel. Visual observations and thin section examinations showed that failure of the cores during compression will be caused by opening of parallel ASR cracks. The slender columns may fail due to a combination of bending, buckling, and/or spalling. The slender concrete columns at the edge of the concrete core in particular tended to open and fail first. A larger amount of ASR cracks corresponds to more slender columns in the concrete core. Consequently, the compressive strength of the concrete core may decrease with increasing ASR cracks parallel to the load direction.

The failure mechanism in drilled cores having ASR cracks perpendicular to the load direction may be more complex than the failure mechanism of cores having parallel cracks. Our visual observations showed that several vertical splitting cracks are formed in the concrete between the perpendicular ASR cracks during loading. Both strength and formation of vertical splitting cracks at these cores may be governed by the strength of and cohesion between aggregate and cement paste. Vonk [34] reported that for normal, uncracked concrete, formation of vertical splitting cracks takes less energy than formation

of inclined shear cracks in a core. The amount of ASR cracks perpendicular to load direction may play a role in the formation of vertical splitting cracks. It will be easier to form vertical splitting cracks when more ASR perpendicular cracks are present in the cores. The length in "intact" concrete between the ASR cracks will be shorter, forming vertical splitting cracks. The development of vertical splitting cracks increases the lateral deformation of the cores. The hardened alkali-silica gel partially filling the cracks may also play a role in the formation of vertical splitting cracks, because a large stress concentration will occur at this specific area. However, this mechanism could not be confirmed by thin section examinations. It is important to state that we do not expect that an increase in the number of ASR perpendicular cracks will always result in continuous decreasing of compressive strength. As seen in Fig. 8, a lower limit in the compressive strength may be reached despite the fact that ASR cracking still develops in the concrete.

As seen in Figs. 9-10 ASR cracks perpendicular to the load direction will lead to larger eccentric deformations, than cracks parallel to the load direction. The crack widths and location of perpendicular cracks were unevenly distributed in the core. Consequently, local areas in the cores will experience large stress concentrations, which will result in a more rapid and negative impact in strength than strength in the direction parallel to the ASR cracks.

6. Conclusions

In this paper the influence of ASR and ASR crack orientation on the uniaxial compressive strength was experimentally studied. The tested cores were drilled vertically and horizontally from three severely ASR-damaged flat slab bridges in service. The ASR cracks in the slabs were oriented parallel to the longitudinal and transverse reinforcement, corresponding to the largest restraint direction. This study shows the same tendency for all three examined bridge slabs. The following conclusions were drawn:

- The compressive strength is valid for an anisotropic ASR damaged concrete; the strength in the direction perpendicular to ASR cracks (vertical drilling) is significantly lower than the strength in the direction parallel to ASR cracks (horizontal drilling). Consequently, evaluation of strength based on vertical drilled cores is rather conservative.
- The compressive strength is highly affected by ASR cracking. Compressive strength reduction up to 64% has been found for vertically drilled cores, cores having perpendicular ASR cracks, and up to 52% for horizontally drilled cores, cores having parallel ASR cracks.

- When oriented perpendicular to the load direction the ASR cracks have a more rapid and more markedly negative impact on strength. Consequently, we may argue that the strength in directions parallel to ASR cracks may be more representative of the degree of ASR deterioration or ASR cracking.
- Increase in ASR cracking within the cores causes a decrease in strength. However, a lower limit of the strength will be reached.
- For an increasing amount of ASR cracks, the anisotropic concrete behaviour in compression will reduce.
- The Young's modulus depends on the crack orientation. Due to closure of perpendicular cracks, the Young's modulus is reduced by up to 90% compared to that of uncracked concrete.

An explanation of the failure mechanism for cores with ASR cracks oriented parallel or perpendicular to the load direction is proposed:

- The failure mechanism of cores with ASR cracks perpendicular to the load direction is governed by crack closure, eccentric deformations and the development of vertical splitting cracks. The development of vertical splitting cracks increases the lateral deformation of the concrete.
- The failure mechanism of cores with ASR cracks parallel to the load direction is governed by opening of parallel cracks. Due to this opening, the parallel slender concrete columns will fail due to bending, buckling, or crushing.
- Thin section examinations confirmed the opening of parallel cracks and closure of perpendicular cracks.
- Closure of uneven distributed perpendicular cracks result in large eccentric deformations and local stress concentrations in the core. Consequently, this eccentric behaviour will result in a more rapid and negatively impact on strength than ASR cracks parallel to the load direction.

References

[1]   R.N. Swamy, Alkali-Silica Reaction in Concrete, Blackie and Son Ltd., Glasgow and London, 1992.

[2]   D.W. Hobbs, Alkali-silica reaction in concrete, American Society of Civil Engineers, Thomas Telford, London, 1988.

[3]   T. Ahmed, E. Burley, S. Rigden, A.I. Abu-Tair, The effect of alkali reactivity on the mechanical properties of concrete, Constr. Build. Mater. 17 (2003) 123–144.

[4]   N. Smaoui, B. Bissonnette, B. Fournier, B. Durand, Mechanical Properties of ASR-Affected Concrete Containing Fine or Coarse Reactive Aggregates, ASTM Int. 3 (2006) 1–16.

[5]   R.N. Swamy, M.M. Al-Asali, Engineering Properties of Concrete Affected by Alkali-Silica Reaction, ACI Mater. J. 85 (1988) 367–374.

[6]   G. Giaccio, R. Zerbino, J.M. Ponce, O.R. Batic, Mechanical behavior of concretes damaged by alkali-silica reaction, Cem. Concr. Res. 38 (2008) 993–1004.

[7]   O. Batic, G. Giaccio, R. Zerbino, On effect of ASR cracking on the mechanical behaviour of concrete in tension and compression, in: 12th Int. Conf. Alkali-Aggregate React. Concr., 2004: pp. 1136–1141.

[8]   S. Fan, J.M. Hanson, Effect of Alkali Silica Reaction Expansion and Cracking on Structural Behavior of Reinforced Concrete Beams, ACI Struct. J. 95 (1998) 498–505.

[9]   S.R.Rigden, J.M. Salam, E. Burley, The influence of stress intensity and orientation upon the mechanical properties of ASR affected concrete, in: 9th Int. Conf. Alkali-Aggregate React. Concr., London, UK, 1992: pp. 865–876.

[10]   G. Giaccio, M.C. Torrijos, J.M. Tobes, O.R. Batic, R. Zerbino, Development of Alkali-Silica Reaction under Compressive Loading and Its Effects on Concrete Behavior, ACI Mater. J. 106 (2009) 223–230.

[11]   A.E.K. Jones, L.A. Clark, S. Amasaki, The suitability of cores in predicting the behaviour of structural members suffering from ASR, Mag. Concr. Res. 46 (1994) 145–150.

[12]   H.W. Reinhardt, O. Mielich, Effects of mechanical properties of ASR damaged concrete on structural design, in: Brittle Matrix Compos. 10, Woodhead Publishing Limited, Warsaw, 2012: pp. 1–9.

[13]   Y. Majlesi, A laboratory investigation into the structural performance and mechanical properties of plain and reinforced concrete elements affected by alkali silica reaction, Queen Mary and Westfield Collage University of London, PhD thesis, 1994.

[14]   H. Marzouk, S. Langdon, The effect of alkali-aggregate reactivity on the

mechanical properties of high and normal strength concrete, Cem. Concr. Compos. 25 (2003) 549–556.

[15]   Y. Hiroi, T. Yamamoto, Y. Toda, H. Manabe, T. Miyagawa, Experimental and analytical studies on flexural behavior of post-tensioned concrete beam specimen deteriorated by alkali-silica reaction (ASR), in: Proc. 15th Int. Conf. Alkali-Aggregate React. Concr., São Paulo, 2016.

[16]   F. Bach, T.S. Thorsen, M.P. Nielsen, Load-carrying capacity of structural members subjected to ASR, Constr. Build. Mater. 7 (1993) 109–115.

[17]   A. Allard, S. Bilodeau, F. Pissot, B. Fournier, J. Bastien,B. Bissonnette, Performance Evaluation of Thick Concrete Slabs Affected by Alkali-Silica Reaction (ASR) - Part I: Materials Aspects, in: Proc. 15th Int. Conf. Alkali-Aggregate React. Concr., São Paulo, 2016.

[18]   The Institution of Structural Engineers, Structural effects of alkali-silica reaction - Technical guidance on the appraisal of existing structures, 1992.

[19]   A. McLeish, Structural implications of the alkali silica reaction in concrete, Report 177, Transport and Research Laboratory, 1990.

[20]   S.G. Hansen, R.A. Barbosa, L.C. Hoang, Prestressing of reinforcing bars in concrete slabs due to concrete expansion induced by Alkali-Silica Reaction, in: Proc. Fib Symp. 2016, Cape Town, 2016.

[21]   N. Østergaard, Aggressive concrete disease attack 600 danish bridges (In Danish), Ingeniøren, 2012. https://ing.dk/artikel/aggressiv-betonsygdom-angriber-600-danske-broer-131714.

[22]   N.M. Plum, Temporary guide in prevention of damaging alkali-silica reaction in concrete (In Danish), The Danish National Institute of Building Research, 1961.

[23]   J.W. Schmidt, S.G. Hansen, R.A. Barbosa, A. Henriksen, Novel shear capacity testing of ASR damaged full scale concrete bridge, Eng. Struct. 79 (2014) 365–374.

[24]   S.G. Hansen, R.A. Barbosa, L.C. Hoang, Shear capacity of ASR damaged structures – In-depth analysis of some in-situ shear tests on bridge slabs, in: Proc. 15th Int. Conf. Alkali-Aggregate React. Concr., São Paulo, 2016.

[25]   DS Standard 12390-3: Testing hardened concrete – Part 3: Compressive strength of test specimens, Danish Standards, 2009.

[26]   Danish Road Directorate, Guide in loading- and basic calculations (In Danish), The Danish Road Directorate, Road regulation council, 2010.

[27]   N. Thaulow, A.D. Jensen, S. Chatterji, P. Christensen, H. Gudmundsson, Estimation of the compressive strength of concrete samples by means of fluorescence microscopy, Nord. Betong. 51 (1982) 2–4.

[28]   DS Standard 1992-1-1, Eurocode 2 : Design of concrete structures – Part 1-1: General rules and rules for buildings, Danish Standards, 2008.

[29]   A.E.K. Jones, Cracking, expansion and strength of concrete subjected to restrained alkali silica reaction, The University of Birmingham, UK, PhD Thesis, 1994.

[30]   T. Ahmed, E. Burley, S. Rigden, The Static and Fatigue Strength of Reinforced Concrete Beams Affected by Alkali-Silica Reaction, ACI Mater. J. 95 (1999) 376–388.

[31]   M. Fujii, K. Kobayashi, T. Kojima, H. Maehara, The static and dynamic behaviours of reinforced concrete beams with cracking due to alkali-silica reaction, in: Proc. 7th Int. Conf. Alkali Aggreg. React., Ottawa, 1986.

[32]   K. Kobayashi, Load carrying behaviours of concrete structures and members affected by alkali-aggregate reactions, Concr. J. 24 (1986) 70–78.

[33]   S. Inoue, M. Fujii, K. Kobayashi, K. Nakano, Structural behaviors of reinforced concrete beams affected by alkali-silica reaction, in: Proc. 8th Int. Conf. Alkali-Aggregate React., Kyoto, 1989: pp. 727–732.

[34]   R.A. Vonk, Softening of concrete loaded in compression, Technical University of Eindhoven, Netherlands, PhD thesis, 1992.

CHAPTER 3

Influence of alkali-silica reaction and crack orientation on the tensile strength of specimens from slab bridges

Paper II

"Influence of alkali-silica reaction and crack orientation on the tensile strength of concrete specimens from severely ASR-damaged slab bridges"

R.A. Barbosa, K.K. Hansen, L.C. Hoang and B. Grelk

Influence of alkali-silica reaction and crack orientation on the tensile strength of concrete specimens from severely ASR-damaged slab bridges

Ricardo Antonio Barbosa[a], Kurt Kielsgaard Hansen[a], Linh Cao Hoang[a], Bent Grelk[a]

[a] *Technical University of Denmark, Brovej, Building 118, 2800 Kgs. Lyngby, Denmark*

Abstract

In Denmark numerous cases of deterioration and cracking in reinforced bridge slabs without shear reinforcement are diagnosed to be caused by alkali-silica reaction (ASR). This paper presents an experimental investigation of the influence of ASR and corresponding ASR crack orientation on the tensile strength of concrete specimens attained from three actual ASR-damaged flat slab bridges. Both direct and indirect tensile test methods were applied to determine the tensile strength. It is shown that the ASR-induced cracks result in significant impact on the tensile strength of concrete. The tensile strength is strongly dependent on the orientation of the ASR-induced cracks. All the applied direct and indirect test methods have significant disadvantages when testing the tensile strength of ASR-damaged concrete.

Alkali-silica reaction, bridge slab, ASR crack orientation, Brazilian split test, wedge splitting test, uniaxial tensile test

1. Introduction

For several decades alkali-silica reaction (ASR) in reinforced concrete structures is and has been a major concern worldwide [1]. In Denmark numerous cases of deterioration and cracking in older reinforced concrete bridge slabs without shear reinforcement are diagnosed to be caused by ASR. Many of these older Danish bridge slabs are built with a highly fast ASR-reactive porous opaline and/or calcareous opaline flint [2]. Normally, most cases of ASR in the Danish reinforced concrete structures occur in the sand fraction.

It is well known that ASR can cause severe cracking in concrete structures. The ASR-induced crack orientation inside the concrete will be governed by the structure's boundary conditions and reinforcement configuration [3]. For the Danish bridge slabs, the ASR-induced cracks are formed parallel to the mesh of reinforcement. This can e.g. be seen in Fig. 1 showing the typical orientation of ASR-induced cracks in a bridge slab. The image has been obtained by impregnating the surface

of a part of a bridge cross section with a fluorescent epoxy without vacuum. This bridge part was cut out before in-situ shear strength testing [4]. A comprehensive ASR crack pattern oriented parallel to the plane of the bridge deck is observed.
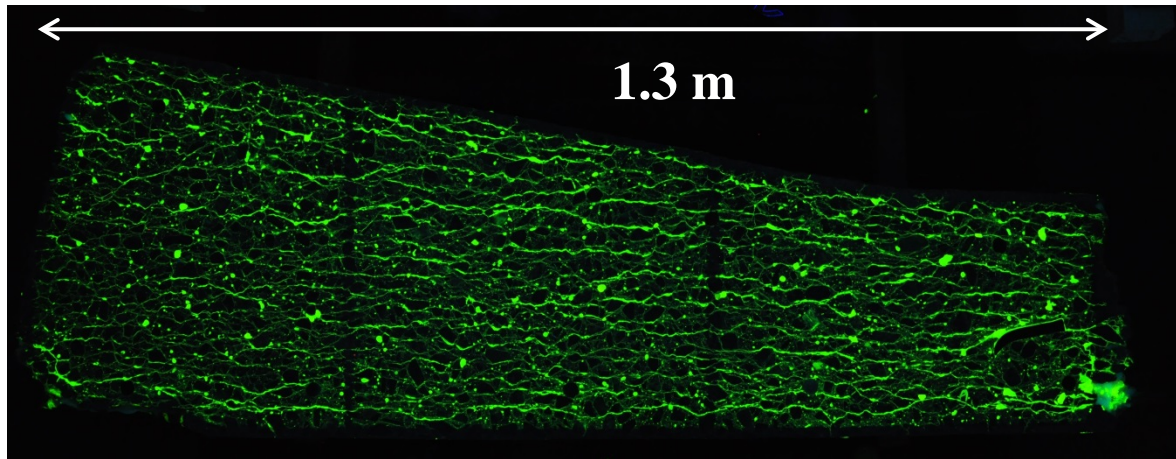

Fig 1: Fluorescence-impregnated surface of a segment cut out from a bridge slab and seen under ultraviolet light. Vertical black lines in the beam surface correspond to the division of the beam length into sections during impregnation.

As a consequence of this specific ASR crack orientation, Barbosa *et al.* [5] reported that the ASR-induced crack orientation within cores drilled horizontally and vertically from actual bridge slabs has a significant anisotropic influence on the concrete compressive strength. For the structural assessment of actual ASR-damaged bridge slabs without shear reinforcement, the concrete tensile strength is as important as the compressive strength. The shear forces in the slabs without shear reinforcement are assumed to be carried solely by the concrete. Consequently, the shear resistance of the slabs essentially depends on the concrete tensile strength.

It is difficult in practice to test the direct tensile strength of concrete. The tensile strength is often estimated from the splitting tensile strength by an empirical conversion factor in the range of 0.6–0.9 [6,7] or by empirical formulas based on the concrete compressive strength. For ASR-damaged concrete, however, these empirical conversion factors are not applicable. For instance, a strong anisotropic behavior of the ASR-cracked concrete in compression may also influence the behavior of the cracked concrete in tension.

A limited number of investigations into the tensile strength of ASR-damaged concrete specimens can be found in the literature. Results of indirect and direct tensile tests have been reported. Most of the studies are based on laboratory-accelerated specimens under free expansion. Consequently, the ASR-induced cracks in the specimens are randomly oriented and not comparable with the crack patterns seen in Fig. 1. Based on the investigations of unrestraint specimens, it is generally reported that the uniaxial tensile strength is more rapidly affected by ASR than the splitting tensile strength.

The uniaxial tensile strength is generally thought of as more sensitive to ASR expansion and therefore suitable to be used as an indicator of damages due to ASR [8–12]. In some studies the splitting tensile strength and compressive strength were reported to be similarly affected by ASR [11,13]. However, in other studies the splitting tensile strength is more affected by ASR than the compressive strength [14,15].

To the authors´ knowledge research concerning the tensile strength of concrete cores drilled from actual ASR-damaged reinforced concrete structures is very limited. Apparently, the studies by Siemens *et al.* [16,17] are the only publications on this topic. Siemens *et al.* investigated the influence of ASR cracking on the uniaxial tensile strength and splitting tensile strength of concrete cores drilled from several ASR-damaged concrete structures. They also investigated the influence of ASR crack orientation on the tensile strength of concrete. Unfortunately, the most cracked concrete cores were not used for tensile strength testing. Statistically, the obtained results would be lower with inclusion of the most cracked cores. Despite this circumstance, the reported uniaxial tensile strength was much lower than could be predicted on the basis of the compressive strength and the splitting tensile strength. In addition, the relationship between uniaxial tensile strength and the splitting tensile strength varied both per individual structure and within the same structure. It was clear that the tensile strength of the cores was orientation dependent. The uniaxial tensile strength in the direction perpendicular to ASR cracks was significantly lower than the strength in direction parallel to ASR cracks. Siemens *et al.* also reported that the splitting tensile strength was not orientation dependent. Surprisingly, Siemens and Visser [17] experienced no significant reduction in compressive strength as a consequence of ASR cracks in concrete. As previously stated, for the Danish bridge slabs, Barbosa *et al.* [5] reported a significant reduction and anisotropic behavior of the ASR-damaged cores in compression.

In this paper the tested tensile strength of cores drilled from three severely ASR-damaged bridges are presented. Several large beam segments cut out from different areas of the bridge slabs were transported to DTU Civil Engineering for testing. Brazilian split tests and direct uniaxial tensile tests were performed on cores drilled horizontally and vertically from beams/strips cut from the slabs. In addition, wedge splitting tests were carried out on cubes sawn from some of the beams.

2. Materials and methods

2.1 Materials

Cores of 100 mm in diameter and between 150 and 200 mm in length were drilled from slab segments of three severely ASR-damaged flat slab bridges. For convenience, the slab bridges are

named A, B and C. A water cooled diamond drill was used for the drilling. After drilling, the ends of the cores were sawn by a water-cooled diamond saw and thereafter grinded. To avoid desiccation, cling-film was wrapped around the cores which then were sealed in plastic bags until the time of testing. The cores were tested approximately 3 weeks after drilling. Most of the cores were in one piece after drilling, despite the comprehensive ASR-induced cracks. The cores were used for the Brazilian split test and for the uniaxial tensile test.

To conduct wedge splitting tests, cubes of 100 x 100 x 100 mm were sawn with a water-cooled diamond saw. The cubes were sawn from the beams/strips cut out from slabs B and C. The cubes were cohesive after the cutting and preparation.

The crack patterns in all slabs and corresponding cores were similar. Cores drilled vertically had ASR cracks that were predominantly oriented perpendicular to the core length, and cores drilled horizontally had ASR cracks predominantly oriented parallel to the concrete length. Fig. 2 exemplifies the crack orientation within the cores. The shown cores were impregnated with a fluorescent epoxy under vacuum to visually amplify the crack pattern. It is important to state that the ASR crack extent may vary both between the different slabs and within the same slab.
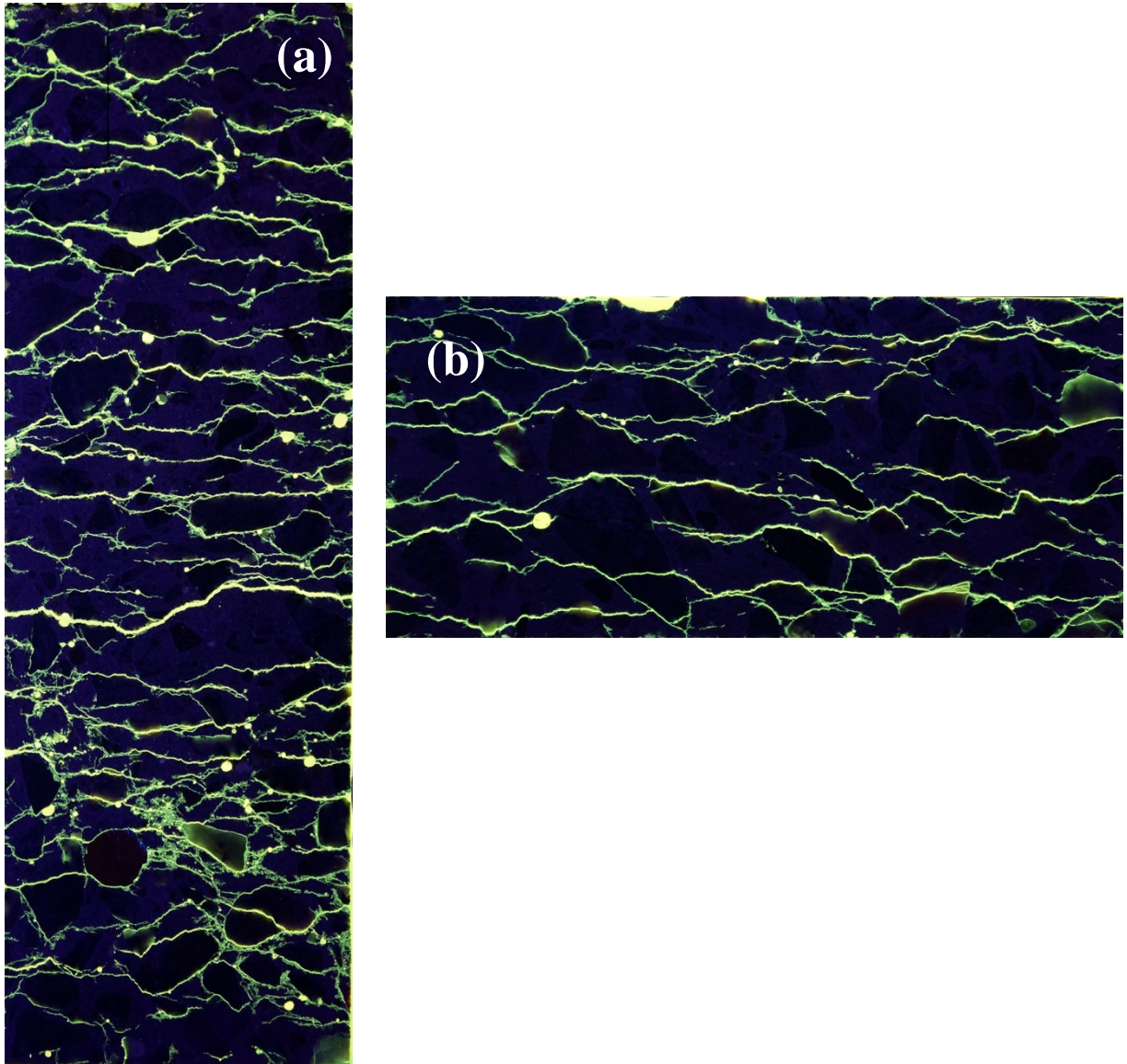
Fig. 2: Fluorescence-impregnated concrete cores seen under ultraviolet light. (a) Impregnated core vertically drilled from slab bridge C. (b) Impregnated core horizontally drilled from slab bridge C.

2.2 Indirect and direct tensile test methods

2.2.1 Split test

Usually the tensile strength of concrete is assessed from the indirect split test, also known as the Brazilian split test, by an empirical conversion factor of 0.6–0.9. In the split test, the load is applied to the cores along diametrically opposed loading platens until failure. The cores measured 100 mm in diameter and 150 to 200 mm in length. The load was distributed to the core over small, narrow strips. The narrow strips used were 10 mm in width and 3 mm in thickness made of high-density wood fiber boards. The split tests were conducted as deformation controlled with a loading rate of 0.5 mm/min; this differs from DS/EN 12390-6:2002 [18], where split tests should be conducted as load-controlled tests.

Fig. 3 illustrates the orientation of the ASR cracks within the cores subjected to the split test setup. The cores used for split test were drilled from slabs A and B.
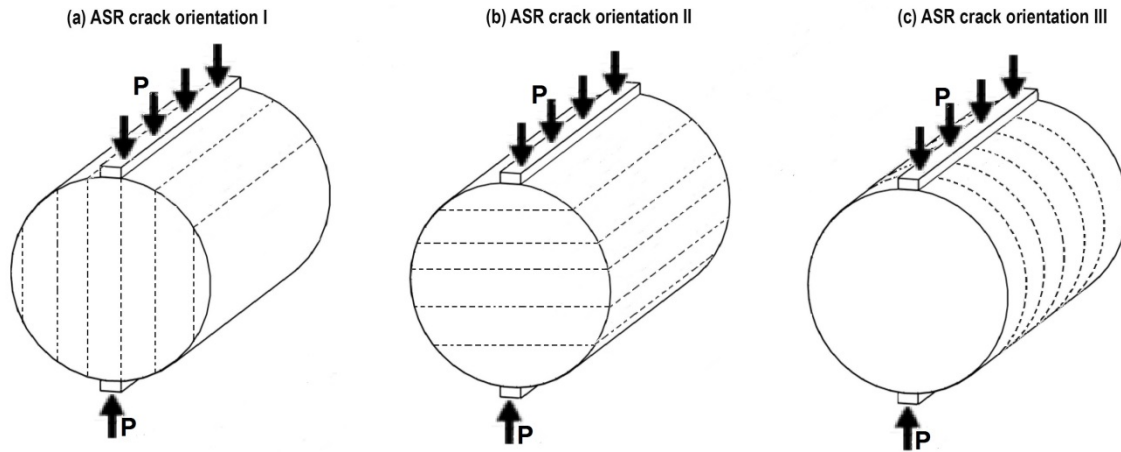

Fig. 3: Illustration of the ASR crack orientations in the Brazilian split test. (a) Orientation I corresponds to cracks parallel to the split load. (b) Orientation II corresponds to cracks perpendicular to the split load. (c) Orientation III corresponds to cracks oriented out of plane.

2.2.2 Wedge splitting test

To the authors' knowledge, the wedge splitting test (WST) has never been used to determine the tensile strength of ASR-damaged concrete. The wedge splitting test was originally proposed by Linsbauer and Tschegg [19] and later developed by Brühwiler and Wittmann [20]. With a suitable model the WST can be used to determine the cohesive law, elastic modulus, and tensile strength for a material through an inverse analysis.

In the wedge splitting test a small cube with a grove and notch is split into two halves while monitoring the applied vertical load P_v and crack mouth opening displacement (CMOD). Fig. 4 shows an illustration of the experimental setup. As seen in Fig. 4(a) the cube is first placed on a line support and two loading devices with roller bearings are mounted on the cube, see Fig. 4(b). Hereafter, the wedge is placed between the roller bearings and the vertical load P_v acts on the roller bearings, see Fig. 4(c). The splitting load P_{sp} is the horizontal component of vertical load acting on the roller bearings.
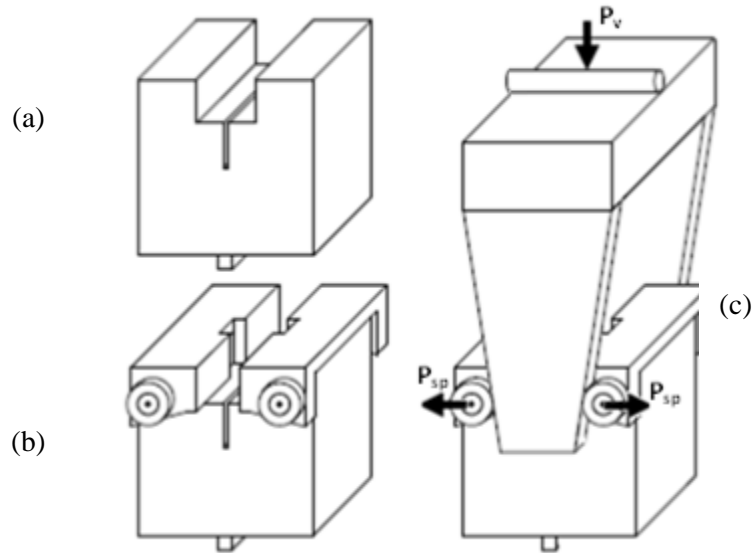
Fig. 4: Illustration of the WST experimental test setup. Adapted from Østergaard [21].

The WST was performed in a universal testing machine, the Instron 6022, equipped for closed-loop testing. A 10 kN static load cell was used for the testing. The CMOD was measured with a clip gauge (Instron type 2670-116) fixed on each side of the notch. The test was controlled using the signal from the clip gauge where a deformation rate of 0.2 mm/min was used. The CMOD is illustrated in Fig. 5.

After the experimental test data was acquired, an inverse analysis established material properties based on the experimental test data. The step-by-step inverse analysis approach provided by Østergaard [21] was used. The inverse analysis was conducted using a MatLab program developed at the Technical University of Denmark by Østergaard [21] and further developed by Skoček [22,23]. The inverse analysis applies the crack hinge model by Olesen [24] which was implemented on the WST geometry. The crack hinge model applies the fictitious crack concept of Hillerborg *et al.* [25]. The crack hinge model is based on the assumption that the crack only changes the stress and strain field locally, while the rest of the structure remains unaffected. By applying the hinge model with a simple and robust inverse analysis algorithm, Østergaard [21] reported that it is possible to produce relevant material parameters of the tested material, such as the tensile strength of concrete.

Fig. 5 shows the geometry of the cubes and an illustration of the crack orientations within the sawn concrete cubes. The cubes were sawn from slabs B and C.
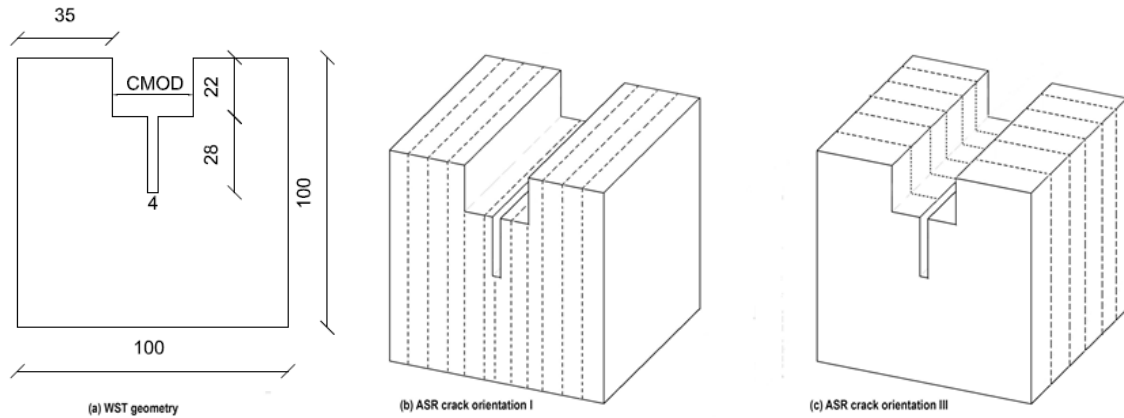
Fig. 5: Illustration of the cubes applied in the WST: (a) WST geometrygiven in mm. (b) Orientation I corresponds to cracks perpendicular to the splitting load. (b) Orientation III corresponds to cracks oriented "out of plane."

2.2.3 Uniaxial tensile test

The uniaxial tensile test setup was conducted in accordance with CRD-C 164-92 [26]. In the uniaxial tensile test, the cores were glued to cylindrical end platens. The cores were 200 mm long and 100 mm in diameter. The end platens were made of steel, 65 mm thick, and 100 mm in diameter. The glue used was a fast-setting epoxy resin. To ensure proper alignment during hardening of the glue, the cores glued to the end platens were placed in a V-shape holder.

The cylindrical end platens were connected to roller chains, each with a length of 400 mm. Steel rods at the end of the roller chains were inserted into the testing machine grips. The test machine used was the 250 kN MTS 180 machine. The tensile load was applied continuously with a rate of 0.002 mm/s to failure of the cores.

Fig. 6 illustrates the uniaxial tensile test setup and the orientation of the ASR cracks. The cores tested in direct uniaxial tension were drilled from slab bridge C.
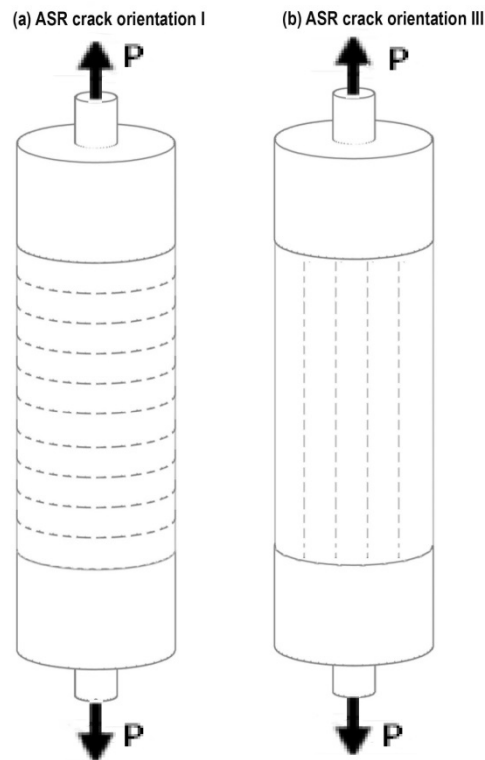
Fig. 6: Illustration of the crack orientation in the uniaxial tensile test. (a) Orientation I corresponds to cracks perpendicular to tension. (b) Orientation III corresponds to cracks parallel to tension.

3. Results

3.1 Slab bridge A - Brazilian split test and influence of ASR crack orientation

Figs. 7(a) and 7(b) show the tested splitting tensile strength, f_{sp}, of cores drilled from slab bridge A. The beams/strips from slab bridge A were cut from the eastern part; see Fig. 7(a), and the western part; see Fig. 7(b), of the slab. The distance between these two positions was approximately 30 m. The test results in Figs. 7(a) and 7(b) illustrate clearly the influence of crack orientation on f_{sp} (see Fig. 3 for orientations I, II, and III).

The test results are plotted as so-called box plots. In the box plots all measurements are included. The tops of the boxes represent the third quartile, the bottoms of the boxes represent the first quartile, and the coarse horizontal lines inside the boxes represent the median of the measurements. The tops and bottoms of the whiskers represent the maximum and minimum splitting tensile strengths, respectively. The red dots inside the boxes represent the average f_{sp}. The circles represent *outliers*, or strengths that are distant from other measurements. To the authors' opinion, the outliers in the splitting test do not indicate an experimental error but may represent differences in the

9

alignment of the cracks to the predetermined separation/splitting surface according to the split test setup.
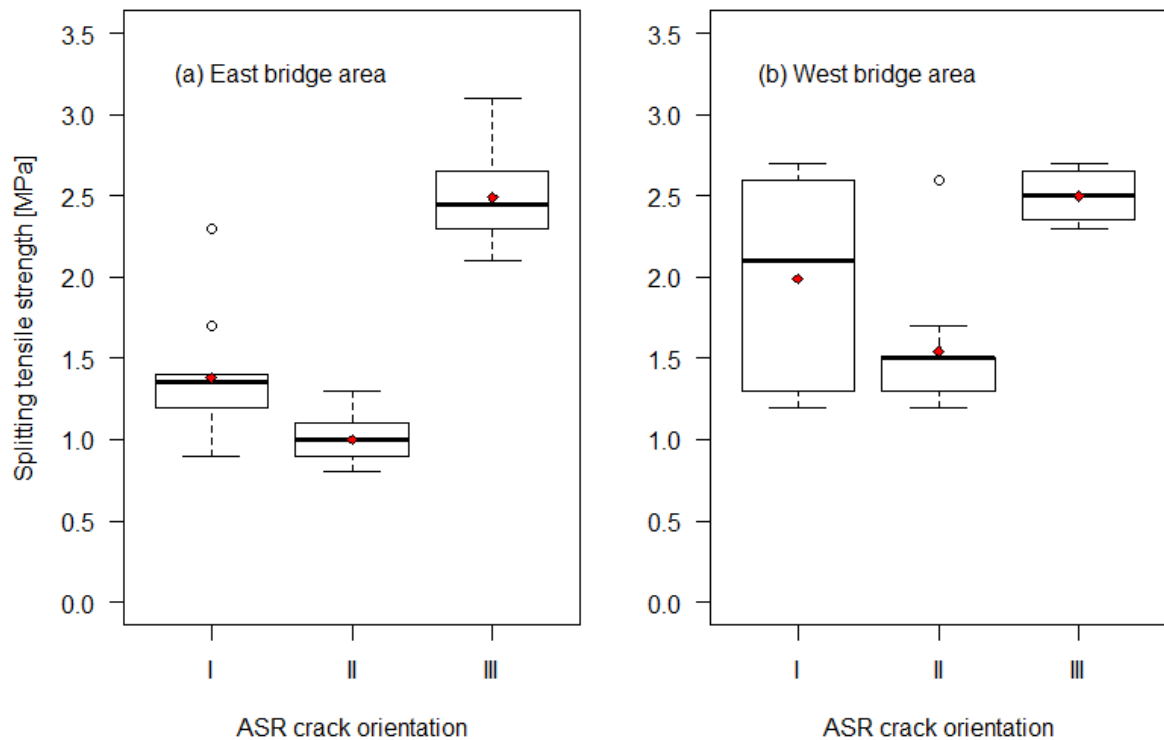
Fig. 7: Splitting tensile strength, f_{sp}, of cores drilled from slab bridge A grouped into three positions of crack orientations.

3.2 Slab bridge B - Influence of crack orientation on Brazilian split test and WST

The f_{sp} and the tensile strength determined from WST, $f_{t,WST}$, are plotted in Fig. 8(a) and Fig. 8(b), respectively. The results belong to cores and cubes from the same area within slab bridge B (see Figs. 3 and 5 for orientations I, II, and III). 10 - 27 splitting test and 10 – 12 wedge splitting tests were conducted on each crack orientation. The results in Figs. 8(a) and 8(b) illustrate clearly the influence of crack orientation on both f_{sp} and $f_{t,WST}$. As expected the $f_{t,WST}$ is significantly smaller than f_{sp}.
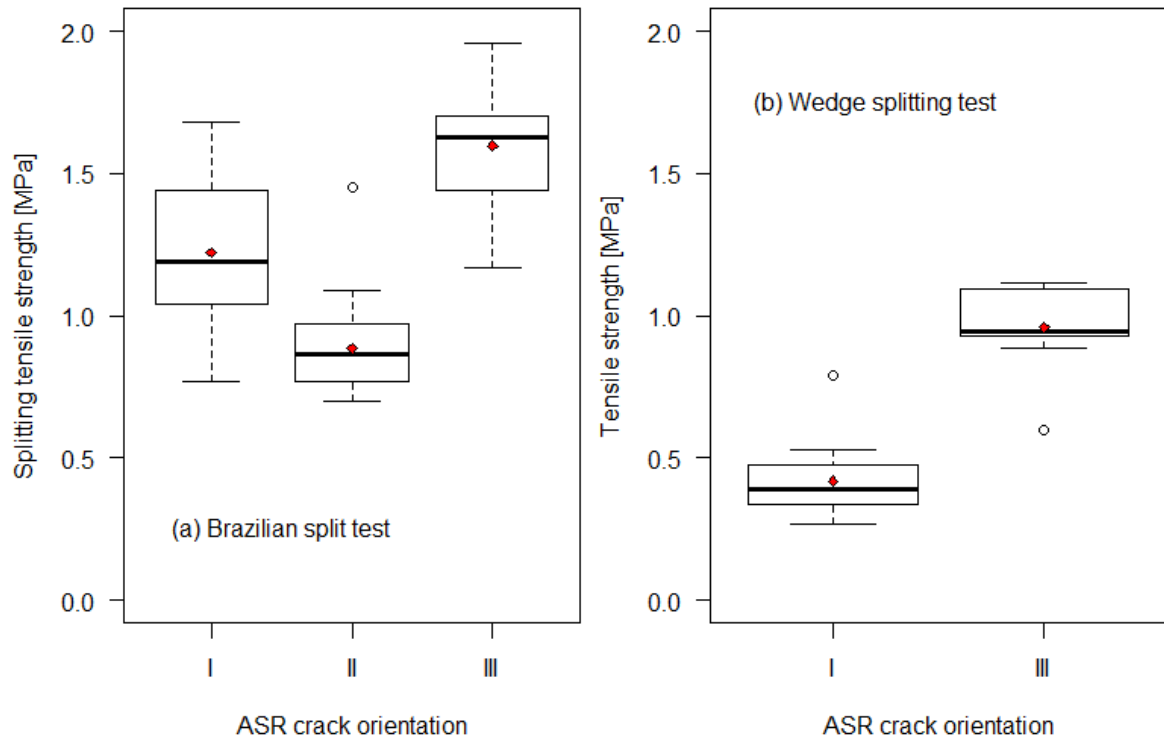
Fig. 8: Splitting tensile strength, f_{sp}, and tensile strength from WST, $f_{t,WST}$, grouped into positions of crack orientation. Specimens sawn and drilled from slab bridge B.

3.3 Slab bridge C - Influence of crack orientation on WST and uniaxial tensile test

The direct tensile strengths, f_t, and $f_{t,WST}$ are plotted in Figs. 9(a) and 9(b), respectively. These results belong to cubes and cores sawn and drilled from the same beam/strip from slab bridge C (see Figs. 5 and 6 for crack orientations I and III). 10-12 wedge splitting tests and 6-9 direct tension tests were conducted on each crack orientation. As seen in Figs. 9(a) and 9(b) f_t is significantly smaller than $f_{t,WST}$. The figures illustrate clearly the influence of crack orientation on the strength.
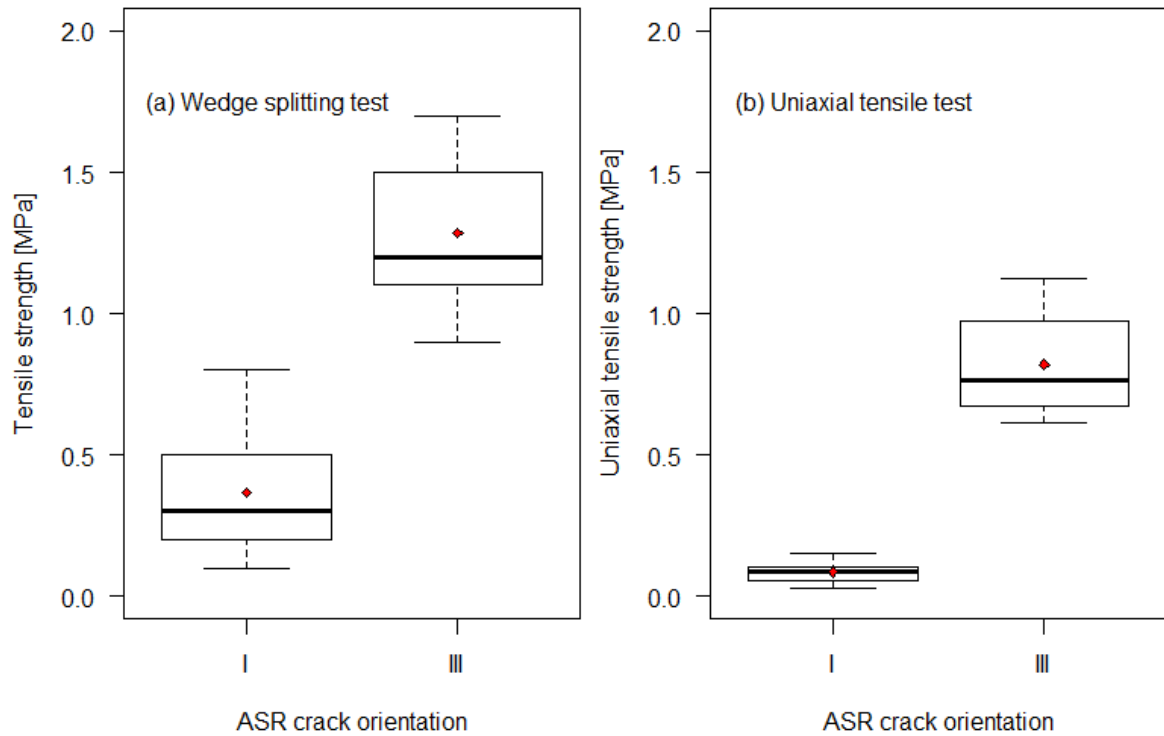
Fig. 9: Tensile strength from WST, $f_{t,WST}$, and direct tensile strength, f_t, grouped into positions of crack orientation. Specimens sawn and drilled from slab bridge C.

4. Discussion

4.1 Influence of crack orientation on the splitting tensile strength

As seen from Figs. 7(a), 7(b), and 8(a) it is clear that f_{sp} is strongly influenced by the orientation of the cracks. On the average, orientation III has the highest and orientation II the lowest f_{sp}. This observation is valid for both slab bridge A and slab bridge B. However, the relationship between the f_{sp} for different crack orientations varies for each individual slab and within the same slab. This may not be a surprise because the extent of cracks was not the same from slab to slab and within the same slab.

Contrary to our study, Siemens *et al.* [16,17] reported that the crack orientations had no significant influence on f_{sp}. Probably the contradiction between the studies may be explained by the differences in ASR-reactive aggregates and the crack extent within the tested cores. In the slabs examined by Siemens *et al.*, ASR occurred in the coarse aggregate fraction, whereas in our examined slabs ASR occurred in the fine aggregate fraction. Consequently, it is expected that the cores from our study contained considerably more ASR cracks, which would influence on f_{sp}. In addition, Siemens *et al.* omitted the most cracked specimens when performing the tests.

From Figs. 7(a) and 7(b), it is seen that the split test may be capable of capturing the extent of cracks for orientation I and II but not for crack orientation III. Visually, the eastern part of slab bridge A had a greater extent of cracks than the western part. Consequently, the distance between the cracks in the western part is larger than in the eastern part. This evaluation was confirmed by the compressive strength of cores. The compressive strength was significantly higher for the western part than eastern part. As seen in Figs. 7(a) and 7(b) $f_{sp,III}$ is similar for both areas in slab bridge A, corresponding to an average $f_{sp,III}$ of 2.5 MPa. Practically, orientation III corresponds to vertically drilled cores, which in many cases is the only possible in-situ drilling orientation in slabs. The fact that $f_{sp,III}$ are above the other orientations may not be a surprise. $f_{sp,III}$ corresponds to of a less-deteriorated cross section. As seen in Fig. 3, the cracks are oriented out of plane.

For orientation I, the alignment of the cracks with the predetermined separation/splitting surface is crucial. In some tests the cracks were split or opened due to loading resulting in low $f_{sp,I}$. However, in other tests the predetermined separation/splitting surface was developed unaffected by the presence of ASR cracks nearby, which resulted in high $f_{sp,I}$. The larger scatter between the minimum and maximum $f_{sp,I}$ seen in Fig. 7(b) may be explained by the lesser extent of and larger distance between the cracks.

As seen in Figs. 7(a), 7(b), and 8(a), $f_{sp,II}$ is generally lower than $f_{sp,I}$ and $f_{sp,III}$, which may be explained by the failure mechanism for this specific crack orientation. For orientation II, the failure was governed by a predetermined separation/splitting surface and by rotation and opening of individual cracks perpendicular to the split load. The rotation due to opening of the cracks also influenced the propagation of the separation/splitting surface. Fig. 10 depicts the combined failure behaviour observed for orientation II, where a significant curvature of the separation surface was observed in most split tests; this curvature influences the stress distribution in the separation surface.
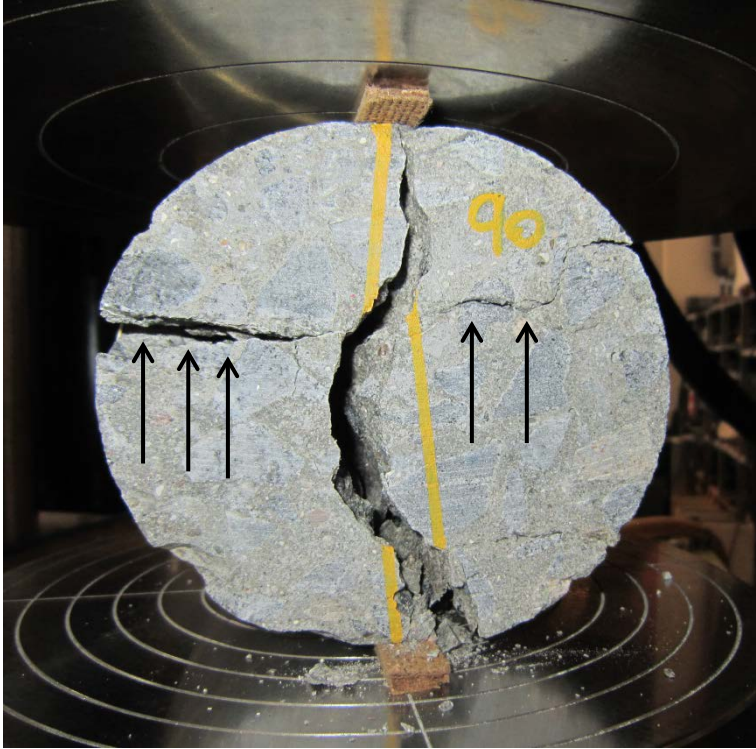
Fig. 10: Split test. Combined effects of failure for orientation II. Cracks perpendicular to the split load are opened.

4.2 Influence of crack orientation on the wedge splitting test

As previously stated, $f_{t,WST}$, is determined from the inverse analysis that applies the crack hinge model. In Figs. 11(a) and 11(b), the ability of the inverse analysis and the crack hinge model to fit the measured splitting load-CMOD curves is shown for both crack orientations. The computational approximation is based on a trilinear softening curve, in order to decrease the total discrepancy between the measurements and computational approximation.
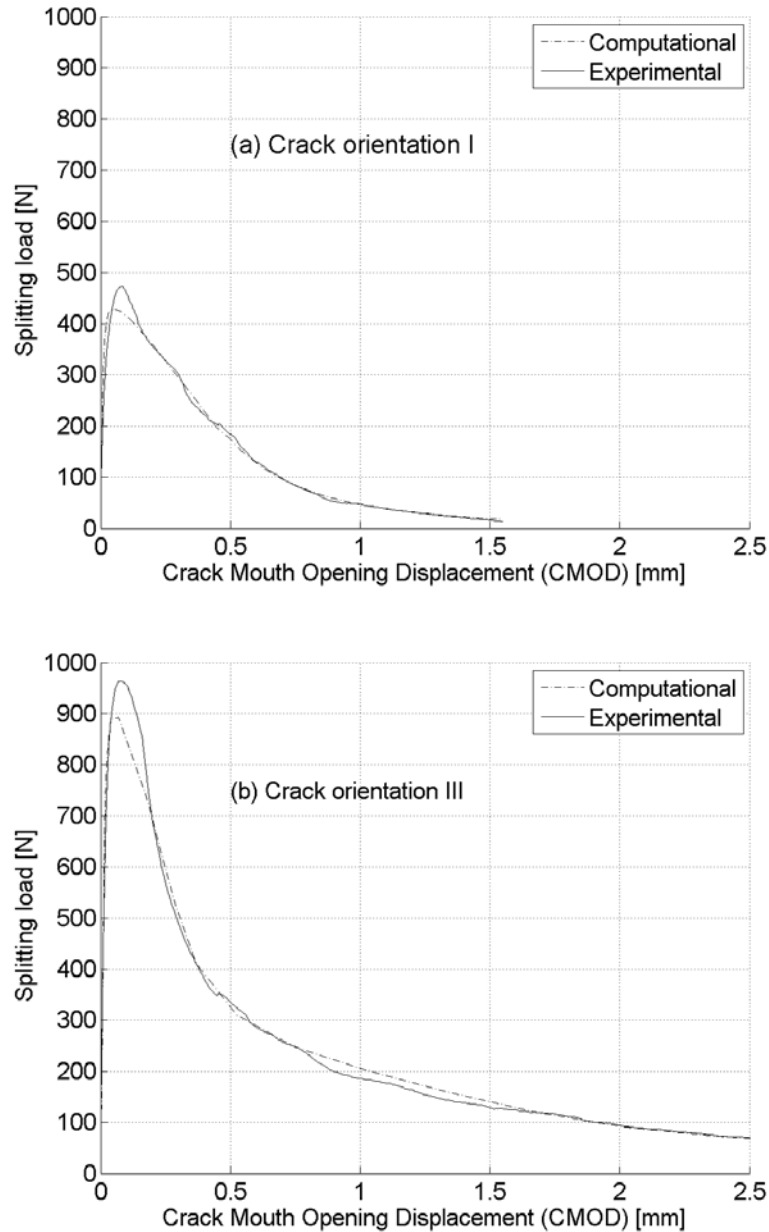
Fig 11: Wedge splitting test. Comparison of the experimental and the computed splitting load-CMOD curve. (a) Orientation I. (b) Orientation III.

As seen in Figs. 11(a) and 11(b), the computational based approximation generally underestimates the ultimate splitting force and may also underestimate $f_{t,WST}$. The fact that the computational approximation does not completely fit to the experimental data was expected. As seen in Fig. 12, the cracks influenced the propagation of the load-induced crack. For orientation I, WST can definitely open existing cracks, although the cracks are not entirely in alignment with the notch. However, the opening of cracks may cause a curvature of load-induced crack, which can result in a failure mode not entirely compatible with the crack hinge model. Theoretically, in the crack hinge model, the load-induced crack will run straight from the notch to the bottom of the cube without any significant curvature.
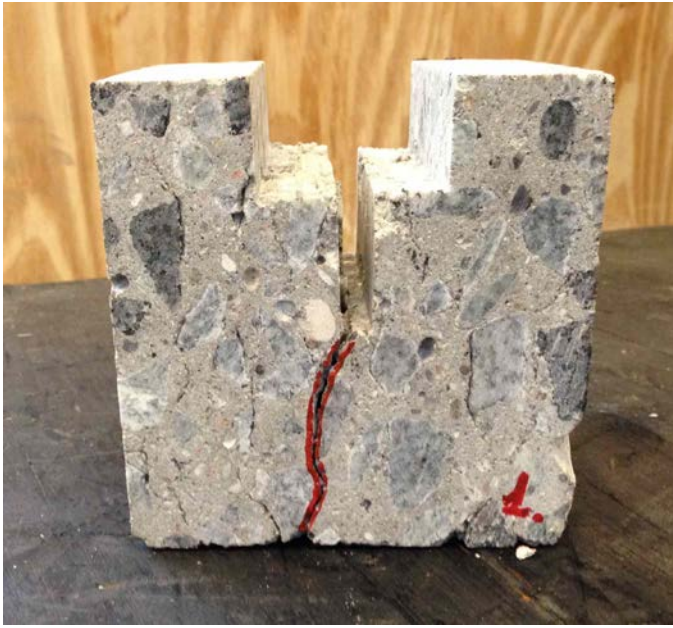
Fig. 12. WST cube with orientation I after testing. The ASR cracks were opened due to the splitting load.

Despite this, it is clear from Figs. 8(b) and 9(a) that the crack orientation has a significant influence on f_{WST}. $f_{WST,I}$ is significantly lower than $f_{WST,III}$. The relationship between f_{WST} and crack orientations will, like f_{sp}, vary between different slabs and possibly within areas of the slab. This is caused by differences in the extent of cracks in the cubes.

4.3 Influence of crack orientation on the uniaxial tensile test

Due to the strong predominant crack orientation observed on the cores, it was expected that f_t would be orientation dependent. Fig. 9(b) illustrates that this expectation is correct. $f_{t,I}$ is significantly lower than $f_{t,III}$.

This significant difference in f_t can be explained by the effective cross section area in the cores for both crack orientations. The effective cross section to support the tensile stresses is much smaller for orientation I than orientation III. The effective cross section area for orientation I may primarily consist of the alkali-silica gel partially filling and binding the cracks; this resulted in $f_{t,I}$ of almost 0 MPa. Although the effective cross section for orientation III is not reduced, $f_{t,III}$ is influenced by the parallel cracks. It is well known that is it difficult to maintain a centric load during the direct tension tests. As seen in Figs. 13-14, in addition to possible load eccentricity, the cracks also cause significant eccentricities and bending moment in the cores during direct tension test. The images presented in Figs. 13-14 were generated with the digital image correlation (DIC) system and analyzed with ARAMIS software [27]. Additional examples of applying this system to measure the

relative surface displacement of concrete specimens were described by Pereira *et al.* [28] and Schmidt *et al.* [4].

Fig. 13(a) shows a core surface with orientation I at the beginning of the testing, where no load was applied to the core. After the load was applied a uniform strain distribution in the core, corresponding to the opening of an existing crack is seen, see Fig. 13(b). However, with increasing load, Fig. 13(c) shows an uneven strain distribution across the specimen due to opening of a coarser crack in the left side of the core, thus resulting in eccentric load distribution during testing. Fig. 13(d) shows that the load-induced cracks propagate from the left side of the core.

The observation of uneven strain distribution and thus eccentric loading during testing is valid for both crack orientations in the direct tension tests. Fig. 14 shows the strain distribution and load propagation for a core with orientation III. Fig. 14(a) shows the core surface at a time where no load was applied. Fig. 14(b) shows how the strains gradually build up in the right side of the core, causing uneven strain and load distribution in the specimen during testing. The strain also gradually builds up in the parallel cracks. Fig. 14(c) shows the core just before separation, where the load-induced crack propagates from the right-hand side of the core.
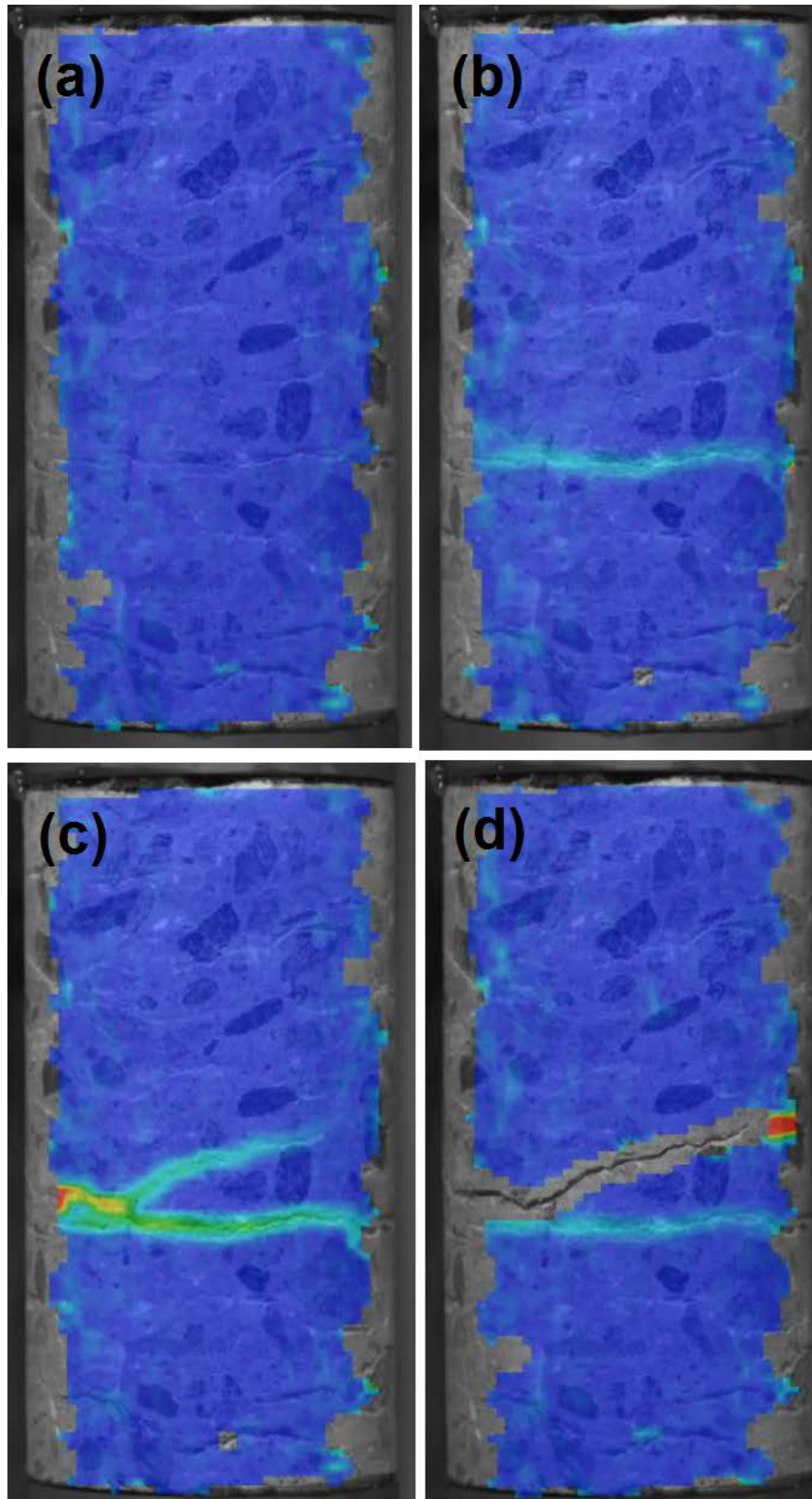
Fig. 13: Major principal strain distribution in a core with orientation I during direct tension test.
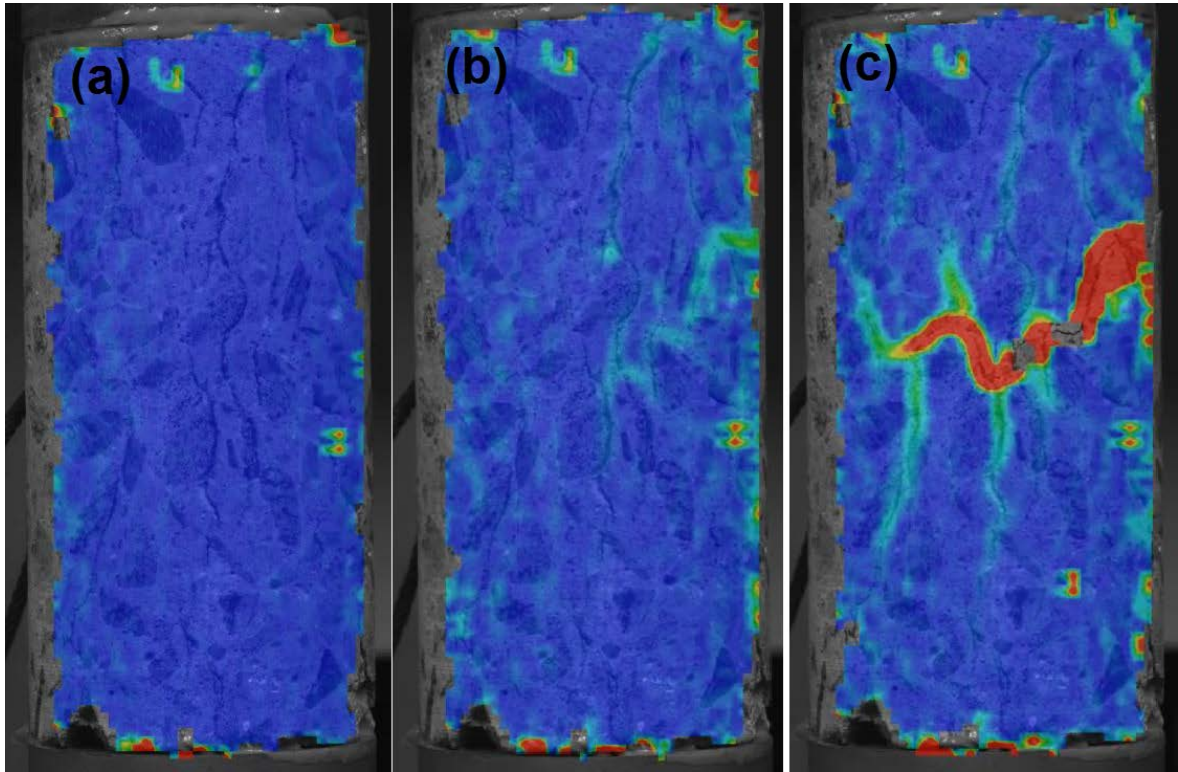
Fig. 14: Major principal strain distribution in a core with orientation III during direct tension test.

4.4 Predictions of tensile strength by means of splitting tensile strength and compressive strength

Table 1 shows the average f_{sp} and average $f_{t,WST}$ for slab bridge B. Additionally, Table 1 shows the average f_t and average $f_{t,WST}$ for slab bridge C. The ratios $f_{t,WST}/f_{sp}$ for slab bridge B are calculated to 0.34 and 0.60 for orientations I and III, respectively. Consequently, the conversion factors or ratios to relate f_{sp} to $f_{t,WST}$ is orientation dependent. The ratio of 0.60 for orientation III is more a coincidence than a fact. Assuming that f_t is the "true" tensile strength of the material we may expect that the ratios f_t/f_{sp} should be considerably smaller than $f_{t,WST}/f_{sp}$. As calculated from Table 1 the ratios $f_t/f_{t,WST}$ for slab bridge C are 0.24 and 0.64 for orientation I and orientation III, respectively.

Table 1: Average f_{sp}, $f_{t,WST}$ and f_t for slab bridge B and C.

| Bridge slab | f_{sp} [MPa] | | $f_{t,WST}$[MPa] | | f_t [MPa] | |
| | Orientation | | Orientation | | Orientation | |
	I	III	I	III	I	III
B	1.22	1.60	0.41	0.96	-	-
C	-	-	0.37	1.29	0.09	0.82

Table 2 shows the average measured f_t, $f_{t,WST}$, f_c and average $f_{t,pre}$. $f_{t,pre}$ was predicted from Eq.(1) given by Nielsen and Hoang [29]. Eq. (1) is used for normal uncracked concrete.

$$f_{t,pre} = \sqrt{0.1f_c} \qquad (1)$$

The compressive strength, f_c, is determined by cores drilled from the same area, from bridge slab C, as those used for the tensile tests. As seen in Table 2, f_t and $f_{t,WST}$ is significantly more reduced than $f_{t,pre}$. The ratios $f_t/f_{t,pre}$ are 0.07 and 0.51 for orientations I and III, respectively. The ratios $f_{t,WST}/f_{t,pre}$ are 0.29 and 0.80 for orientations I and III, respectively.

Table 2: Average f_t, f_{sp}, f_c and $f_{t,pre}$ for slab bridge C.

	f_t [MPa]		$f_{t,WST}$ [MPa]		f_c[MPa]		$f_{t,pre}$ [MPa]	
Orientation	I	III	I	III	I	III	I	III
Slab bridge C	0.09	0.82	0.37	1.29	16.13	25.98	1.27	1.61

It is clear from the above results that the normally used empirical conversion factor in the range of 0.60–0.90 when estimating f_t from f_{sp} is not applicable for ASR-cracked concrete. $f_{t,pre}$ yields significant higher values than the measured f_t and $f_{t,WST}$. Consequently, $f_{t,pre}$ overestimate the "true" tensile strength. We expect that the ratios between the applied direct and indirect tests will, as reported by Siemens *et al.* [17], vary both for individual slabs and within the same slab due to differences in extent of ASR cracks.

4.5 Evaluation of the test methods

The remarkable differences between the direct and indirect tensile strengths illustrate clearly the difficulties in measuring a "true" tensile strength of ASR-damaged concrete from actual slabs. In addition, it is difficult to determine which tensile strength to use in structural calculations.

Although the split test may be capable of capturing the extent of ASR cracks for crack orientations I and II, it is clear from our results that the split test is less indicative for the effects of ASR cracks. Due to the predetermined separation/splitting surface, the alignment of the cracks will be important in order to obtain a true f_{sp} for the ASR-cracked cross section, especially for crack orientation I.

In our opinion the direct tensile test may be too sensitive for the effects of ASR cracks. Firstly, due to the presence of cracks it is difficult if not impossible to maintain a centric load during testing. Secondly, f_t will not indicate the effects of ASR cracks but will only provide the strength of local defects and cracks. As an example, if only one crack is visible in the core, the failure will happen at this local crack due to a decrease in effective cross-sectional area. Furthermore, we may argue that in practice most tensile situations are more similar to the wedge splitting test than the direct tension test. Therefore, f_t of ASR-damaged concrete may not be directly applicable to structural situations.

The wedge splitting test is capable of evaluating the tensile strength in the cracks, meaning that for crack orientation I an existing ASR crack was opened due to the splitting force, even though some of the cracks were not in alignment with the notch. However, in most cases the computational approximations by the inverse analysis may underestimate the ultimate splitting force, thus predicting lower $f_{t,WST}$. Most importantly, the propagation of the splitting force-induced cracks and corresponding failure mode may not be entirely compatible with the assumptions in the crack hinge model that is applied in the inverse analysis and used to determine $f_{t,WST}$. Despite this fact, it is still surprising how good the crack hinge model fits the measurements.

In practice, vertical drilling of cores, corresponding to orientation I in Fig. 6, is the only possible and cost-effective drilling orientation in actual bridge slabs. Consequently, the tensile strength for the vertical drilled cores determined from the Brazilian split test will provide the highest f_{sp} and the direct tension test will provide very low f_t – almost 0. For the wedge splitting test, the concrete cores must be at least 150 mm in diameter in order to obtain concrete cubes with 100 mm in length, width, and thickness. However, as reported by Brühwiler and Wittmann [20], it is possible to apply drilled cores in the wedge splitting; this was not investigated in this study.

5. Conclusions

This study experimentally investigates the tensile strength of ASR-damaged concrete. The ASR-damaged concrete specimens were drilled and sawn from segments from three severely ASR-damaged flat slab bridges. Three tensile test methods were used: Brazilian split test, wedge splitting test, and uniaxial tensile test. The main conclusions from the study can be summarized as follows:

- Both direct and indirect tested tensile strengths are negatively affected by the ASR cracks.
- Both direct and indirect tested tensile strengths are strongly dependent on the orientation of the ASR cracks.
- All the three applied test methods have disadvantages that affect the measured tensile strength.
- The Brazilian split test may be less indicative for the effects of ASR cracks. The normally used conversion factors of 0.6–0.9 to predict the uniaxial tensile strength is not applicable for ASR-damaged concrete.
- The wedge splitting test is a rather simple test. Although, the failure observed on the concrete cubes may not be compatible with the assumptions of the crack hinge model, it seems, surprisingly that the crack hinge model fits fairly well with the experiments. However, in-situ drilled cores have at least to be 150 mm in diameter to saw the cores into cubes.

21

- The uniaxial tensile strength is more negatively affected by the ASR cracks than the other test methods. However, due to the ASR cracks it is nearly impossible to maintain a centric load during testing.
- The formula, used for normal uncracked concrete, to predict the uniaxial tensile strength from the compressive strength is not applicable to ASR-damaged concrete. The measured uniaxial tensile strength is considerably lower than the predictions.
- Due to the significant differences between all the applied test methods it is very difficult to analyse which tensile strength to be used for structural calculations for ASR-damaged bridge slabs.

Acknowledgments

References

[1]   R.N. Swamy, Alkali-Silica Reaction in Concrete, Blackie and Son Ltd., Glasgow and London, 1992.

[2]   N. Østergaard, Aggressive concrete disease attack 600 danish bridges (In Danish), Ingeniøren. (2012). https://ing.dk/artikel/aggressiv-betonsygdom-angriber-600-danske-broer-131714.

[3]   A. McLeish, Structural implications of the alkali silica reaction in concrete, Report 177, Transport and Road Research Laboratory, 1990.

[4]   J.W. Schmidt, S.G. Hansen, R.A. Barbosa, A. Henriksen, Novel shear capacity testing of ASR damaged full scale concrete bridge, Eng. Struct. 79 (2014) 365–374.

[5]   R.A. Barbosa, S.G. Hansen, K.K. Hansen, L.C. Hoang, B. Grelk, Influence of alkali-silica reaction and crack orientation on the uniaxial compressive strength of concrete cores from bridge slabs, Submitted to Cem. Concr. Res. 2017.

[6]   A.D. Herholdt, C.F.P. Justesen, P. Nepper-Christensen, A. Nielsen, The Concrete Book (In Danish), 2nd ed., Aalborg Portland, 1985.

[7]   Danish Standard, Eurocode 2 - Design of concrete structures – Part 1-1: General rules and rules for buildings, Danish Standards, 2008.

[8]   H.W. Reinhardt, O. Mielich, Effects of mechanical properties of ASR damaged concrete on structural design, in: Brittle Matrix Compos. 10, Woodhead Publishing Limited, Warsaw,

2012: pp. 1–9.

[9]   L.A. Clark, Critical Review of the Structural implications of the alkali silica reaction in concrete, Department of Civil Engineering Univerity of Birmingham, UK, PhD thesis, 1989.

[10]   T. Ahmed, E. Burley, S. Rigden, A.I. Abu-Tair, The effect of alkali reactivity on the mechanical properties of concrete, Constr. Build. Mater. 17 (2003) 123–144.

[11]   N. Smaoui, B. Bissonnette, B. Fournier, B. Durand, Mechanical Properties of ASR-Affected Concrete Containing Fine or Coarse Reactive Aggregates, ASTM Int. 3 (2006) 1–16.

[12]   H. Marzouk, S. Langdon, The effect of alkali-aggregate reactivity on the mechanical properties of high and normal strength concrete, Cem. Concr. Compos. 25 (2003) 549–556.

[13]   N. Clayton, R.J. Currie, R.M. Moss, The effects of alkali-silica reaction on strength of prestressed concrete beams, Struct. Eng. 68 (1990) 287–292.

[14]   S. Fan, J.M. Hanson, Effect of Alkali Silica Reaction Expansion and Cracking on Structural Behavior of Reinforced Concrete Beams, ACI Struct. J. 95 (1998) 498–505.

[15]   R.N. Swamy, M.M. Al-Asali, Engineering Properties of Concrete Affected by Alkali-Silica Reaction, ACI Mater. J. (1988) 367–374.

[16]   T. Siemens, N. Han, J. Visser, Unexpectedly low tensile strength in concrete structures, HERON. 47 (2002) 111-124.

[17]   T. Siemens, J. Visser, Low tensile strength in older concrete structures with alkali-silica reaction, in: Proc. 11th Int. Conf. Alkali-Aggregate React., Québec, 2000: pp. 1029–1038.

[18]   DS Standard 12390-6:2000. Testing of hardened concrete - Part 6: Tensile splitting strength of test specimens, Danish Standards, 2000.

[19]   H.N. Linsbauer, E.K. Tschegg, Fracture energy determination of concrete with cube shaped specimens (in German), Zement Und Bet. 31 (1986) 38–40.

[20]   E. Brühwiler, F.H. Wittmann, The Wedge Splitting Test, a New Method of Performing Stable Fracture Mechanics Tests, Eng. Fract. Mech. 35 (1990) 117–125.

[21]   L. Østergaard, Early-Age Fracture Mechanics And Cracking of Concrete, Technical University of Denmark, Denmark, PhD thesis, 2003.

[22]   J. Skoček, Fracture propagation in cementitious materials - Multi-scale approach: measurements and modeling, Technical University of Denmark, Denmark, PhD thesis, 2010.

[23]   J. Skoček, H. Stang, Inverse analysis of the wedge-splitting test, Eng. Fract. Mech. 75 (2008) 3173–3188.

[24]   J.F. Olesen, Fictitious crack propagation in fibre-reinforced concrete beams, J. Eng. Mech. 127 (2001) 272–280.

[25]   A. Hillerborg, M. Modéer, P.E. Peterson, Analysis of Crack Formation and Crack Growth in Concrete by means of Fracture Mechanics and Finite Elements, Cem. Concr. Res. 6

(1976) 773–782.

[26] CRD-C 164-92 Standard Test Method for Direct Tensile Strength of Cylindrical Concrete or Mortar Specimens, U.S. Army Engineering Research developemnt Center (ERDC), Vicksburg, 1992.

[27] G. für O. Messtechnik, ARAMIS v 5.3.0 - User Manual, 2004.

[28] E.B. Pereira, G. Fischer, J.A.O. Barros, Image-based detection and analysis of crack propagation in cementitious composites, in: C. Leung, K.T. Wan (Eds.), Int. RILEM Conf. Adv. Constr. Mater. Trough Sci. Eng., RILEM Publications SARL, 2011: pp. 343–350.

[29] M.P. Nielsen, L.C. Hoang, Limit Analysis and Concrete Plasticity, 3rd ed., Taylor and Francis Group, 2011.

Residual shear strength of a severely ASR-damaged flat slab bridge

Paper III

"Residual shear strength of a severely ASR-damaged flat slab bridge"

R.A. Barbosa, S.G. Hansen, K.K. Hansen and L.C. Hoang

Residual shear strength of a severely ASR-damaged flat slab bridge

Ricardo Antonio Barbosa[a], Søren Gustenhoff Hansen[b], Kurt Kielsgaard Hansen[a], Linh Cao Hoang[a]

[a] *Technical University of Denmark, Brovej, Building 118, 2800 Kgs. Lyngby, Denmark*
[b] *University of Southern Denmark, Campusvej 55, 5230, Odense M, Denmark*

Abstract

Although the residual shear strength of ASR-damaged slab bridges without shear reinforcement has been discussed for several decades, the amount of published research on this topic is very limited. This paper presents the results of a test series on 18 reinforced beams sawn from a severely ASR-damaged flat slab bridge. The test results indicate that the tested load-carrying capacities are strongly influenced by the applied bending test setup. The ASR cracks in the beams strongly influenced the propagation of load-induced cracks. The measured load-carrying capacities in the three-point bending setup are an expression of the moment capacity and not for the shear strength of the beams. Generally, the calculated sectional moment capacity of beams tested in the three-point bending setup was lower than the maximum moment carried by the beams. For the beams tested in the four-point bending setup an increase in shear span-to-effective depth ratios resulted in decrease in measured shear strengths. We compared the measured shear strengths with calculations using the Eurocode 2 design code and found the calculations based on the compressive strength of drilled cores was rather conservative at low shear span-to-effective depth ratios. However, the conservatism of Eurocode 2 calculations decreased with increasing shear span-to-effective depth ratios. With the inclusion of ASR-induced pre-stress effect the calculated shear strengths correlated better with the measured shear strengths. But, the calculated shear strengths were higher than the measured shear strengths at higher shear span-to-effective depth ratios. The test results indicated that the ASR-induced pre-stress effect can, to some extent, compensate for the significant loss in material properties; however, the types of failure mechanism in some beams influenced the measured shear strengths.

Alkali-silica reaction, uniaxial compressive strength, crack orientation, slab without shear reinforcement, shear strength, moment capacity, pre-stress effect, Digital Image Correlation, Eurocode 2

The notations used in tables and figures are shown in Appendix A.

1. Introduction

The consequences of ASR cracks on the residual shear strength of slabs without shear reinforcement have been discussed for several decades. In Denmark, four ASR-damaged slab bridges have been demolished in recent years due to uncertainties about their residual shear strength. Unfortunately, the number of published studies regarding the residual shear strength of slabs in service remains limited. Execution of full-scale tests on slabs can be complicated and expensive. Consequently, most studies concerning the shear strength of ASR-damaged reinforced specimens are based on small-scale laboratory-prepared and laboratory-conditioned beams [1–12]. The shear test results from these accelerated specimens are generally contradictory: both increases and decreases in shear strength were reported. The contradictory nature of these test results is, however, not surprising. The degree of deterioration at the time of testing, the reinforcement configuration, the test setup and the type of reactive aggregates differs between all tests. These essential differences result in significant challenges in the interpretation and comparison of the shear test results. Most importantly, the correlation between laboratory-conditioned specimens and ASR-damaged slabs in service is unclear. To the authors knowledge, only three destructive shear tests on ASR-damaged slab bridges in service have been conducted recently [13–16].

In the Netherlands full-scale shear tests were conducted on six large reinforced beams sawn from two ASR-damaged slabs [13,14]. Two shear tests were conducted on each of the six beams. Four of the six beams were strengthened by steel strips that were glued onto the bottom side over the entire beam length to enhance its bending capacity. Since the steel strips have not been exposed to the ASR-induced expansion they are not comparable to ordinary internal reinforcement; neither in moment capacity or shear strength. It was reported that the failure of the beams occurred at about 75 percent of the predicted theoretical shear capacity and that the variation in shear span-to-depth ratio between 2.5 and 4.5 did not influence on the shear capacity. It must be recognized that in the slabs tested in the Netherlands ASR occurs in the coarse aggregate fraction whereas the ASR occurs in the fine aggregate fraction in Denmark. This circumstance may cause significant differences in the ASR implications in the structure.

In Denmark, an in-situ full-scale test was conducted on a severely ASR-damaged slab bridge before it was demolished due to concerns about its residual shear capacity [16]. The scope was to investigate whether the test could assess a lower limit for the shear capacity (not the ultimate shear capacity) of the slab and to develop a method to predict the shear capacity based on drilled cores. The investigation included a destructive in-situ

shear test as well as tests of the tensile and compressive strength of vertically drilled cores. Unfortunately, due to a statically indeterminate test setup, the actual applied shear force could not be determined with sufficient accuracy. Consequently, a method to predict the actual shear capacity was not achieved.

In 2013 a new round of in-situ full-scale shear tests were conducted on parts of another slab [15]. The investigation consisted of shear tests in four areas on the slab. The purpose of the tests was to verify the shear capacity of the bridge slab. Unfortunately, in depth-analysis of the shear tests revealed that some of the essential tensile longitudinal bars were cut during the preparation of the test rig setup [17]. This means that three out of four test results could not be considered as shear capacities. However, the one valid shear test resulted in residual shear strength that was 30 percent higher than the predicted shear strength estimated by use of the compressive strength of cores [17]. Despite the incorrect preparation of three tests, the results could be used as a lower limit for the shear capacity. The results provided enough knowledge in order to extend the remaining service life of the ASR-damaged slab.

Despite the questionable quality and validity of the existing shear tests, we acknowledged that the residual shear strength is not as low as expected when judged solely on the residual compressive strength of the drilled cores. Researchers agree this could be due to an ASR-induced pre-stress effect on the longitudinal reinforcement [5–7,13,14,17–19]. The pre-stress effect is caused by the elastic restraint of the ASR expansion by the reinforcement. However, to the best of our knowledge, no quantification of the pre-stress effect in actual ASR-damaged bridge slabs has been reported in the literature.

In order to develop reliable methods and models to predict the residual shear strength of actual ASR-damaged slabs, there is a need for additional testing on specimens sawn from actual ASR-damaged slabs in service. In that context quantification and understanding of the ASR-induced pre-stress effect correlated with loss of material properties are needed. This paper does not provide a new theory for the residual shear capacity of ASR-damaged reinforced concrete. However, this paper presents research on the residual shear strength of 18 beams sawn from a severely ASR-damaged flat slab bridge without shear reinforcement. Nine of the beams were loaded until failure in an asymmetrical four-point bending test setup and the remaining nine beams were loaded until failure in a three-point bending test setup. The influence of shear span on the residual shear strength was investigated. During testing, Digital Image Correlation (DIC) was applied to evaluate the failure mechanism and propagation of load-induced cracks in the beams. Quantification

of the ASR-induced pre-stress effect in the longitudinal tensile reinforcement bars was measured by strain gauges on sawn beams and compared to in-situ measurements on the slab bridge.

2. Materials

The shear tests were conducted on beams sawn from a severe ASR-damaged flat slab bridge located in the northern part of Denmark. The bridge was built in 1966-1967 as a multi-span pile supported slab.

Figure 1: (a) Sawn slab segment at laboratory facility of the Technical University of Denmark. (b) The bridge slab after sawing of a segment.

The bridge slab is 312 m long, 10 m wide and 0.3 m thick. Six large slab segments, 2.2 m wide and ranging from 2.4 to 4.2 m long; see Fig. 1a, were sawn from the western part of the slab; see Fig. 1b, and transported to laboratory facilities at the Technical University of Denmark. Each slab segment was then sawn into seven beams with different widths and lengths; see Fig. 2. Three of these beams, denoted A, were used for shear tests and the remaining four beams, denoted B, were used for core drilling and quantification of the ASR-induced pre-stress in the tensile reinforcement.
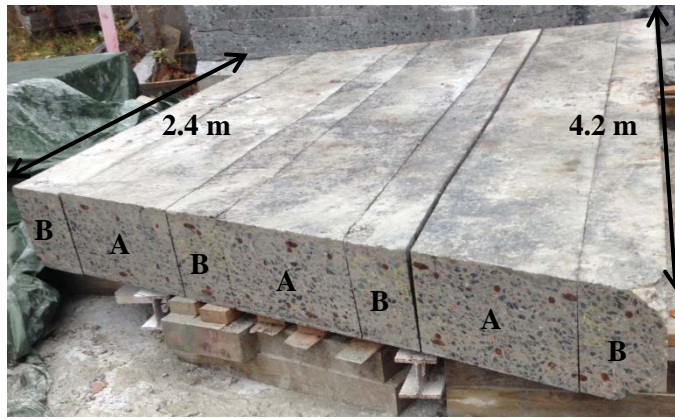
Figure 2: The slab segments sawn into beams. Beams A used for shear tests. Beams B used for core drilling and quantification of ASR-induced pre-stress effect.

The width of the 18 beams used for shear testing varied from 0.41 to 0.45 m, the length varied from 2.6 to 3.7 m and the height was 0.30±0.03 m. The beams were reinforced with three longitudinal Ø16 mm ribbed bars at the bottom and two longitudinal Ø 16 mm ribbed bars at the top.

2.1 Visual appearance and condition of the ASR-damaged slab segments

ASR cracks were observed in all segments. Fig. 3 shows the typical ASR crack pattern on a sawn beam surface. The cracks are predominantly oriented parallel to the longitudinal reinforcement. This crack pattern was expected since the slabs were not provided with shear reinforcement, which mean that the vertical ASR expansion was not restrained.

Figure 3: Typical ASR crack pattern on the section of segment 5.

Visually, segment 2 had less cracks compared to the other segments. There were no visual differences in the extent of ASR cracks between segments 1 and 3 to 6. Thin-section examinations confirmed that ASR was the main cause for the cracking. The ASR cracks were formed due to reactions of porous opaline flint in the sand fraction. However, reinforcement corrosion was found to contribute to an increase in crack widths. Locally, larger crack widths around the top and bottom reinforcement were observed in segments 4 and 6. The largest crack widths due to corrosion and ASR were observed at the top of segment 6, see Fig. 4. As can be seen in the figure, the crack widths in the bottom face of the beam are considerably smaller than in the compression zone.

Figure 4: Local increase in crack widths in compression zone of a beam from segment 6 due to combined effect of ASR and corrosion.

2.2 Compressive strength of drilled cores

In total 93 cores were drilled vertically or horizontally from the beams. Fig. 5 shows the average compressive strength from these cores and Table 1 shows the estimated original (undamaged) compressive strength, $f_{c,ori}$. $f_{c,ori}$ was estimated by means of fluorescence microscopy in accordance with the method proposed by Thaulow *et al.* [20]. The variations of $f_{c,ori}$ are due to inhomogeneity in the water-cement ratio and air content on each individual segment. As seen in Fig. 5 the compressive strength of the cores is dependent on crack orientation; the strength in the direction perpendicular to ASR cracks ($f_{c,90}$) corresponding to vertical drilling, is significantly lower than the strength in the direction parallel to ASR cracks ($f_{c,0}$).
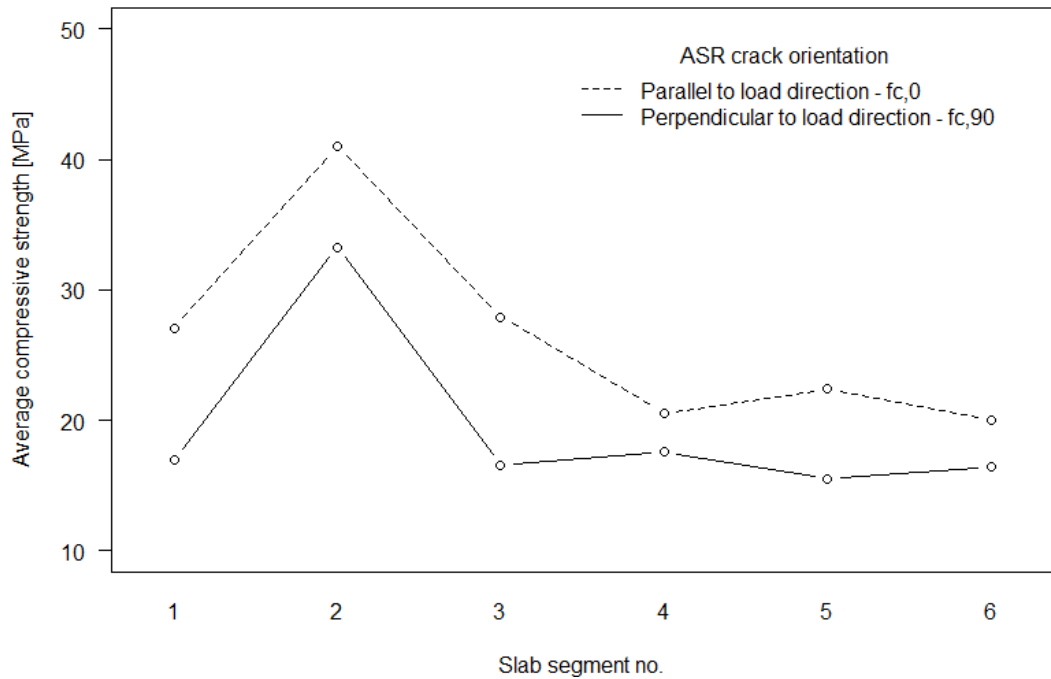
Fig. 5: $f_{c,0}$ (parallel cracks) and $f_{c,90}$ (perpendicular cracks) for the six slab segments.

$f_{c,0}$ and $f_{c,90}$ in segment 2 are significantly higher than the other segments. This difference in strengths corresponded well to the visual appearance of segment 2 compared to the other segments. For the other segments there was no visual difference between the extents of ASR cracks. However, it seems that $f_{c,0}$ is higher for segments 1 and 3 than for segments 4, 5 and 6. Comparing Fig. 5 and Table 1 it is seen that $f_{c,0}$ and $f_{c,90}$ for most segments are significantly lower than $f_{c,ori}$. $f_{c,90}$ has decreased by up to 64%.

Table 1: Estimated original compressive strength, $f_{c,ori}$ and variations determined by means of fluorescence microscopy.

Slab segment no.	1	2	3	4	5	6
$f_{c,ori}$ (and variations) [MPa]	37.5 (35-40)	45 (40-50)	42.5 (40-45)	42.5 (40-45)	42.5 (40-45)	37.5 (35-40)

3. Experimental program

3.1 Test setup

Shear tests on 18 beams were conducted. Nine beams (from segments 2, 3 and 6) were tested in a three-point bending test setup, see Fig. 6. Nine beams (from segments 1, 4 and 5) were tested in an asymmetrical four-point bending setup, see Figs. 7 and 8. In the

8

three-point bending setup all beams were simply supported and subjected to one point load. In the asymmetrical four-point setup the specimens were subjected to two point loads by means of a steel spreader beam. Figs. 6 and 7 illustrate the bending test setups which include bending moment and shear diagrams. 12 mm low-density wood fiber boards were used as intermediate layer between the beams and the supports to compensate for minor geometrical imperfections in the beams. For beams from the same segment in the three-point bending setup the shear span $a = M_u/V_u$, where M_u being the maximum moment carried by the beams and V_u the shear force, varied corresponding to an a/d-ratio of 2.8 to 4.2. For beams tested in the four-point bending setup the shear span $a = M_{C,u}^+/V_{II,u}^+$, where $M_{C,u}^+$ being the ultimate positive moment at C and $V_{II,u}^+$ the ultimate shear force carried by the beams at shear zone II, varied corresponding to an a/d-ratio of 2.2 to 4.4. Appendices B and C provide detailed geometrical parameters of the beams in both experimental setups.
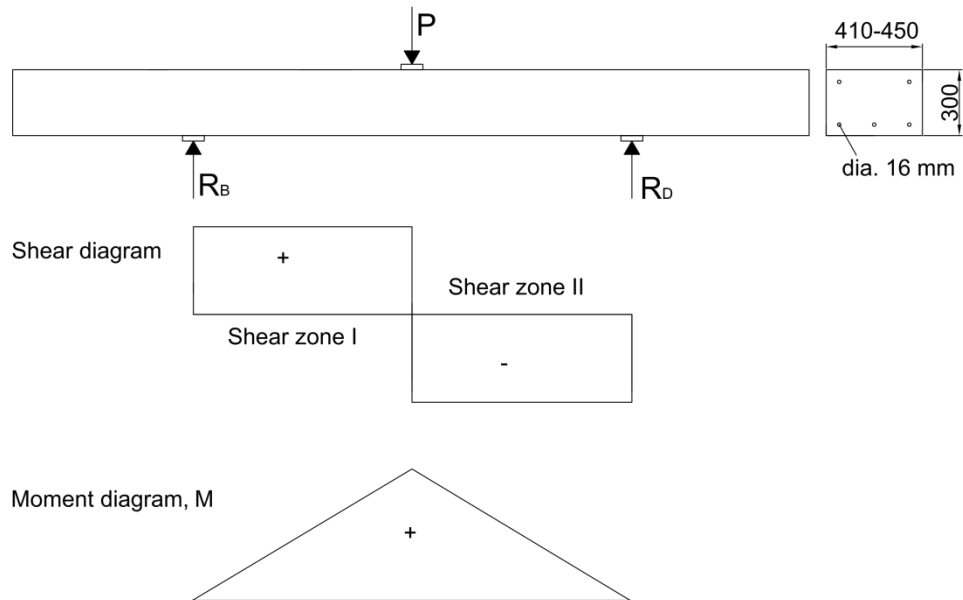
Fig. 6: Illustration of the three-point bending test setup with corresponding shear diagram and moment diagram. Dimensions are given in mm.
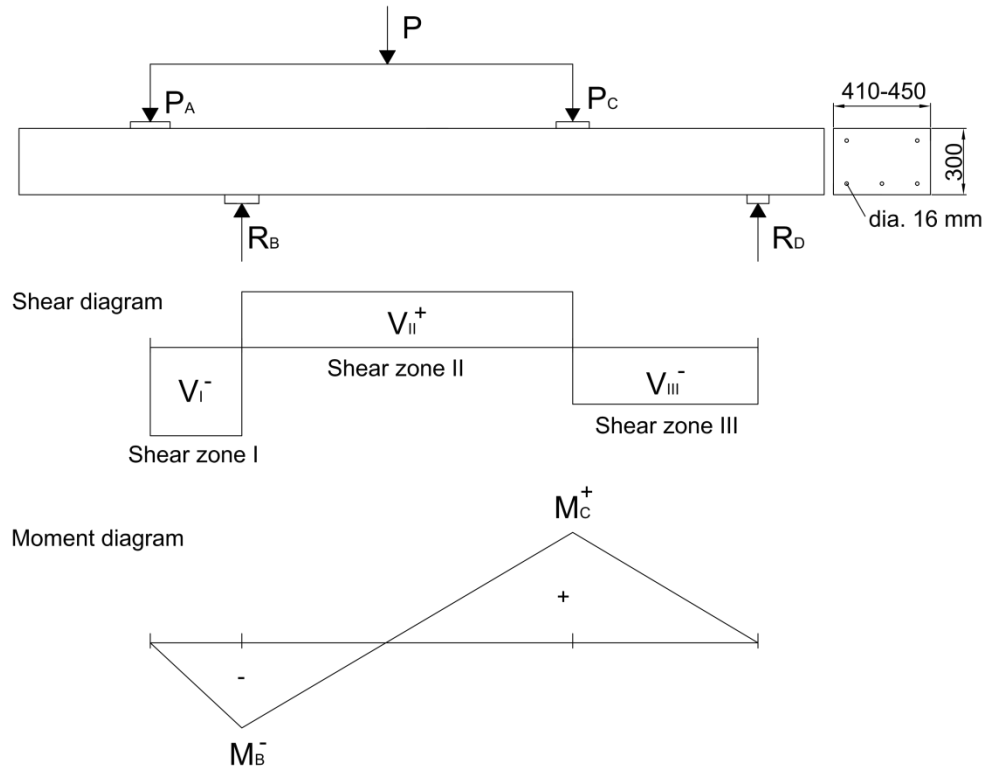
Fig. 7: Illustration of the asymmetrical four-point bending test setup with corresponding shear diagram and moment diagram. Dimensions are given in mm.

3.2 Load and deflection measurements

The beams were loaded by a displacement controlled servo-hydraulic actuator. The load was applied by a constant displacement rate of 0.5 mm/min. The beam deflection was measured on top of the beams by LVDT's fastened to an external steel frame; see Fig. 8. The deflection was measured on each side of the beam to evaluate possible rotation during loading. A total of 14 LVDT's were used in the four-point bending setup and 8 LVDT's were used in the three-point bending setup.
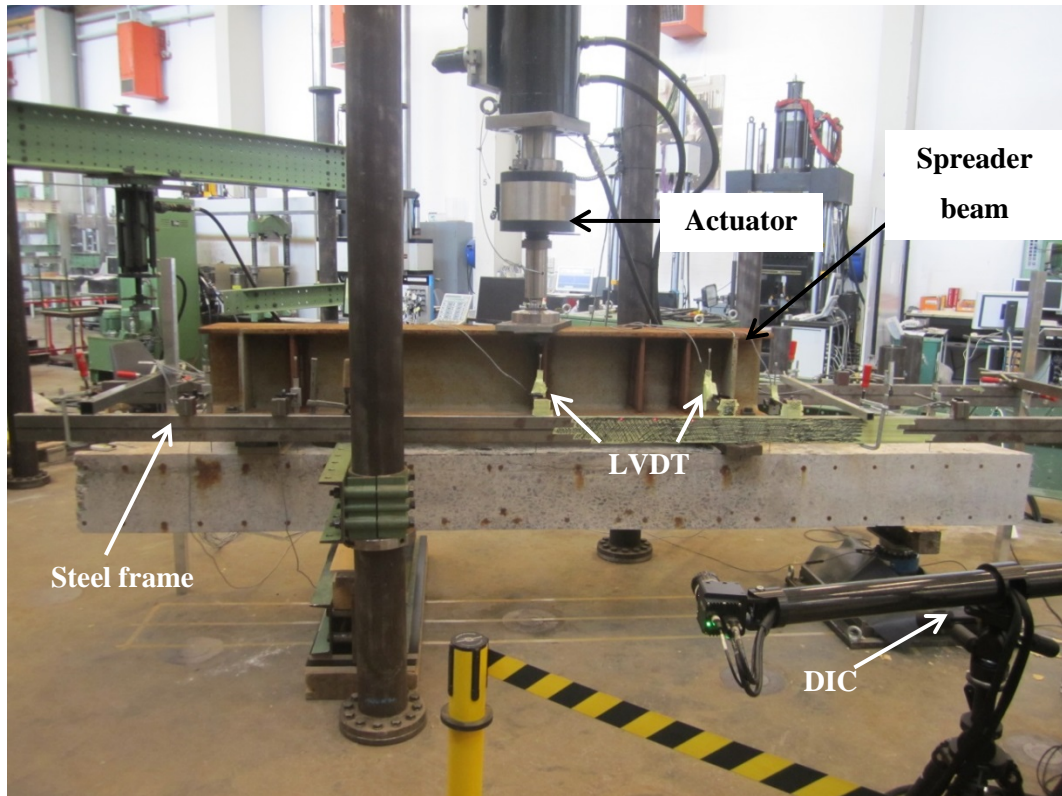
Fig. 8: Photo of the four-point bending test setup.

3.3 Digital Image Correlation measurements

DIC system was applied to evaluate the failure mechanism and the propagation of load-induced cracks on the surface of the beams; see Fig.8. A 3D measuring system was used in this shear test series. The digital images acquired by two 12 megapixels cameras were analysed by a commercial DIC software system called ARAMIS.

3.4 Quantification of ASR-induced pre-stress

Measurements of the tensile strains on a number of longitudinal reinforcing bars embedded in the beam specimens (of type B in Fig. 2) were performed to quantify the ASR-induced pre-stress effect.The method used basically consisted of removing (locally) the concrete around the bar over a length of 20 mm. Linear strain gauges of type HBM LY41-6/120 were then installed on the exposed part of the bars. Finally, each bar was cut 0.15 m from location of the strain gauge. The contraction measured by the strain gauge due to the cutting is a measure of the pre-stress in the bar. Measurements continued for approximately 10 to 20 minutes after cutting in order to avoid possible thermal influence from the cutting. In total, 21 strain gauge measurements were performed on bars embedded in the beam specimens. Additionally, three in-situ strain gauge measurements were conducted on bars in the slab bridge to compare them with results from the sawn beams.

4. Test results and discussions

4.1 Quantification of ASR-induced pre-stress effect

Fig. 9 shows the measured tensile strains, ε_{ASR}, in reinforcement bars where each point corresponds to one strain gauge measurement. ε_{ASR} varied from 0.7‰ to 1.4‰ which corresponds to tensile stresses of 150 to 300 MPa, respectively. On the average the Young's modulus, E_s, of the bars was measured to 214 GPa. For segments 1, 2, 4 and 5 the yield strength of the bars, f_y, was measured to 580 MPa whereas for segment 3 and 6 f_y was measured to 623 MPa. Thus, the reinforcement was pre-stressed to yielding due to ASR expansion.
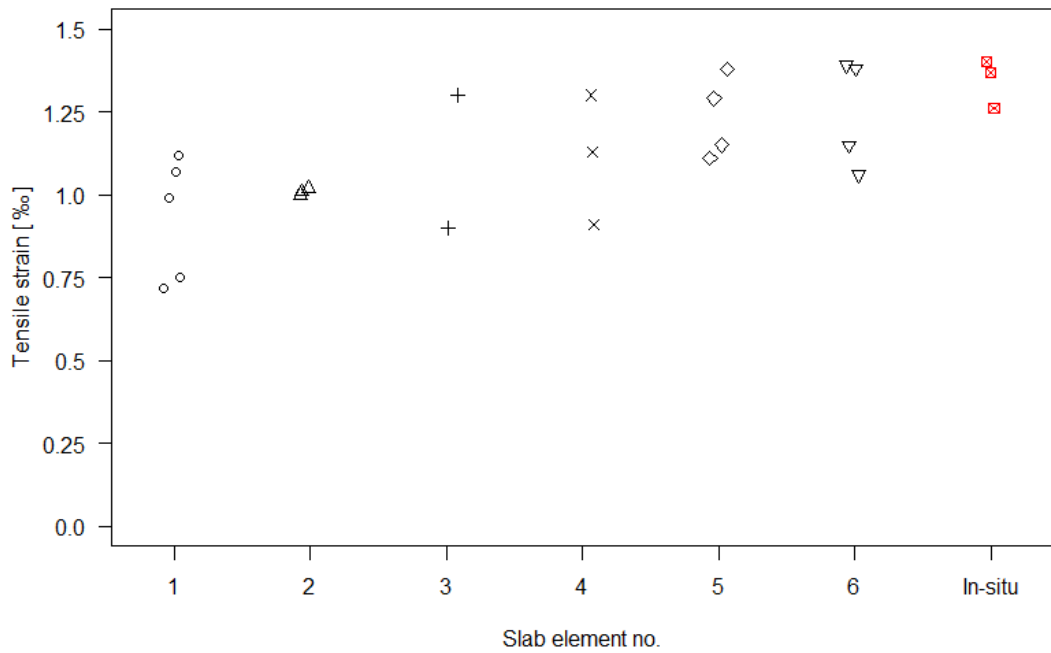
Figure 9: Tensile strains, ε_{ASR}, measured in tensile reinforcement bars.

As seen in Fig. 9 the ASR-induced expansion caused significant tensile strains in the bars. The in-situ strain measurements are comparable to ε_{ASR} on segment 3 to 6. The large scatter of ε_{ASR} in the beams may be explained by insufficient anchorage of the reinforcing bars due to ASR cracks. Based on the results we may argue that ε_{ASR} is not proportional to the visual appearance of ASR cracks and the compressive strength of the segments. Segment 2 had fewer ASR cracks and both $f_{c,0}$ and $f_{c,90}$ were significantly higher than the other segments. Despite this, ε_{ASR} in segment 2 is equal to ε_{ASR} in segment 1 and not significantly smaller than ε_{ASR} in the other segments. These results indicate that ε_{ASR} develops rapidly in the early formation of ASR cracks.

4.2 Shear tests in three-point bending setup

Eight beams were tested symmetrically in the three-point setup. Beam 6.1 was tested asymmetrically. The most severe deteriorated areas in the beams from segment 6, see Fig. 4, were placed at shear zone I in Fig. 6. The geometrical parameters and test results of each beam in the three-point setup are listed in Table 2. The calculated sectional moment capacity, M_{calc}, is based on $f_{c,0}$.

4.2.1 Load-deflection response

Fig. 10 shows the load-deflection response of the beams. The depicted deflection is based on the average deflection of four LVDTs located next to the point load, P. As can be seen from the figure there was a problem in collecting data for beam 2.3 until approximately 280 kN. Generally, it was observed that most of the beams (with the exception of beam 6.3) suffered a ductile failure. Nevertheless, beams 2.1, 2.2 and 2.3 were more ductile than the other beams. Table 2 shows the deflection δ_u at ultimate load P_u.
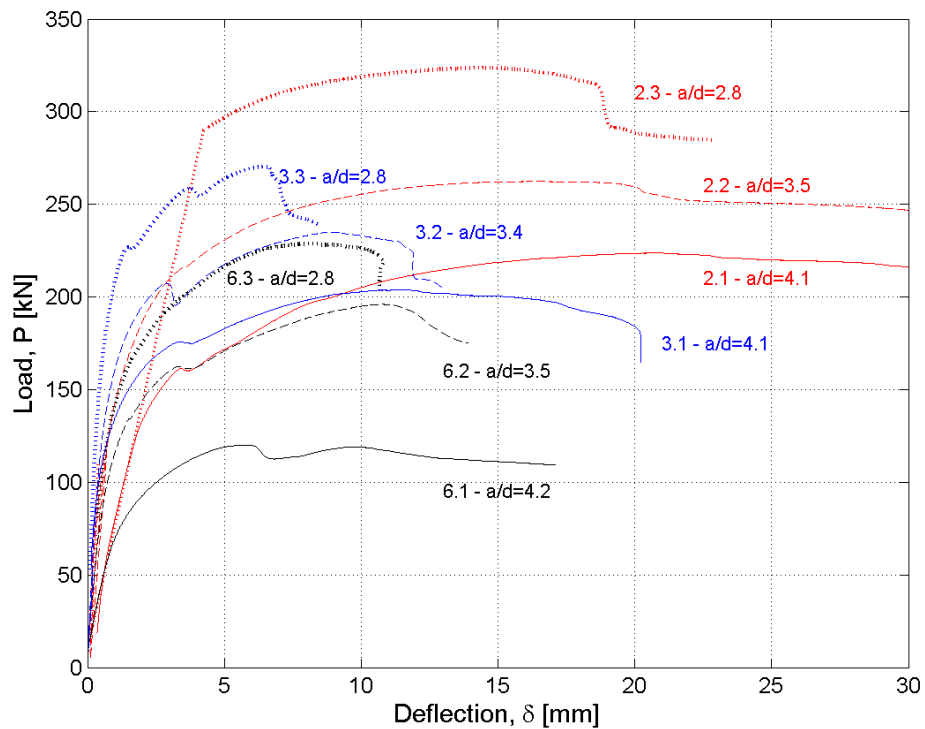
Fig. 10: Three-point bending setup. Load-deflection response.

13

Table 2: Geometrical parameters and test results of each beam tested in the three-point bending setup.

	Beam no.	b [mm]	d [mm]	P_u [kN]	V_u [kN]	M_u [kNm]	τ_u [MPa]	δ_u [mm]	a [mm]	a/d [-]	M_u/M_{cal} c
Slab segment 2	2.1	435	247	224	112	112.2	1.04	20.6	1002	4.1	1.22
	2.2	410	242	262	131	111.2	1.32	16.4	849	3.5	1.27
	2.3	445	247	324	162	113.4	1.47	14.7	700	2.8	1.25
Slab segment 3	3.1	450	242	204	102	102.0	0.94	11.5	1000	4.1	1.15
	3.2	450	247	235	118	99.9	1.06	8.9	851	3.4	1.10
	3.3	445	252	270	135	94.2	1.20	6.5	698	2.8	1.04
Slab segment 6	6.1	425	237	120	74	73.8	0.73	5.8	997	4.2	0.90
	6.2	440	242	196	98	83.6	0.92	10.8	853	3.5	1.01
	6.3	430	247	229	114	80.1	1.08	8.2	703	2.8	0.94

4.2.2 Failure mechanism

Fig. 11 shows major strain plots from DIC measurements at the ultimate load, P_u. As can be seen, the failure mechanism in the beams varied from beam to beam and within beams with same a/d-ratio. Generally, most beams suffered a rotational failure in diagonal cracks with yielding of the tensile longitudinal bars and formation of horizontal cracks in the compressive zone. This evaluation is supported by the M_u/M_{calc} in Table 2, and the ductile load-deflection response in Fig. 10. The ASR cracks clearly influenced the propagation of the load-induced cracks, where horizontal ASR cracks along the tensile bars particularly affected the propagation of bending cracks (beams 2.2, 2.1 and 6.1). In experiments with concrete without ASR, we expected that a fan of bending cracks would form around the point load. These bending cracks propagate from the bottom of the beams towards the compressive zone. However, for Beams 2.2, 2.1 and 6.1 the bending cracks were affected the horizontal ASR cracks at level of tensile bars.

In similar experiments with concrete without ASR, the diagonal shear cracks were convex in shape due to the distribution of the principal stresses in the uncracked concrete. However, it was observed that diagonal cracks in some beams (beams 2.3, 2.2, 3.2, 6.2 and 2.1) tended to have a concave shape, where they partially followed the horizontal ASR cracks. Once the diagonal cracks reached the tensile bars they followed the horizontal ASR-induced cracks along the bars. In other beams (beams 3.3, 6.3, 3.2, 6.2, 3.1 and 6.1) the diagonal cracks developed almost straight from the support to P. In beams 3.2 and 6.2 both types of diagonal cracks were observed in each shear zone.

As can be seen in Fig. 11 the failure mechanisms of beams 6.1 and 6.3 are significantly different from those of corresponding beams with same a/d-ratios. The DIC measurements indicate that the failure of beam 6.1 might be a bending failure with horizontal movements between the layers seperated by the horizontal ASR cracks. The measurements for beam 6.3 did not indicate bending failure. Nonetheless, as Fig. 11 shows the crack propagation differs significantly from the expected pattern in a similar test with concrete without ASR. It may not be a coincidence that both of the beams from segment 6, differ from the other beams. $f_{c,0}$ for segment 6 was lower than for the other segments. Additonally there were significantly larger crack widths in parts of the compression zone of segment 6 due to combined effect of corrosion and ASR.

15
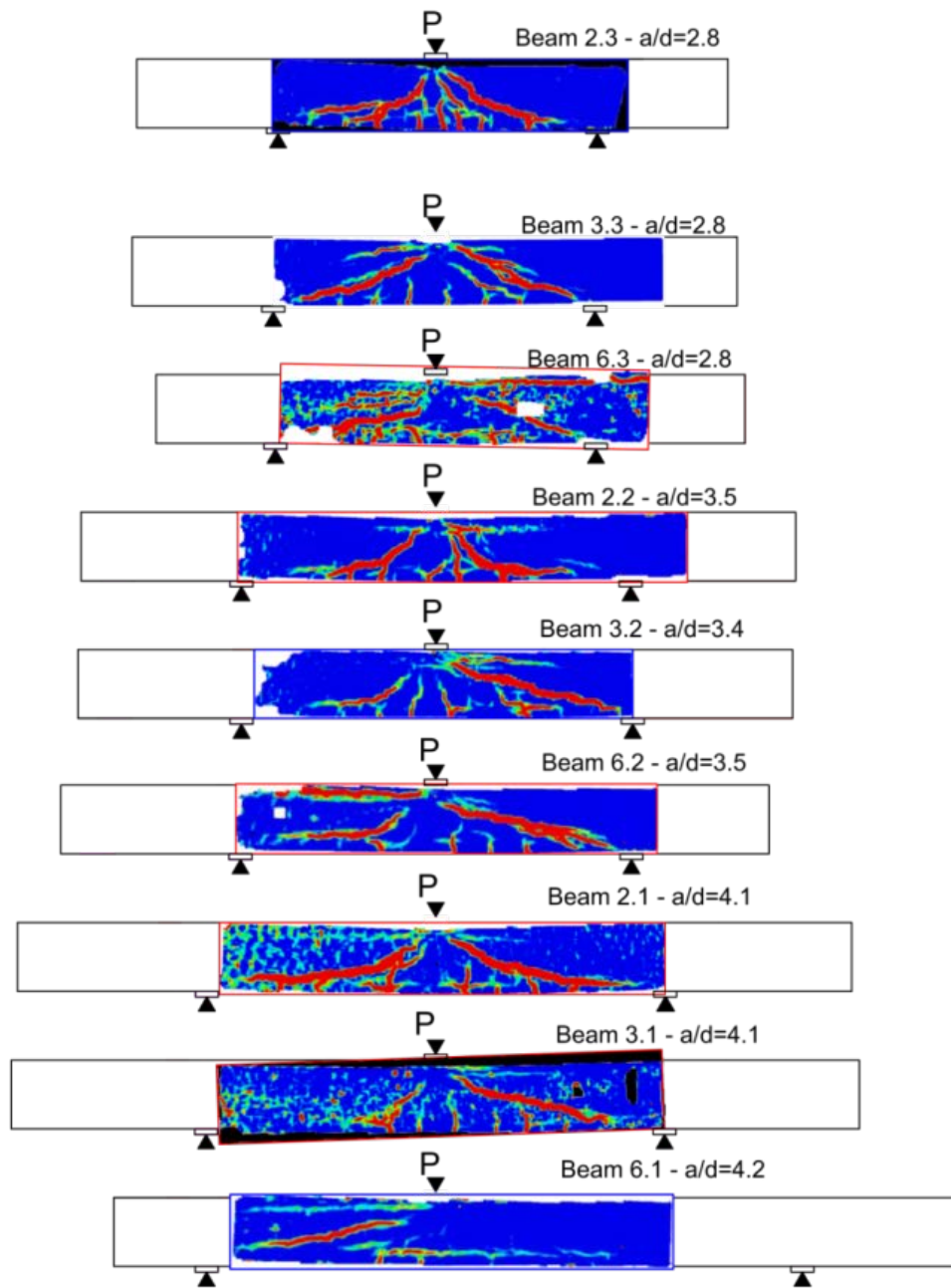
Fig. 11: Major strain plot at P_u for the three-point bending setup.

4.2.3 Strength as function of a/d-ratio

Figs. 12 and 13 present the test results in terms of the measured shear strengths $\tau_u = V_u/bd$ as well as M_u/bd^2, as a function of the a/d-ratios. Here $M_u = V_u \cdot a$. Since the beams suffered rotational failure in diagonal cracks (bending type of failure) the results from the three-point setup (with exception of beam 6.3) are not an expression for the shear strength but for the moment capacity of the beams. However, it can be concluded that the actual shear strength of the beams is larger than the measured shear strengths governed by the rotational failure. Therefore the shear test results for the three-point bending setup can be

16

regarded as lower limit for the actual shear strengths. Due to this type of failure, the decrease of τ_u for increasing a/d-ratios as can be seen in Fig. 12 is simply caused by a larger moment; see Fig. 13.
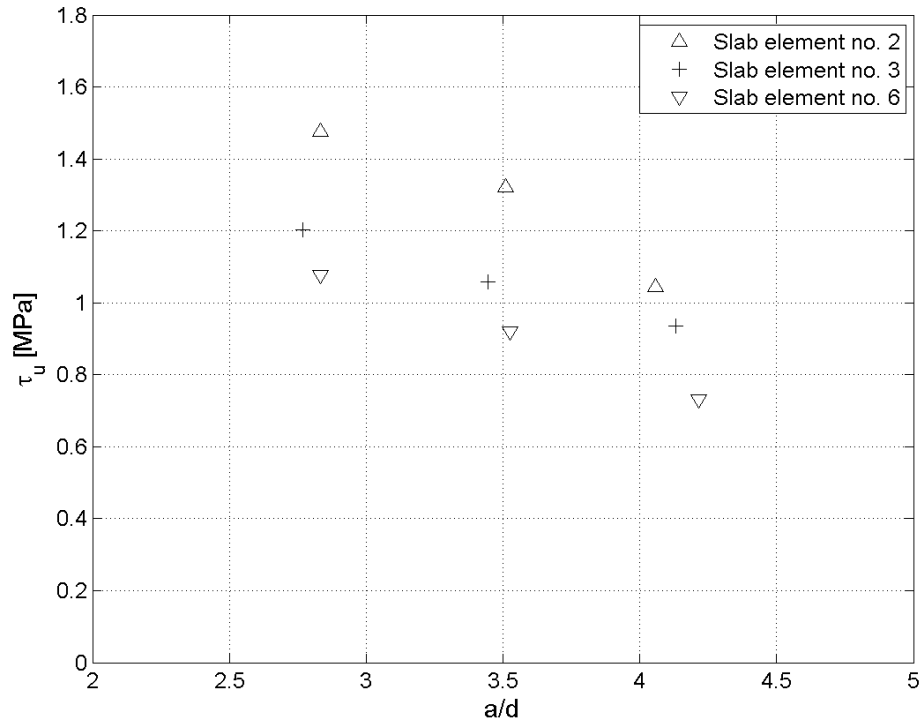

Figure 12: Thee-point bending setup. τ_u as a function of a/d-ratio.
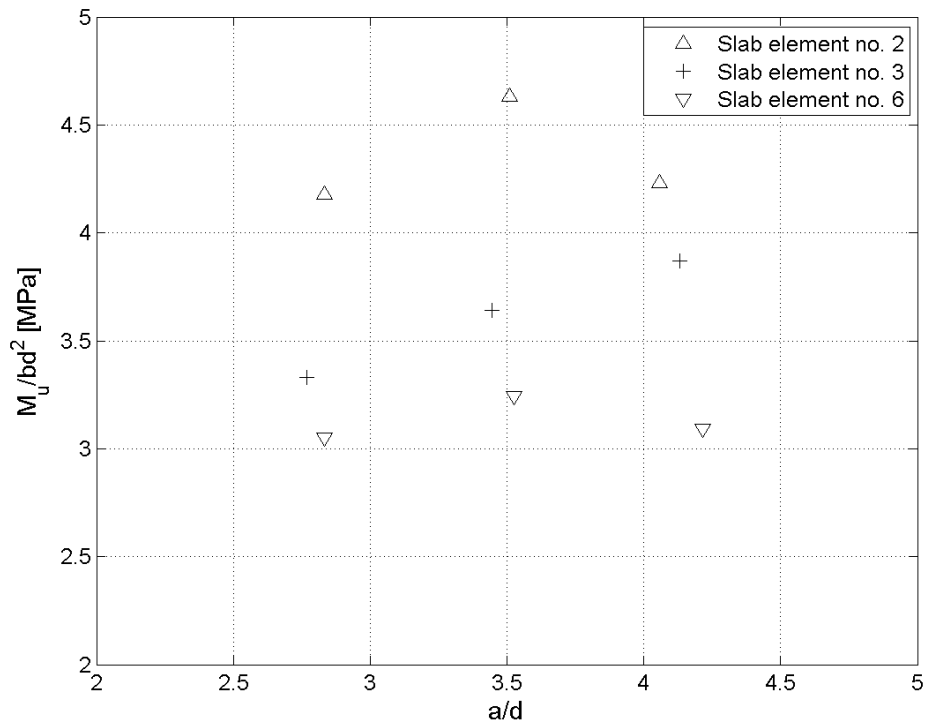
Figure 13: Three-point bending setup. M_u/bd^2 as a function of a/d-ratio.

Clearly, as seen in Fig. 12 and 13, the measured strengths (τ_u and M_u) depends on which segment the beams were sawn from. $f_{c,0}$ and $f_{c,90}$ for segment 2 were considerably higher than the other segments. $f_{c,0}$ for segment 3 was higher than for segment 6. However, $f_{c,90}$ was almost the same for both segments no. 3 and 6. This may indicate that $f_{c,0}$ better illustrates the moment capacity of the beams than $f_{c,90}$.

4.3 Shear tests in four-point bending setup

Nine beams were tested asymmetrically in the four-point bending setup. The geometrical parameters and test results of each beam tested in the four-point setup are listed in Table 3. M_{calc} in table 3 is based on $f_{c,0}$.

4.3.1 Load-deflection response

Fig. 14 shows the load-deflection response of the beams. The depicted deflection is based on two LVDTs located at the left side of the point load, P_c; see Fig. 7. As can be seen the majority of the beams suffered a ductile failure. However, as can be seen from Table 3, $\delta_{c,u}$ for beams 5.1 and 1.2 are considerably lower than for corresponding beams with same a/d-ratios. Contrary to the three-point bending tests, the load-deflection curves here display both a concave and a convex part in the pre-peak regime. This may be explained by the closure/compaction of horizontal ASR cracks. Apparently, the flatter the concave part, the lower the $P_{c,u}$.
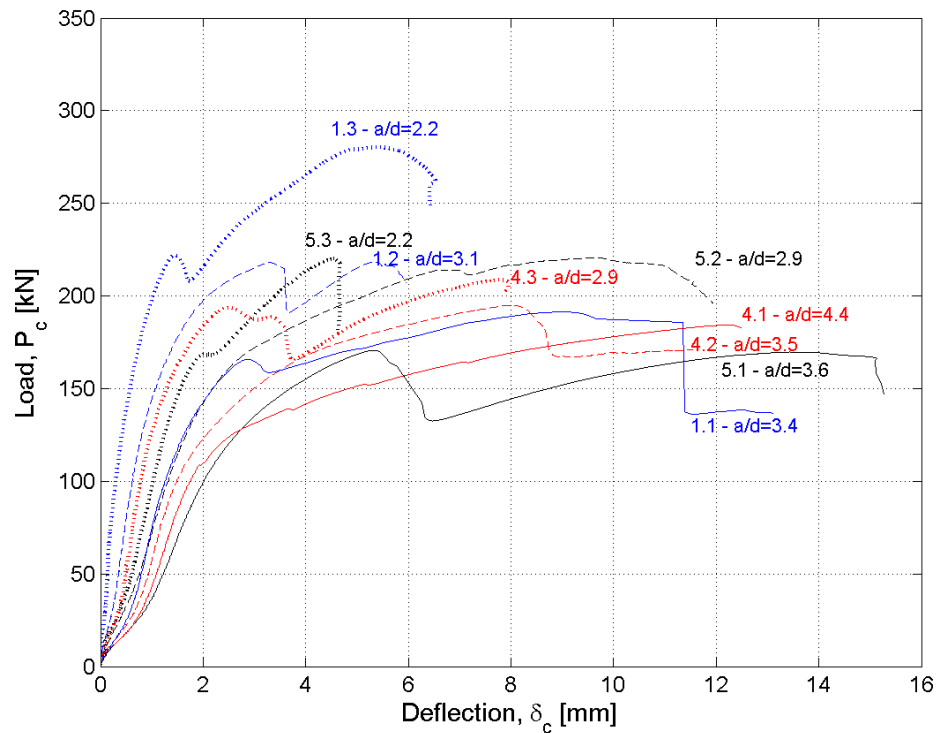
Fig. 14: Four-point bending setup. Load-deflection response.

4.3.2 Failure mechanisms

Fig. 15 shows major strain plots from DIC measurements at ultimate load, P_u. Generally, it was observed that the failure of the beams could be roughly divided into three types of shear failure mechanisms:

1) Formation of almost straight diagonal cracks from R_B to P_c (beams 4.3, 5.1 and 5.3). The diagonal crack followed stepwise the horizontal ASR cracks and therefore had a flatter nature than the diagonal cracks in the other beams.

2) Formation of both concave and convex diagonal cracks (beams 1.1, 1.3, 4.1 and 5.2). A concrete compressive strut is observed between these two diagonal cracks. For beam 4.1, large ASR-induced cracks in the compression zone seems to affect the failure mechanism.

3) Formation of concave diagonal crack (beams 1.2 and 4.2). In the beginning, the diagonal cracks follow stepwise the ASR cracks until they reach the level of tensile bars. Subsequently, the crack propagated along the tensile bars. Additionally, for beam 4.2 bending cracks were formed discontinuously due to horizontal movements in the horizontal cracks in the level of tensile bars. In beam 4.2 large crack widths were observed in the level of tensile bars due to the combined effect of ASR and corrosion.

19
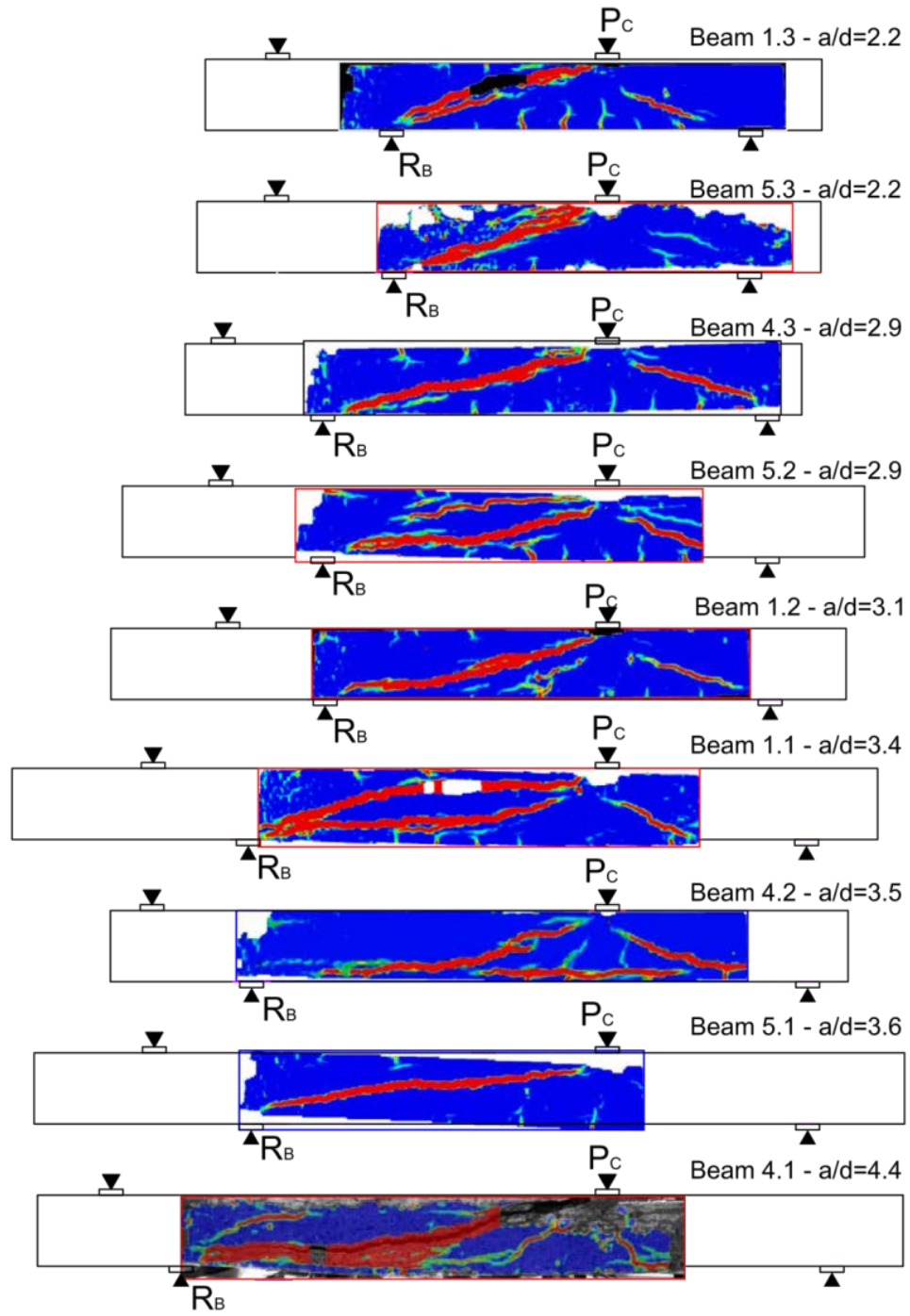
Fig. 15: Four-point bending setup. Major strain plots at P_u.

Table 3: Geometrical parameters and test results of each beam tested in the four-point bending setup.

Slab no.	Beam no.	b [mm]	d [mm]	P_u [kN]	$P_{A,u}$ [kN]	$V_{u,I}^-$ [kN]	$M_{B,u}^-$ [kNm]	$P_{C,u}$ [kN]	$V_{II,u}^+$ [kN]	$M_{C,u}^+$ [kNm]	$\delta_{C,u}$ [mm]	τ_u [MPa]	a [mm]	a/d [-]	$M_{C,u}^+/M_{calc}$ [-]
Slab segment 1	1.1	420	247	341	150	-150	-62.1	191	95	80.8	9,0	0.92	851	3.4	0.96
	1.2	435	242	333	115	-115	-47.1	218	104	77.5	3.1	0.99	745	3.1	0.91
	1.3	425	247	394	113	-113	-54.4	281	148	80.2	5.4	1.41	542	2.2	0.95
Slab segment 4	4.1	445	237	409	224	-224	-66.2	185	88	91.5	12.2	0.83	1040	4.4	1.19
	4.2	425	242	347	152	-152	-63.8	195	97	82.5	8.0	0.94	851	3.5	1.06
	4.3	450	247	325	116	-116	-48.9	209	101	72.5	7.8	0.91	718	2.9	0.90
Slab segment 5	5.1	450	242	302	131	-131	-53.5	171	84	73.1	5.3	0.77	870	3.6	0.92
	5.2	430	242	344	123	-123	-53.1	221	108	76.2	9.6	1.04	706	2.9	0.97
	5.3	410	247	304	84	-84	-41.5	220	116	62.6	4.5	1,15	540	2.2	0.78

4.3.3 Shear strength as function of a/d-ratio

Fig. 16 shows the measured shear strengths $\tau_u = V_{II,u}^+/(bd)$, as a function of a/d-ratio. As can be seen the variation in a/d-ratio between 2.2 to 4.4 had a significant influence on the measured shear strengths. Generally, τ_u for beams with similar a/d-ratios did not differ significantly from each other. However, it was observed that beams 4.3, 5.1 and 5.3 had lower τ_u than beams with similar a/d-ratios. These beams had the same type of failure mechanism; a diagonal crack direct from R_B to P_c; see Fig. 15. It may not be a coincidence that the failure of beams from slab segments 4 and 5 were more influenced by the ASR cracks. These segments had a lower $f_{c,0}$ and a larger ε_{ASR} than segment 1.
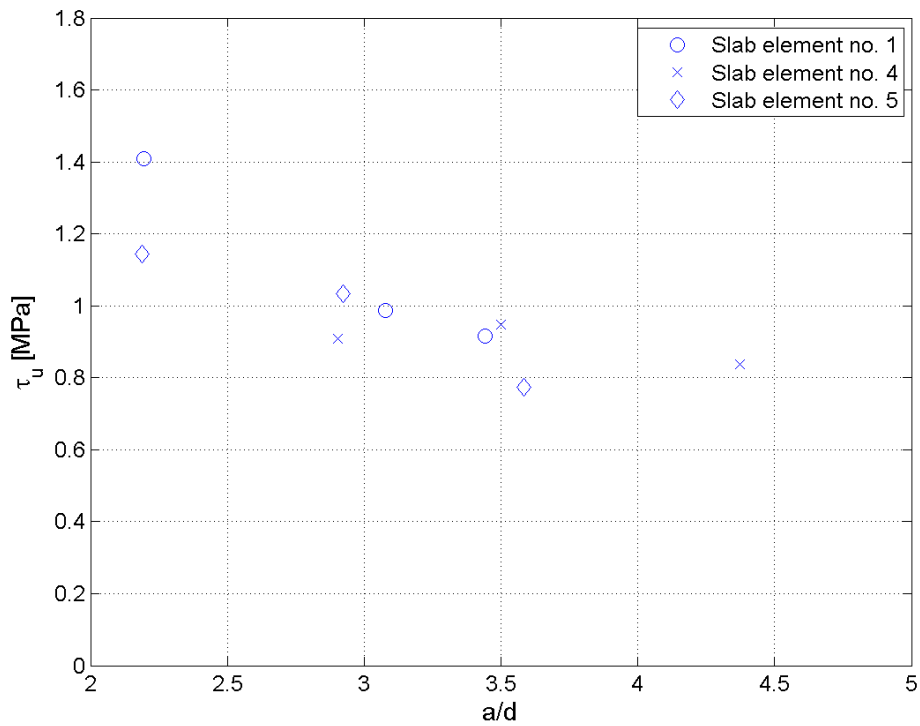
Figure 16: Four-point bending setup. τ_u as a function of a/d-ratio.

4.4 Comparison of three-point and four-point bending setup

Fig. 17 shows the measured shear strengths from the six segments. Despite that the results from the three-point bending setup are a lower limit for the shear strength, it can be seen that τ_u determined from the four-point bending setup (blue marks) is generally lower than τ_u from the three-point bending setup (black marks). Consequently, the test setup has a considerable influence on τ_u. This may not be a surprise, since the failure

mechanisms and load-deflection response of the beams were considerably different between the two test setups.
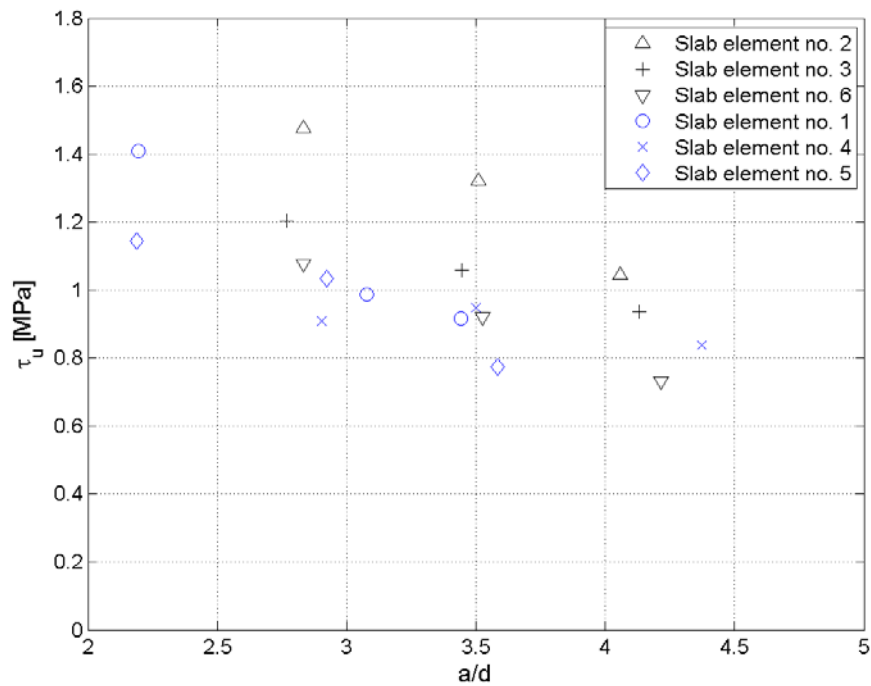

Figure 17: Three-point (black marks) and four-point bending setup (blue marks). τ_u as a function of a/d-ratio.

5. Comparison of the test results and Eurocode 2 calculations

The shear test results are compared with shear strength calculations, τ_{calc}, in accordance with Eurocode 2 design code, EC2, (DS/EN 1992-1-1 incl. the Danish Annex) [21,22]. The EC2-formula for shear capacity of members without shear reinforcement is empirical and developed for design of new structures and is not intended for ASR-damaged structures. Nonetheless, since there are no commonly accepted methods with which to assess the residual shear strength for ASR-damaged structures, the residual shear strength in Denmark is often assessed by use of the EC2. To evaluate the influence of various parameters on the calculated capacity, calculations based on the EC2-formula have been performed by use of $f_{c,90}$, $f_{c,0}$ as well as $f_{c,ori}$. In addition, the calculations were also performed with and without inclusion of the ASR-induced pre-stress effect.

For beams from segments 2, 3 and 6 (except beam 6.3) the maximum moment carried by the beams M_u are compared to the calculated sectional moment capacity M_{calc} due to the

bending type of failure for these beams. For beams from segments 1, 4 and 5 the measured shear strengths τ_u are compared with calculated shear strengths τ_{calc}, since the beams suffered ductile shear failure.

5.1 Calculations based on $f_{c,90}$ without pre-stress effect

Fig. 18 shows the ratios between the test results (τ_u and M_u) and the calculated strengths (τ_{calc} and M_{calc}). The calculated strengths in Fig. 18 are based on $f_{c,90}$ without inclusion of the pre-stress effect. As can be seen in Fig. 18a there is poor agreement between τ_{calc} and τ_u. τ_u is larger than τ_{calc}. Especially, at lower a/d-ratios the shear strength calculations are lower than the measured shear strengths. From Fig. 18a we may argue that by use of $f_{c,90}$ without inclusion of pre-stress effect, the shear strength calculations may always be rather conservative. As can be seen in Fig. 18b M_{calc} (using $f_{c,90}$) are in most cases lower than M_u for the three-point bending tests. However, for beam 6.1 M_u is 93% of M_{calc}. Despite severe crack widths in the compressive zone of beams from segment 6, M_{calc} is not significantly smaller than M_u for beam 6.1. Consequently, M_{calc} (using $f_{c,90}$) may be rather conservative to be used for ASR-damaged beams.
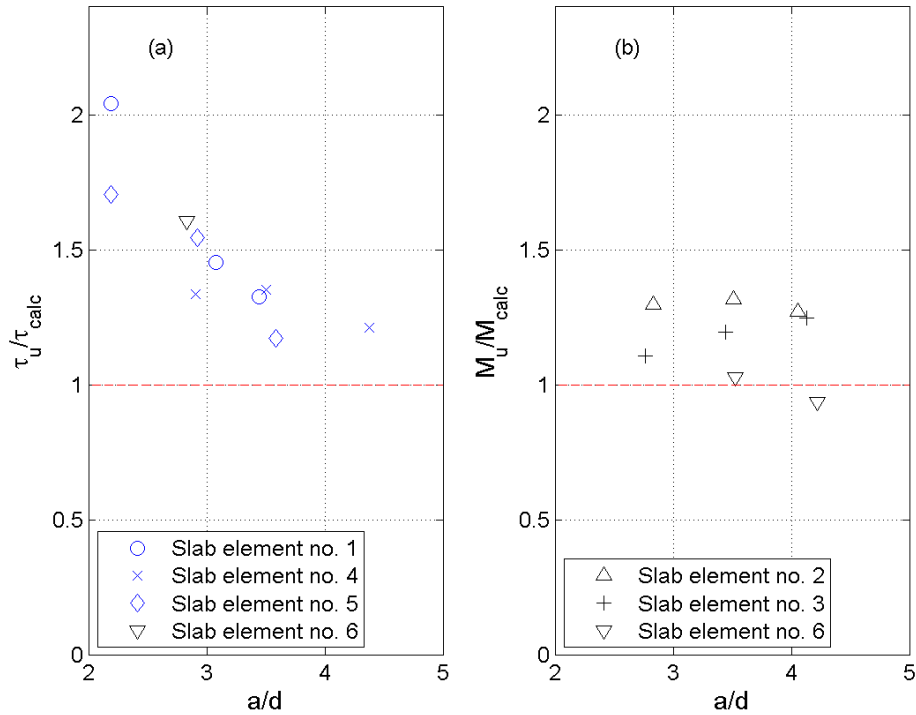

Figure 18: (a) τ_u/τ_{calc} as a function of a/d-ratio. (b) M_u/M_{calc} as a function of a/d-ratio. τ_{calc} and M_{calc} based on $f_{c,90}$ without inclusion of pre-stress.

5.2 Calculations based on $f_{c,0}$ without pre-stress effect

Fig. 19 shows the ratios between the test results (τ_u and M_u) and the calculated strengths (τ_{calc} and M_{calc}). In Fig. 19 the calculated strengths are based on $f_{c,0}$ without inclusion of the ASR-induced pre-stress effect. As can be seen from Fig. 19a the shear strength calculations are still conservative at lower a/d-ratios. As can be seen in Fig. 19b M_u is larger than M_{calc} for most beams except for beam 6.1. For beam 6.1 M_{calc} is as expected higher than M_u (now by 10%) since $f_{c,0}$ is 23% bigger than $f_{c,90}$ for this segment. For beams from segment 2 with high $f_{c,0}$ and a lesser degree of ASR cracking M_u is approximately 25% higher than $M_{calc.}$ Comparing Fig. 18 with Fig. 19 shows that the benefit of applying $f_{c,0}$ instead of $f_{c,90}$ in the calculations is negligible. Consequently, for ASR-damaged slabs the use of $f_{c,90}$ is recommended since it is the most cost-effective in-situ drilling orientation.
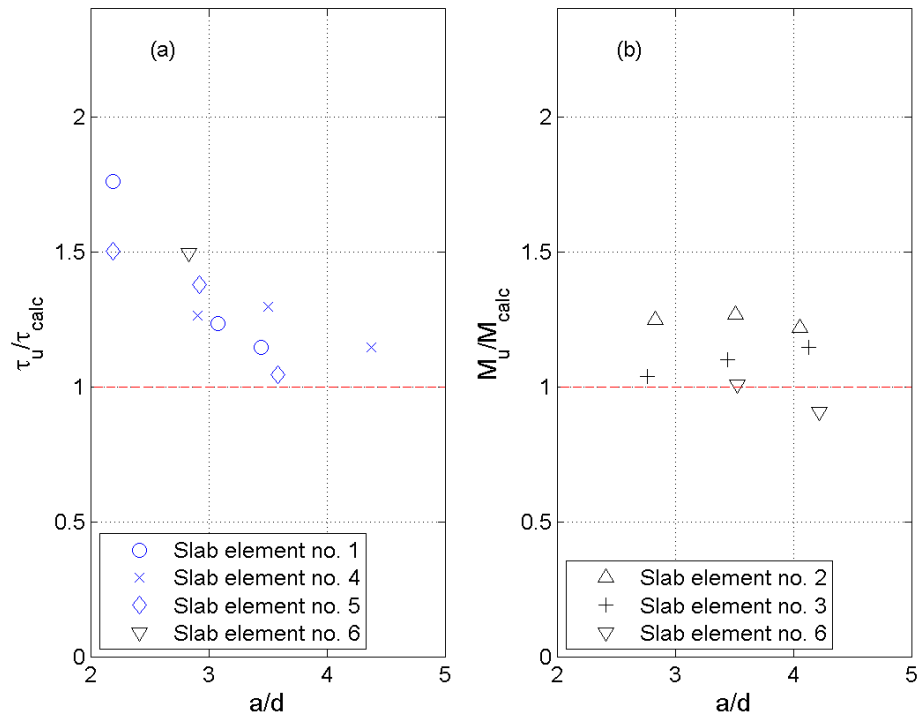
Figure 19: (a) τ_u/τ_{calc} as a function of a/d-ratio. (b) M_u/M_{calc} as a function of a/d-ratio. τ_{calc} and M_{calc} based on $f_{c,0}$ without inclusion of pre-stress.

5.3 Calculations based on $f_{c,ori}$ without pre-stress effect

Fig. 20 shows the ratios between the measured strengths (τ_u and M_u) and the calculated strengths (τ_{calc} and M_{calc}). The calculated strengths are based on $f_{c,ori}$ without inclusion of pre-stress effect. As can be seen in Fig. 20a, for beams 5.1 and 4.1, τ_u is 9% and 16% smaller than τ_{calc}, respectively. For beams 6.1, 6.2 and 3.3 M_{calc} is larger than M_u.

Especially, for beam 6.1 M_u is 18% smaller than M_{calc}. By use $f_{c,ori}$ there is a considerable risk that the calculated strengths are higher than the measured strengths. Consequently, it is not recommended to use the estimated original strength in the calculations of ASR-damaged beams.
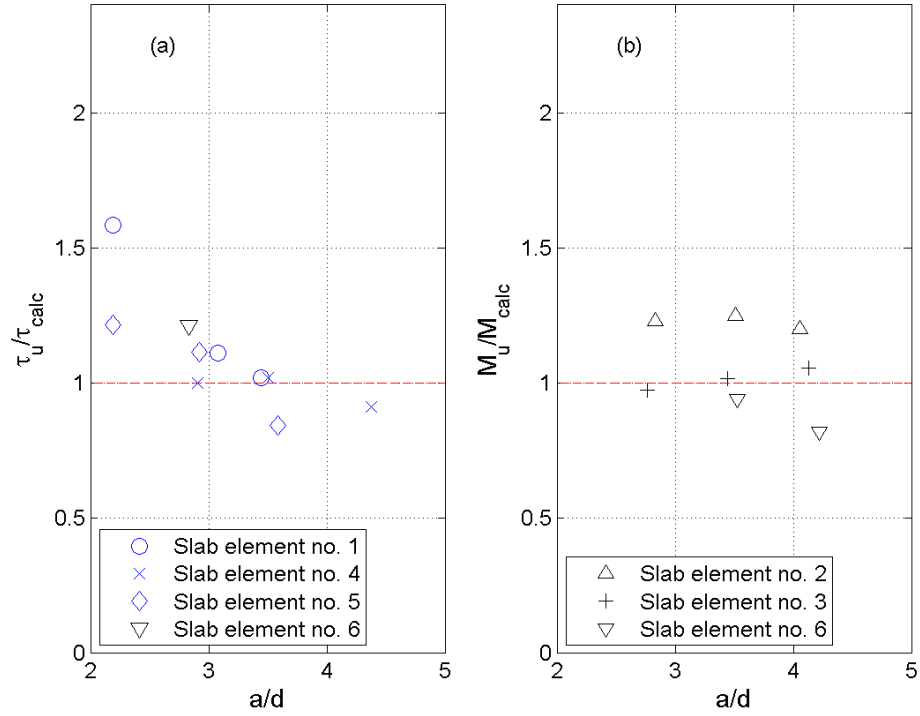

Figure 20: (a) τ_u/τ_{calc} as a function of a/d. (b) M_u/M_{calc} as a function of a/d. τ_{calc} and M_{calc} based on $f_{c,ori}$ without inclusion of pre-stress effect.

5.4 Calculations based on $f_{c,90}$ with pre-stress effect

Fig. 21 shows the ratios between the measured strengths (τ_u and M_u) and the calculated strengths (τ_{calc} and M_{calc}). The calculated strengths are based on $f_{c,90}$ with inclusion of the ASR-induced the pre-stress effect. The average tensile strains, ε_{ASR}, measured on the beam specimens are included in both the tensile and compressive reinforcing bars. As can be seen in Fig. 21a, with a/d-ratios between 2.8 and 3.5, the calculations are in better agreement with the measured shear strengths. However, for beams 4.1 and 5.1 τ_u is smaller than τ_{calc}, by up to 19%. For a/d-ratio of 2.2 the pre-stress effect alone cannot explain the enhancement in τ_u. From Fig. 21a we may argue that the pre-stress effect can, to some extent, compensate for the loss in material properties for ASR-damaged concrete. However, we may argue that the failure mechanism for beams 4.1 and 5.1 had an influence on the measured shear strengths which cannot be accounted for in the calculations. Consequently, it can be argued that the inclusion of the average ε_{ASR} in both

the tensile and compressive longitudinal bars should not be recommended. Comparing Fig. 21b with Fig. 18b shows that inclusion of the pre-stress effect does not have any significant effect on M_{calc}. Consequently, is most cases M_u is larger than $M_{calc.}$
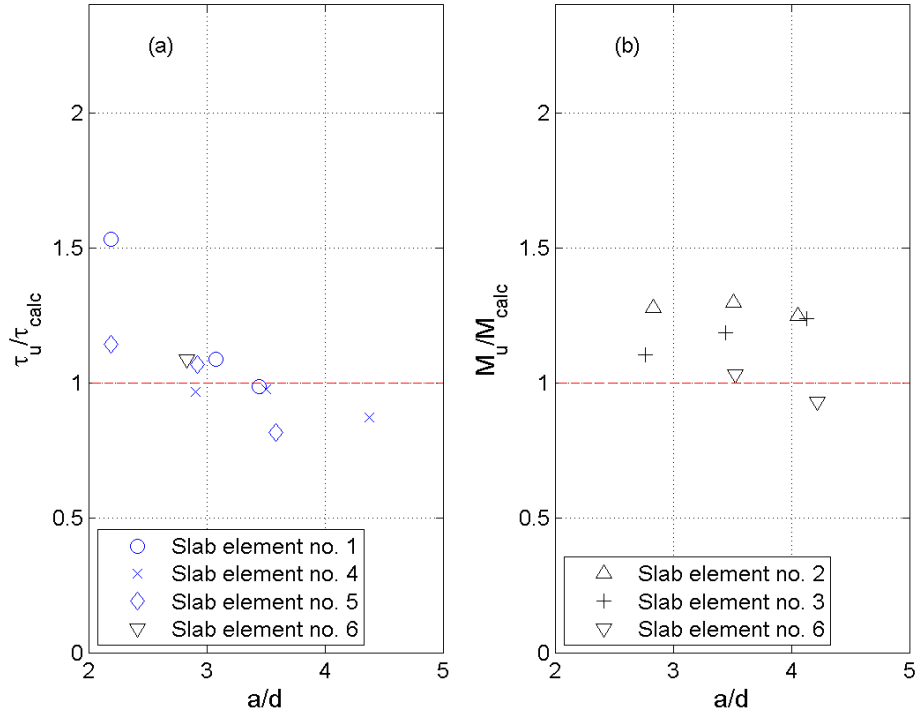

Figure 21: (a) τ_u/τ_{calc} as a function of a/d. (b) M_u/M_{calc} as a function of a/d. τ_{calc} and M_{calc} based on $f_{c,90}$ with inclusion of pre-stress.

Generally, without inclusion of the pre-stress effect, the shear strength calculations cannot predict the influence of the a/d-ratio on the measured shear strengths (see Figs. 18a to 20a). However as seen in Fig. 21a, where the ASR-induced pre-stress has been accounted for in the calculations, a better prediction of the influence of a/d-ratio on τ_u is obtained. Again we argue that the ASR-induced pre-stress effect is essential for the shear strength for ASR-damaged concrete. Having compared Figs. 18b and 19b we argue that the calculated sectional moment capacity based on be compressive strength in direction parallel to ASR cracks better represents the maximum moment carried by the beams.

27

6. Strength results and safety of the examined ASR-damaged flat slab bridge in service

Although it is not within the scope of this research, it is worth mentioning that the measured load-carrying capacities were found to be adequate to guarantee the required level of codified structural safety for the ASR-damaged bridge slab and to prolong its lifespan. The immediate demolition and reconstruction (which was initially expected) turned out to be unnecessary resulting in considerable economical saving for Danish Road Directorate. However, strengthening and repair of the slab will be conducted to avoid further acceleration of ASR combined with reinforcement corrosion within the near future.

7. Conclusions

The objective of this paper was to report a shear test series on ASR-damaged reinforced beams. The ASR-damaged beams were sawn from six large slab segments without shear reinforcement taken from a severely ASR-damaged flat slab bridge. The shear tests included nine tests on a three-point bending setup and nine tests on an asymmetrical four-point bending setup. The influences of the shear span-to-effective depth (a/d) ratio on the strengths were investigated in both test setups. Strain gauge measurements were conducted to quantify the ASR-induced pre-stress effect in reinforcing bars. The main conclusions from this research can be summarized as follows:

- The ASR cracks significantly influenced the propagation of load-induced cracks and failure mechanism of the beams.
- The failure of the majority of beams tested in both setups was rather ductile.
- The majority of the three-point bending tests failed in bending. Therefore, the actual shear strength of the beams must be higher than the measured shear strengths. The results from the three-point bending tests are thus a lower limit for the actual shear strength of the beams.
- For beams tested in the three-point bending setup the calculated sectional moment capacity (using the compressive strength of drilled concrete cores) was generally lower than the maximum moment carried by the beams. The calculated sectional moment by use of the compressive strength in direction parallel to ASR cracks more accurately represented the maximum moment carried by the beams.

- The beams tested in the four-point bending setup suffered ductile shear failure. The measured shear strengths determined from the four-point bending setup were generally lower than the shear strengths determined from the three-point bending setup. Consequently, the test setup had a considerable influence on the measured shear strengths.

- For the four-point bending setup the variation in shear span-to-effective depth ratio had considerable influence on the measured shear strengths. Increase in a/d-ratio resulted in significantly decrease in shear strengths.

- Significant tensile strains in the reinforcement due to ASR expansion were measured. This pre-stress effect was not proportional to the visual appearance of ASR cracks and the compressive strength of the slab segments.

- Without inclusion of the ASR-induced pre-stress effect and based on the compressive strength of drilled cores there was poor agreement between calculated and measured shear strengths. On the positive side, shear strength calculations by Eurocode 2 were in most cases conservative. But, the conservatism of the calculations decreased as the a/d-ratio increased.

- With inclusion of the ASR-induced pre-stress effect, the calculated shear strengths at larger a/d-ratios were higher than the measured shear strengths. On the contrary, the calculations are in better agreement with the measured shear strengths at a/d-ratios between 2.8 and 3.5. At a lower a/d-ratio of 2.2 the pre-stress effect alone could not explain the enhancement in measured shear strengths.

- Generally, the shear test results indicated that the ASR-induced pre-stress effect seems to have a positive effect on the shear strength of ASR-damaged beams.

Acknowledgements

References

[1]   F. Bach, T.S. Thorsen, M.P. Nielsen, Load-carrying capacity of structural members subjected to ASR, Constr. Build. Mater. 7 (1993) 109–115.

[2]   Danish Road Directorate, Load carrying capacity of structural members subjected to alcali-silica reactions, Ministry of Transport Denmark, The Road Directorate, 1990.

[3]   T. Ahmed, E. Burley, S. Rigden, The Static and Fatigue Strength of Reinforced Concrete Beams Affected by Alkali-Silica Reaction, ACI Mater. J. 95 (1999) 376–388.

[4]   D.J. Deschenes, O. Bayrak, K. Folliard, ASR/DEF-Damaged Bent Caps: Shear Tests and Field Implications, in: Proc. of 2009 Structures Congress - Don't Mess with Structural Engineers: Expanding our role., Texas, 2009: pp. 1049-1057 .

[5]   P.S. Chana, G.A. Korobokis, Structural performance of reinforced concrete affected by alkali-silica reaction: Phase I, Contractor Report 267, Trans. and Road Res. Lab., 1991.

[6]   S. Bilodeau, A. Allard, J. Bastien, F. Pissot, B. Fournier, D. Mitchell and B. Bissonnette, Performance Evaluation of Thick Concrete Slabs Affected by Alkali-Silica Reaction (ASR) - Part II: Structural Aspects, in: Proc. 15th Int. Conf. Alkali-Aggregate React. Concr., São Paulo, 2016.

[7]   S. Inoue, M. Fujii, K. Kobayashi, K. Nakano, Structural behaviors of reinforced concrete beams affected by alkali-silica reaction, in: Proc. 8th Int. Conf. Alkali-Aggregate React., Kyoto, 1989: pp. 727–732.

[8]   K. Okada, M. Tezuka, T. Yoshikawa, M. Himeno, M. Komada, Alkali Aggregate Reaction: An investigation on its causes and strength evaluations of materials subjected to its effects, in: Proc. 8th Int. Conf. Alkali-Aggregate React., Tokyo, 1989: pp. 609–615.

[9]   M. Fujii, K. Kobayashi, T. Kojima, H. Maehara, The Static and Dynamic Behavior of Reinforced Concrete Beams with Cracking Due to Alkali-Silica Reaction, in: Proc. 7th Int. Conf. Alkali Aggreg. React., Ottawa, 1986: pp. 126–130.

[10]   W. Koyanagi, K. Rokugo, H. Ishida, Failure Behavior of Reinforced Concrete Beams Deteriorated by Alkali-Silica Reactions, in: Proc. 7th Int. Conf. Alkali Aggreg. React., Ottawa, 1986: pp. 141–145.

[11]   K. Kobayashi, Load carrying behaviours of concrete structures and members affected by alkali-aggregate reactions, Concr. J. 24 (1986) 70–78.

[12]   E.R. Giannini, Evaluation of Concrete Structures Affected by Alkali-Silica Reaction and Delayed Ettringite Formation, University of Texas at Austin, PhD thesis, 2012.

[13]   J.A. Uijl, N. Kaptijn, Shear Tests on Beams Cut from ASR-Affected Bridge Decks, ACI Int. (2004) 115–133.

[14]   J.A. Uijl, N. Kaptijn, J.C. Walraven, Shear resistance of flat slab bridges affected by ASR, in: Proc. 11th Int. Conf. Alkali-Aggregate React., Québec, 2000: pp. 1129–1138.

[15]   J.W. Schmidt, S.G. Hansen, R.A. Barbosa, A. Henriksen, Novel shear capacity testing of ASR damaged full scale concrete bridge, Eng. Struct. 79 (2014) 365–374. doi:10.1016/j.engstruct.2014.08.027.

[16]   H. Mørup, C. von Scholten, V. Wegan, Have ASR damaged bridges sufficient strength? (In Danish), Trafik & Veje. March (2013) pp. 23–26.

[17]   S.G. Hansen, R.A. Barbosa, L.C. Hoang, Shear capacity of ASR damaged structures – In-depth analysis of some in-situ shear tests on bridge slabs, in: Proc. 15th Int. Conf. Alkali-Aggregate React. Concr., São Paulo, Brazil, 2016: p.

[18]   The Institution of Structural Engineers, Structural effects of alkali-silica reaction - Technical guidance on the appraisal of existing structures, 1992.

[19]   L.A. Clark, Critical review of the structural implications of the alkali silica reaction in concrete, Birmingham, PhD thesis, 1989.

[20]   N. Thaulow, A.D. Jensen, S. Chatterji, P. Christensen, H. Gudmundsson, Estimation of the compressive strength of concrete samples by means of fluorescence microscopy, Nord. Betong. 51 (1982) 2–4.

[21]   DS Standard 1992-1-1, Eurocode 2 : Design of concrete structures – Part 1-1: General rules and rules for buildings, Danish Standards, 2008.

[22]   DS Standard 1992-1-1 DK NA:2003, The Danish National Annex for Eurocode 2: Design of concrete structures – Part 1-1: General rules and rules for buildings, Danish Standards, 2013.

Appendix A- Nomenclature

a   Shear span

b   Width

d   Effective depth for the bottom reinforcement

$f_{c,0}$ Concrete compressive strength in direction parallel to ASR cracks

$f_{c,90}$ Concrete compressive strength in direction perpendicular to ASR cracks

$f_{c,ori}$ Estimated undamaged concrete compressive strength

f_y Yield stress of longitudinal reinforcement

E_s Young's modulus of longitudinal reinforcement

ε_{ASR} Tensile strain in reinforcement induced by ASR expansion

τ_{calc} Theoretically calculated shear strength

M_{calc} Theoretically calculated sectional moment capacity

Three-point bending setup

P   Point load

P_u Ultimate load

M_u Ultimate moment

V_u Ultimate shear force

δ_U Deflection at P_u

τ_u Measured shear strength (V_u/bd)

Four-point bending setup

P   Point load

P_A Point load at A

P_C Point load at C

$P_{A,u}$ Ultimate load at A

$P_{C,u}$ Ultimate load at C

$M_{B,u}^{-}$ Ultimate negative moment at B

$M_{C,u}^{+}$ Ultimate positive moment at C

$V_{I,u}^{-}$ Ultimate negative shear force in shear zone I

$V_{II,u}^{+}$ Ultimate positive shear force in shear zone II

$\delta_{C,u}$ Deflection at $P_{C,u}$

τ_u Measured shear strength ($V_{II,u}^{+}/bd$)

Appendix B: Geometrical parameters in the three-point bending setup
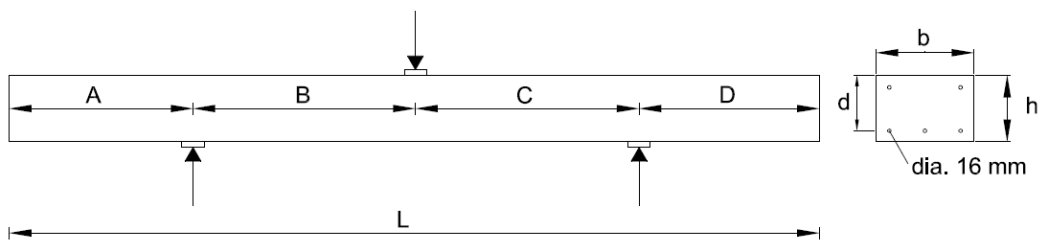
	Beam no	Dimensions, beam cross section			Distances in three point bending setup				
		b [mm]	h [mm]	d [mm]	L [mm]	A [mm]	B [mm]	C [mm]	D [mm]
Slab segment 2	2.1	435	300	247	3640	826	999	1005	810
	2.2	410	300	242	3118	700	848	850	720
	2.3	445	300	247	2580	610	695	705	570
Slab segment 3	3.1	450	300	242	3700	850	1002	998	850
	3.2	450	300	247	3118	713	850	852	703
	3.3	445	300	252	2640	625	700	695	620
Slab segment 6	6.1	425	300	237	3670	405	1000	1600	665
	6.2	440	300	242	3090	784	852	854	600
	6.3	430	300	247	2570	521	700	699	650

Appendix C: Geometrical parameters in the four-point bending setup
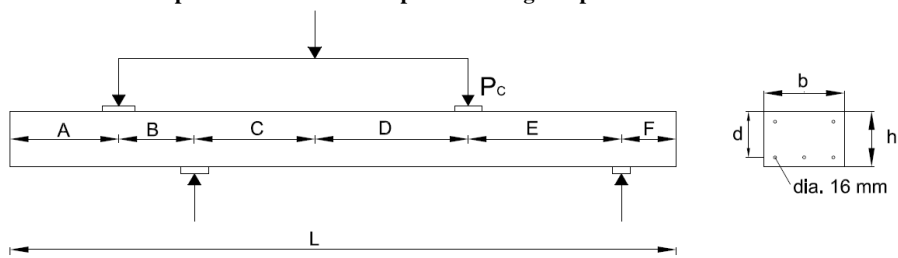
	Beam no	Dimensions, beam cross section			Distances in four point bending setup						
		b [mm]	h [mm]	d [mm]	L [mm]	A [mm]	B [mm]	C [mm]	D [mm]	E [mm]	F [mm]
Slab segment 1	1.1	420	300	247	3650	595	415	660	840	840	300
	1.2	435	300	242	3100	493	410	645	555	677	320
	1.3	425	300	247	2600	305	480	510	400	605	300
Slab segment 4	4.1	445	300	237	3658	320	295	650	1150	945	298
	4.2	425	300	242	3110	175	420	660	840	845	170
	4.3	450	300	247	2600	160	420	620	580	675	145
Slab segment 5	5.1	450	300	242	3670	507	408	672	830	845	408
	5.2	430	300	242	3130	415	430	615	585	675	410
	5.3	410	300	247	2630	335	495	515	385	600	300

Time-dependent influence of alkali-silica reaction on the physical and mechanical properties of laboratory-accelerated reinforced slabs

5.1 Introduction

Destructive examinations of ASR-damaged bridge slabs in service provide just a snapshot of the condition of the examined structure at one point in the alkali-silica reaction (ASR) deterioration progress. The three ASR-damaged slab bridges examined as a part of this PhD study had ASR cracking through the entire bridge slab cross section. However, visually the extent of ASR cracking in the cross section could vary within areas in the same slab bridge. From destructive examinations of the slab bridges in this PhD study, it can be concluded that the ASR cracking has a significant influence on the uniaxial compressive strength (Chapter 2), the Young's modulus (Chapter 2), and the tensile strength (Chapter 3) of drilled cores. In addition, ASR cracking and related expansion may have both negative and positive influences on the residual shear strength of reinforced beams sawn from an ASR-damaged flat slab bridge (Chapter 4).

Such destructive examinations of severely ASR-damaged slab bridges are unique and essential for the understanding and assessment of their residual load-carrying capacity. However, it must be recognized that from destructive studies of already severely ASR-damaged bridge slabs we are not able to completely determine or understand how and how fast the propagation of ASR cracking influences the physical, mechanical and structural behavior of the ASR-affected structure.

Obviously, in order to develop valuable assessment methodologies or improve existing methodologies for ASR-affected slab bridges we must understand and include the time-dependent influence of ASR-deterioration on the evaluation of

the structural integrity of these bridges. By that approach it may be possible to improve remedial actions and to predict the future development of ASR when no remedial actions are executed.

For bridge slabs in service it is difficult to follow this time-dependent influence. When the first visual signs of ASR cracking are detected from beneath the bridge slab, large parts of the bridge cross section may already be severely ASR cracked. Differences between ASR cracking in different areas on the structure may be considerable. Additionally, periodic in-situ drilling may not be cost effective for most bridges and may only provide the condition of the bridge slab in small, selected areas.

In Denmark, determination of the time-dependent influence of external supply of alkalis to the bridge slab must be included in the assessment methodology. The Na_2O eq. content in older Danish bridge slabs is assumed to be around 2.0 to 2.5 kg Na_2O eq. per m^3 of concrete, which is far below the current accepted alkali threshold value to initiate deleterious ASR of 3 kg Na_2O eq. per m^3 of concrete (Nielsen *et al.*, 2004). Therefore, for the Danish bridge slabs, an external supply of alkalis from de-icing salts, i.e. NaCl, is assumed to be essential to initiate ASR cracking. This assumption is valid for road bridge slabs, where in this assumption the possibility of alkali release from aggregates is not included. Due to possible leakage of waterproofing membrane on top surface of bridge slabs, we may expect a significant supply of alkalis and water to the bridge slab during its lifespan. During the Danish winter period, with several annual freeze-thaw cycles, a considerable amount of de-icing salt is used on roads and consequently on road bridges. The specific water and alkalis transport direction from the top surface of the slabs to the concrete may result in gradual development of ASR cracking as a function of water and de-icing salt transport. Consequently, this gradual cracking development could have a significant time-dependent impact on the physical, mechanical and structural behavior of bridge slabs.

To the author's knowledge, literature regarding the time-dependent influence of ASR cracking on the physical and mechanical properties of reinforced slabs is very limited, if it exists at all. Even though international studies could address this research topic, in Denmark we may only be able to use these studies if the exposure conditions, alkali content in the cement and reactive aggregate types are comparable to the conditions observed in the Danish bridge slabs in service. In Denmark, only one study (Road Directorate, 1990; Bach *et al.*, 1993) investigates the time-dependent influence of ASR deterioration on the physical, mechanical and structural behavior of reinforced concrete beams and not of slabs. Although the reactive fine aggregate type used in the study (Road Directorate, 1990; Bach *et al.*, 1993) is comparable to reactive aggregates observed on Danish bridge slabs in service, the accelerated exposure condition, beam size, and reinforcement configuration resulted in crack patterns that are not comparable with those observed on ASR-damaged slabs in service. Hansen *et al.* (Hansen *et al.*, 2016) reported the differences in crack pattern observed in laboratory-accelerated beams and bridge slabs in service. The difference between crack patterns in the laboratory-accelerated beams and bridge slabs was mainly caused by differences in exposure condition and reinforcement configuration. As an example in the study (Road Directorate, 1990; Bach *et al.*,

1993), the reinforced beams were immersed in a saturated NaCl solution at 50 °C. Consequently, the concrete was exposed to the solution from all beam surfaces. This exposure condition is rarely comparable to the exposure condition observed in bridge slabs, where one may assume a one-way water-and-alkali transport from the upper surface of the bridge deck or through existing mainly horizontal ASR cracks.

Clearly, there is a significant lack of knowledge concerning the time-dependent influence of ASR-deterioration on slabs in Denmark. Therefore, the aim of this accelerated laboratory exposure on reinforced slabs is to improve the understanding of the time-dependent influence of ASR on the physical and mechanical properties of reinforced slabs. Another aim of this study is to provide data that can be applied in the future to establish assessment methodologies for Danish ASR-affected bridge slabs.

In this laboratory research, seven 1.5 x 1.5 x 0.25 m^3 reinforced slabs were casted and stored under accelerated conditions at 40 °C and high relatively humidity. Three reinforced slabs were exposed to saturated NaCl solution from the top surface of the slabs in order to simulate an external supply of alkalis to the concrete, as expected in bridge slabs in service. In two additional slabs, the alkali content in the concrete was raised in order to compare the behavior of the slabs when high alkali content are in-built in the concrete. Finally, two slabs were used as control slabs. The internal vertical expansion and surface expansion on the slabs were periodically measured. Cores were periodically drilled vertically from the slabs and tested in compression. Meanwhile, corresponding cores were impregnated under vacuum by fluorescent epoxy, to evaluate the ASR crack extent and crack orientation within the cores. An image analysis program developed at the Technical University of Denmark was used, to obtain an objective evaluation of crack orientation within the impregnated cores. As ASR can be a long, time-dependent deterioration mechanism, only the results achieved to date are reported in this chapter.

5.2 Materials, exposure conditions and measurement methods

5.2.1 Materials

5.2.1.1 Concrete mix design

In total, seven 1.5 x 1.5 x 0.25 m^3 reinforced slabs were casted. Six slabs were casted with Danish reactive fine aggregate (Øde Hastrup sand) and Danish nonreactive crushed granite (Rønne granite) as coarse aggregate. One slab was casted with Danish nonreactive sea-dredged fine aggregate and the same nonreactive crushed granite as coarse aggregate. Before the mixing of each concrete mix, the moisture content of aggregates was measured. The amount of mixing water was adjusted if the aggregate moisture content differed from the moisture content of a saturated, surface-dry condition. Table 5.1 shows the concrete mix design for the slabs. The reinforcement configuration is described in section 5.2.1.2. Due to insufficient mixer capacity, each slab was casted in three layers of 0.2 m^3. The time it took to blend the mix and cast each layer was approximately 20 minutes. A hand held concrete

vibrator was used during placement of each layer, to eliminate larger air voids and to ensure even distribution of the fresh concrete mix. Each layer of the newly casted concrete was covered by a plastic sheet until placement of the next layer.

Table 5.1: Concrete mix design. Values are given in kg/m^3. The kg/m^3 amount of aggregates corresponds to their saturated surface-dry condition.

Constituents	kg/m^3
Cement (Rapid cement - CEM I 52.5 N (LA))	350
Water	175
Fine aggregate (reactive Øde Hastrup sand in six reinforced slabs and nonreactive sea-dredged sand in one reinforced slab)	860
Coarse aggregate, 4-8 mm (nonreactive Rønne granite)	345
Coarse aggregate, 11-16 mm (nonreactive Rønne granite)	667

Aalborg Portland Rapid cement (CEM I 52.5 N (LA)) with Na$_2$O eq. content $\leq 0.6\%$ was used for the mixes. The Na$_2$O eq. content on five slabs is ≤ 2.1 kg/m^3. In two slabs, the Na$_2$O eq. content was raised to approximately 7 kg/m^3 by adding NaOH to the mixing water. The cement content of 350 kg/m^3 is within the range of the cement content used in older Danish bridge slabs (Nielsen *et al.*, 2004). The water-cement ratio is 0.5 in all casted slabs.

After casting of the three layers, and while placed in the form, the slabs were covered by plastic sheets. The slabs were demolded 3-4 days after casting. After demolding all surfaces in the slabs were covered by plastic sheets. The plastic-covered slabs were allowed to cure at room temperature for approximately 3 weeks and were afterwards allowed to cure in a tent at outside temperature for several weeks. The outside temperature corresponded to the Danish climate in the months of November to April with an average outside temperature of 5 °C. Table 5.2 shows the curing time of each slab. As supplement to the slabs, six concrete cylinders (diameter/height=100/200 mm) were casted on a vibrating table from one concrete mix from each slab production.

5.2.1.2 Reinforcement configuration

The slabs were not provided with vertical/shear reinforcement. The slabs consisted of two layers of reinforcement nets made of ribbed bars with a diameter of 12 mm. The heart distance between the ribbed bars was 150 mm. The concrete cover thickness was 20 mm in the bottom and 20-30 mm in the top of the slabs. Figure 5.1a and Figure 5.1b show an illustration of a slab with reinforcement configuration. In Figure 5.1a the location of five DEMEC plates on the top slab surface and the location of four vertical expansion measurement devices are shown.

Table 5.2: Reactive fine aggregate composition, curing time, Na₂O eq. content in the concrete mix during slab production. Exposure condition condition for each slab and indication of vertical expansion measurement.

	Slab production			Exposure	Measurement
Reinforced slab	Reactive fine aggregate	Curing time in weeks	Na_2O eq. content in the mix (kg/m^3)	External alkali and/or high humidity exposure	Internal vertical expansion
1	Yes	22	≤ 2.1	Ex. sat. NaCl from top surface	Yes (4 locations)
2	Yes	21	≤ 2.1	90-100 % RH	No
3	Yes	20	≤ 7	90-100 % RH	Yes (4 locations)
4	Yes	20	≤ 7	90-100 % RH	Yes (4 locations)
5	Yes	28	≤ 2.1	Ex. sat. NaCl from top surface	Yes (1 locations)
8	Yes	11	≤ 2.1	Ex. sat. NaCl from top surface	Yes (4 locations)
9	No	11	≤ 2.1	90-100 %	Yes (4 locations)
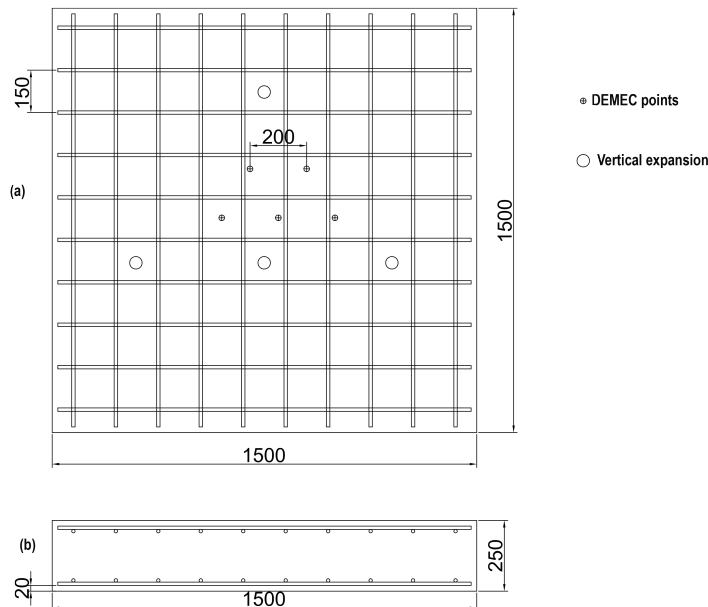
Figure 5.1: Illustration of a reinforced slab with dimensions given in mm and reinforcement configuration. (a) Plan view of the slab with location of five DEMEC points and location of four vertical expansion measurement devices. (b) Cross section of the slab.

5.2.1.3 Exposure conditions

The slabs were conditioned inside a 40-ft insulated container. Figure 5.2 shows the slabs inside the insulated container.

The temperature inside the insulated container was held constant at $40 \pm 2°$C by use of external heaters. The relative humidity inside the container varied in the range of 90 to 100 %. An external humidifier was used to maintain the relative humidity.

Figure 5.2: Reinforced slabs inside the insulated 40-ft container.

Before installation of the slabs inside the insulated container, the vertical side surfaces of all slabs were painted with a two-component epoxy painting, Conpox EB 1040, to prevent ingress of moisture and NaCl solution into the slabs from the vertical side surfaces. Three slabs (slab 1, 5 and 8) were exposed to an external supply of saturated NaCl solution poured onto the top surface of the slabs; see Table 5.2. 3 liters of saturated NaCl solution was poured onto the top surface of the slabs every second week.

5.2.2   Measurements and methods

5.2.2.1   Free expansion of concrete cylinders

Concrete cylinders (diameter/height=100/200 mm) from two mixes are exposed to the accelerated exposure conditions provided by the Danish mortar-bar test method TI-B51 (TI-B 51, 1985). The cylinders were demolded 24 hours after casting and were cured for seven days at room temperature, wrapped in plastic sheets. Four cylinders with a Na_2O eq. content of 2.1 kg/m^3 were immersed in a saturated NaCl solution, and three concrete cylinders with a Na_2O eq. content of 7 kg/m^3 were stored above water and exposed to a high-humidity environment. All cylinders were stored at 50°C.

Before exposure, metal studs were fixed to the end surfaces of the cylinders in order to periodically monitor their longitudinal expansion. The longitudinal expansion measurements were conducted using a Mitutoyo digital indicator with resolution of 0.001 mm. The longitudinal expansion measurements were conducted after the cylinders had cooled to room temperature.

5.2.2.2   Internal vertical expansion of slabs

The internal vertical expansion of slabs was measured periodically as function of the exposure time. Figure 5.3 illustrates the vertical expansion setup casted inside the slabs.
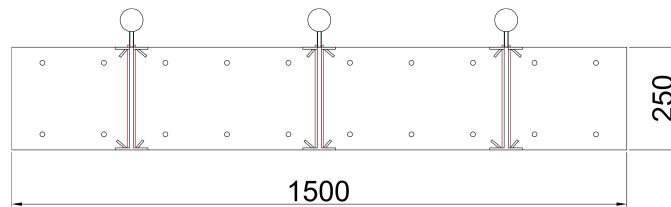

Figure 5.3: Illustration of the internal vertical expansion measurement device inside the slab with dimensions given in mm.

Figure 5.4a shows a photo of the internal vertical expansion measurement device which consists of a vertical plane reinforcement bar welded to a steel foot. The plane bar was protected by a rubber tube that, prevents anchorage of plane bar to the concrete. A Mitutoyo dial gage with 0.01-mm precision was installed on top of the vertical device. Round steel plates were casted on the top surface of the slabs in order to ensure a plane surface for the vertical expansion measurements. Figure 5.4b shows the vertical measuring device after casting on the slabs. Glass jars installed onto the slab surface were used to protect the dial gages from the high-humidity environment inside the container. Small silica-gel packs were placed inside the glass jars. Between the jars and the concrete, closed-pore flexible heat insulation material was glued to the surface, to prevent moisture entering to the dial gages. The vertical expansion was measured on six slabs; see Table 5.2. In slab 5, only one vertical expansion measurement device was installed in the slab. The first readings of the dial gages was conducted at 20°C and all the following readings were conducted at 40°C inside the container.

5.2.2.3   Top surface expansion of slabs

The top surface expansion of the slabs was measured periodically with the same frequency as the vertical expansion. For measuring the surface expansion, small DEMEC steel plates, 25 mm in diameter with a 2 mm diameter centered hole, were glued into the surface of the slabs with a two-component fast curing adhesive. Figure 5.1a shows an illustration of the locations of the DEMEC steel plates on the surface of a slab. The surface expansion was measured longitudinally and diagonally by use of a mechanical Berry device. The Mitutoyo dial gage on the mechanical Berry device has a resolution of 0.01 mm. Before the surface expansion measurements, the mechanical Berry device was placed inside the insulated container for 30 minutes. An invar calibration bar was used before Berry measurements of each slab. The first measurements of surface expansion were conducted at 20°C, and the following measurements were conducted at 40°C inside the container.
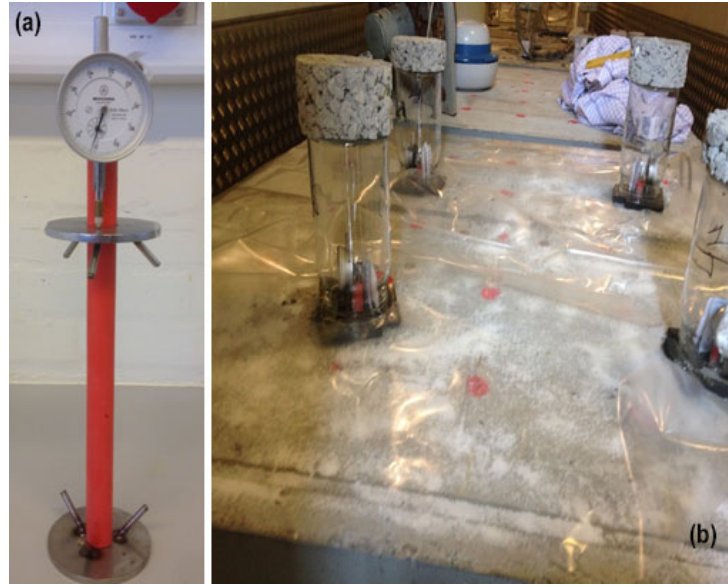
Figure 5.4: Internal vertical expansion measurement setup. (a) Vertical expansion measurement device. (b) Vertical expansion measurement device casted inside the slabs.

5.2.2.4   Uniaxial compressive strength tests

Cores were drilled periodically from the slabs. A diamond drill cooled by water circulation was used for drilling. The cores were tested in compression 1-2 weeks after drilling. The top end of the drilled concrete cores was grinded plane, and approximately 25 mm of the bottom end was sawn with a water-cooled diamond saw and afterwards grinded plane. The cores tested in compression were 100 mm in diameter and approximately 200 mm in length.

The cores were tested in a displacement-controlled hydraulic TONI 3000 kN machine. The tests were carried out with a constant displacement rate of 0.5 mm/minute. Between the cores and the steel loading platens, 3-mm high-density wood fiberboards were used to compensate for small imperfections at the end faces of the core.

5.2.2.5   Ultrasonic pulse velocity measurements

Before compressive strength testing, the ultrasonic pulse velocity of all cores and reference cylinders was measured by use of a Pundit ultrasonic instrument with 150-kHz transducers. Direct transmission was conducted to ensure maximum signal transmission between the transmitter and receiver. Alignment between the transducer and receiver was ensured before the measurements. An aqueous transmission gel ensured good acoustical coupling between the concrete surfaces and the transmitter and receiver. The core end surfaces were plane, to ensure proper contact between the concrete and the transmitter and receiver. The ultrasonic pulse velocity measurements were conducted on the prepared cores and reference cylinders, having a length of approximately 200 mm.

5.2.2.6 Thin-section examinations

Fluorescence-impregnated thin-sections were prepared from cores drilled from the slabs. The fluorescence-impregnated thin-sections were examined by use of a polarization microscope with possibility for fluorescence microscopy. During the thin-section examinations, the following parameters were of primary interest: cause of cracking, type and size of possible reactive aggregates, development of ASR gel, homogeneity of the cement paste, and possibility of another deterioration mechanism influencing the development of ASR.

5.2.2.7 Impregnated plane polished section and image analysis

Cores with diameter/height=100/200 mm were impregnated with fluorescent epoxy under vacuum, in order to visualize possible development of ASR cracking inside the slabs. In this study, before impregnation the cores were cut into two longitudinal halves. Only one half of the core was impregnated. This was done to ensure fluorescence impregnation of all ASR cracks in the sawn surface of the core. After hardening, 2-4 mm of the impregnated surface was ground for removing excess of hardened epoxy. Possible ASR cracking in the cores was visualized by use of ultraviolet light. The visible ASR cracking under ultraviolet light was photographed with a high-resolution camera. The photo was stored as a TIFF file for optimal image analysis as described in the following.

To quantify the orientation of the ASR-induced cracks from the high-resolution photo, the image analysis program developed by Andreassen *et al.* (Andreassen *et al.*, 2016) used a correlation process through application of Prewitt operator for edge detection. According to Paulsen and Moeslund (Paulsen and Moeslund, 2015), an edge is defined as a position in the image where a significant change in grayscale values occurs between neighboring pixels. A thorough description of the used image analysis program is given by Andreassen *et al.* Basically, the image analysis program converts a RGB color image to a grayscale image. To detect edges in the image, the concept of gradients is used. A gradient is a two-dimensional vector that points to the direction in which the image intensity grows faster. By application of Prewitt operator to the grayscale image, the operator calculates the gradient of image intensity at each point in the image. At each point in the image there is one component in x-direction and one component in the y-direction of the gradient. Moreover, the gradients have a direction and a magnitude. The edge of the ASR-induced crack is determined based on the gradient magnitude. The gradient magnitude gives the amount of difference between neighboring pixels, which presents the strength of the edge. The orientation of the ASR cracks in each pixel was calculated as the perpendicular direction to the largest gradient magnitude. The orientation of the ASR cracks was converted to the range of 0 to 180 degrees, where 0 and 180 degrees refers to horizontal ASR cracks, and 90 degrees refers to vertical ASR cracks. One very important feature in the image analysis program provided by Andreassen *et al.* was the selection of a threshold value. If the largest gradient magnitude in the pixel was below the threshold value, the investigated pixel is not taken as a part of the crack edge. Thus, pixels below

the threshold value were not considered as an edge.

5.3 Results and discussion

5.3.1 Free expansion of concrete cylinders

Figure 5.5 shows the free expansion of the concrete cylinders, containing 2.1 kg/m^3 Na$_2$O eq. content immersed in a saturated NaCl solution as well as cylinders containing 7.0 kg/m^3 Na$_2$O eq. content storage at 100 % RH environment condition. Cylinders having high initial alkali content stored at 100 % RH have a rapid expansion from the beginning of the storage period compared to cylinders immersed in the NaCl solution. After the first 5 weeks of exposure, the expansion of cylinders immersed in NaCl solution continues to increase while the expansion of cylinders exposed to 100 % RH stagnates. Although the phenomenon of alkali leaching from specimens stored over water in 100 % RH environments has been reported by several studies (Thomas *et al.*, 2006; Rivard *et al.*, 2007; Lindgård *et al.*, 2012; Lindgård, 2013), this phenomenon is not expected to be the primary explanation to the lower expansion of the cylinders having high initial Na$_2$O eq. content.
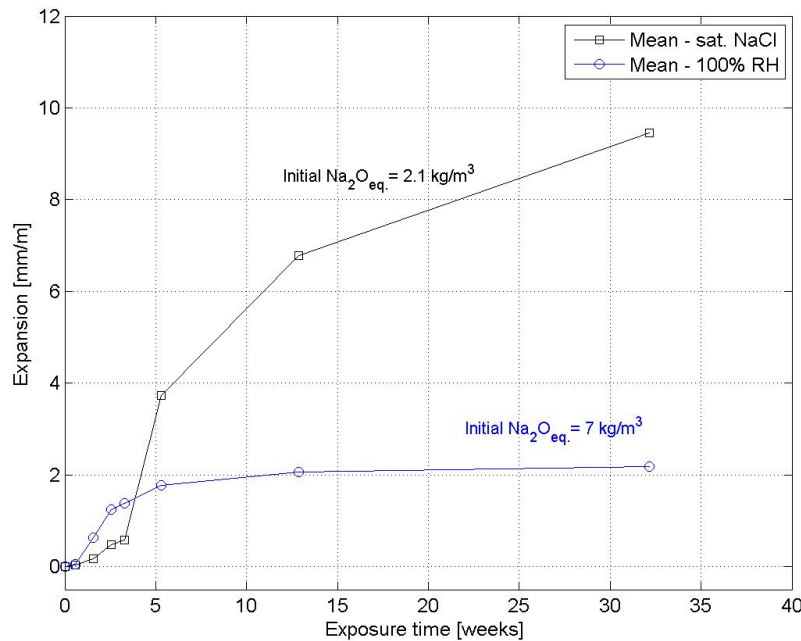
Figure 5.5: Free expansion of concrete cylinders stored at 50 °C.

A similar trend, as seen in Figure 5.5, based on mortar bars casted with Danish reactive Nymølle sand, has been reported by Chatterji *et al.* (Chatterji *et al.*, 1987; Swamy, 1992). In the tests performed by Chatterji *et al.*, all mortar bars were casted with low-alkali Portland cement and were afterward immersed in 3N NaCl solution and 3N NaOH solution, respectively. Thus, there is no risk of

alkali leaching in the tests. Chatterji *et al.* reported that mortar bars stored in NaOH solution had a high expansion in the beginning, but the final expansion was considerably lower than mortar bars stored in NaCl solution; see Figure 5.6. According to Chatterji *et al.*, when stored in NaOH solutions the penetration of Ca^{2+}, K^+, Na^+ and OH^- ions into reactive particles increases with increasing NaOH concentration. However, at the same time $Ca(OH)_2$ concentration surrounding the reactive aggregate will be lowered, resulting in increased leakage of dissolved silica from aggregates causing lower expansion. In this case, according to Chatterji *et al.*, NaOH plays two opposing roles. According to Chatterji *et al.*, a high concentration of $Ca(OH)_2$ accelerates the penetration of Ca^{2+}, K^+, Na^+ and OH^- into the reactive aggregate particle and at the same time limits the amount of silica diffused out of the reactive aggregate particle. Consequently, when immersed into the NaCl solution the leakage of dissolved silica will be lower than mortar bars immersed in NaOH solution, resulting in higher expansion, because both the $Ca(OH)_2$ concentration and Na^+ concentration are high in the concrete pore solution.
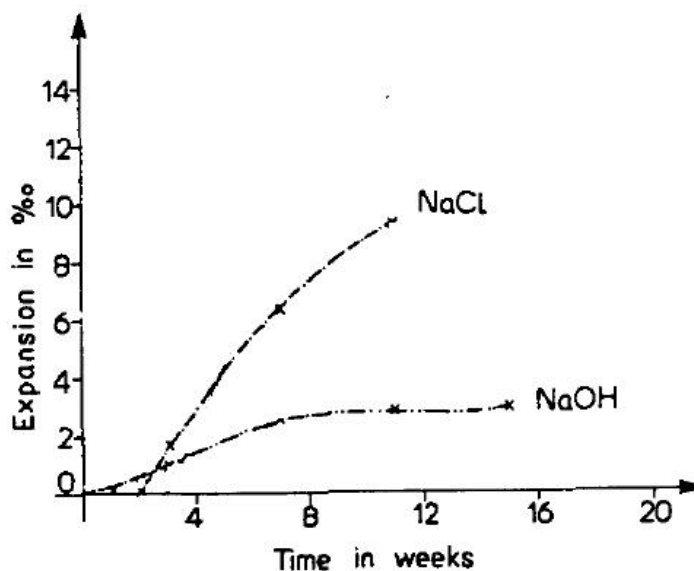
Figure 5.6: Free expansion of mortar bars stored at 50 °C in 3N sodium salt solutions. Adapted from Chatterji *et al.* (Chatterji *et al.*, 1987).

Assuming the proposed mechanism of Chatterji *et al.* to be valid a more plausible explanation for Figure 5.5 is that the fast-reactive Danish opaline flint instantly dissolves, causing increasing leakage of dissolved silica from the aggregates when a high amount of NaOH concentration is mixed into the concrete. In this case, the high NaOH concentration results in increased Na^+, Ca^{2+}, K^+ and OH^- ion penetration into reactive aggregate particles but at the same time lowers $Ca(OH)_2$ concentration. Simultaneously, water molecules migrate to the reactive particles. The lower expansion represents that more dissolved silica leaks out of reactive aggregate particles compared to the cylinders immersed in NaCl solution. Although the results in Figure 5.5 may support the view of Chatterji *et al.*, some studies do

not confirm this view regarding the influence of NaCl and NaOH on ASR expansion. Duchesne and Bérubé (Duchesne and Bérubé, 2003) reported that mortar bars immersed in 1M NaOH solution resulted in larger expansion than mortar bars immersed in 1M NaCl solution. As reported by Giebson *et al.* (Giebson *et al.*, 2016) there is currently no accepted mechanism that can explain the influence of external supply of NaCl on ASR expansion and development. However, Giebson *et al.* argued that NaCl solution may promote the dissolution of reactive silica particles more directly than through their conversion to corresponding alkali hydroxides. To some extent, the results by Giebson *et al.* support the view of Chatterji *et al.* (Chatterji *et al.*, 1987; Swamy, 1992).

5.3.2 Internal vertical expansion of slabs

Figure 5.7 shows the mean internal vertical expansion in the slabs as function of exposure time. Note that slab 1 was replaced by slab 5 at 10 weeks of exposure. As can be seen, the vertical expansion of slabs exposed to external supply of saturated NaCl solution has a significantly larger expansion than slabs with a high initial Na_2O eq. content. The lower vertical expansion of slabs with high alkali content is not considered to be caused by alkali leaching. Possible combined effects of this lower expansion are: 1) the orientation of the developed ASR cracking inside the slabs (see section 5.3.7); 2) the possibility that the ASR cracking in the slabs with high Na_2O eq. content may already be developed before the beginning of the accelerated exposure and measurements; and 3) the view of Chatterji *et al.* (Chatterji *et al.*, 1987; Swamy, 1992) reported in section 5.3.1.

It is seen in Figure 5.7 that the initiation of the vertical expansion for slab 5 is approximately 5 weeks slower than the other slabs exposed to the external supply of saturated NaCl solution. In slab 5 only one vertical expansion device is casted inside the slab. Several factors may influence the initiation of ASR cracking and corresponding expansion; in this case slab 5 was cured 10 weeks more than the other slabs before exposure, which may have an influence on the vertical expansion. By thin-section examinations, the water-cement ratio of slab 5 is compatible to the other reinforced slabs. The vertical expansion of slab 8 increases in linear fashion, and further expansion is expected after 33 weeks of exposure time. The vertical expansions of slabs 3 and 4 are similar to each other as expected. The vertical expansions of slabs 3 and 4 stagnate and stabilize after approximately 28 weeks. The vertical expansion of slabs 3 and 4 stabilize at expansion levels corresponding to the free expansion of cylinders, which may be a coincidence. Slab 9 contracts after the first week of exposure, possibly due to shrinkage. The vertical contraction of slab 9 is constant and stable after the first week of exposure time.

5.3.3 Surface expansion of slabs

Figure 5.8 shows the mean surface expansion as a function of exposure time for the slabs. As previously stated, slab 1 was replaced by slab 5 at 10 weeks of exposure. The surface expansion represents both longitudinal and diagonal expansion measurements. As seen in Figure 5.9, there is no considerable difference between
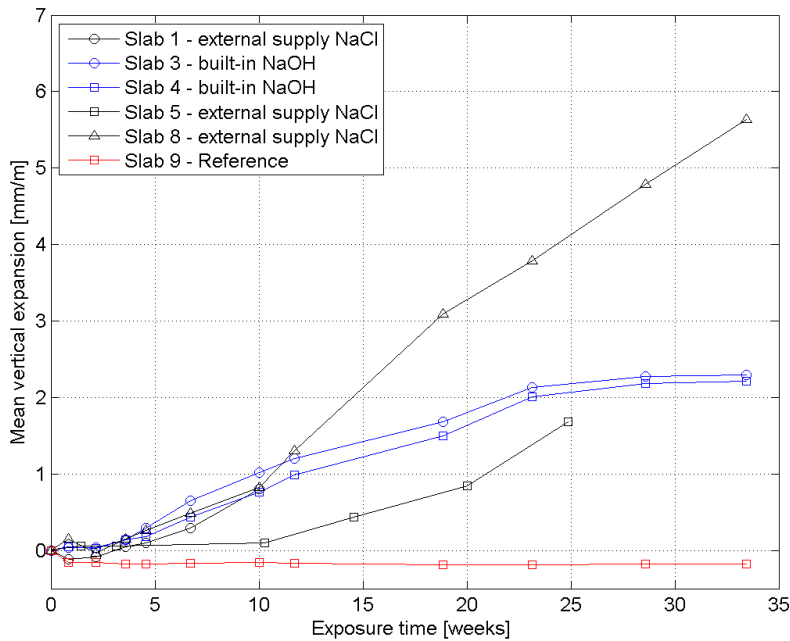
Figure 5.7: Mean internal vertical expansion of slabs.

the longitudinal and diagonal surface expansion for slab 4. The relation between the longitudinal and diagonal surface expansion in Figure 5.9 is representative for all other slabs. As seen in 5.8, the surface expansion of most of the slabs with exception of the reference slabs is almost the same within the first 10 weeks of exposure. However, after 10 weeks of exposure slab 8 shows a remarkable increase in surface expansion, where after 23 weeks the surface expansion begins to stagnate. Although slab 5 is exposed to NaCl solution, the delayed vertical expansion observed in Figure 5.7 is also observed for the surface expansion in Figure 5.8 within the first 20 weeks of exposure, where subsequently the rate of surface expansion increases. In general, the surface expansion is, like the vertical expansion, higher for slabs exposed to NaCl solution.

The surface expansion of the reference slabs shows equal trends, with an increase in surface expansion to approximately 0.29 mm/m within the first 10 weeks of exposure. After 10 weeks of exposure, a sudden increase and subsequent stabilization of surface expansion occurs. The calibration of the mechanical Berry was the same at weeks 10 and 12. Consequently, there is no clear explanation for the increase in surface expansion from week 10 to week 12. In order to drill cores from the slabs, at week 10 the temperature inside the container was lowered to $20 \pm 2°$C. The temperature of $20 \pm 2\,°$C was held constant for three days, whereafter the temperature was again raised to $40 \pm 2\,°$C. This temperature effect is not expected to cause any further increase in surface expansion of the reference slabs between weeks 10 and 12. The surface expansion in the reference slabs within the first 10 weeks may be explained by thermal expansion of the reinforced slab when heated
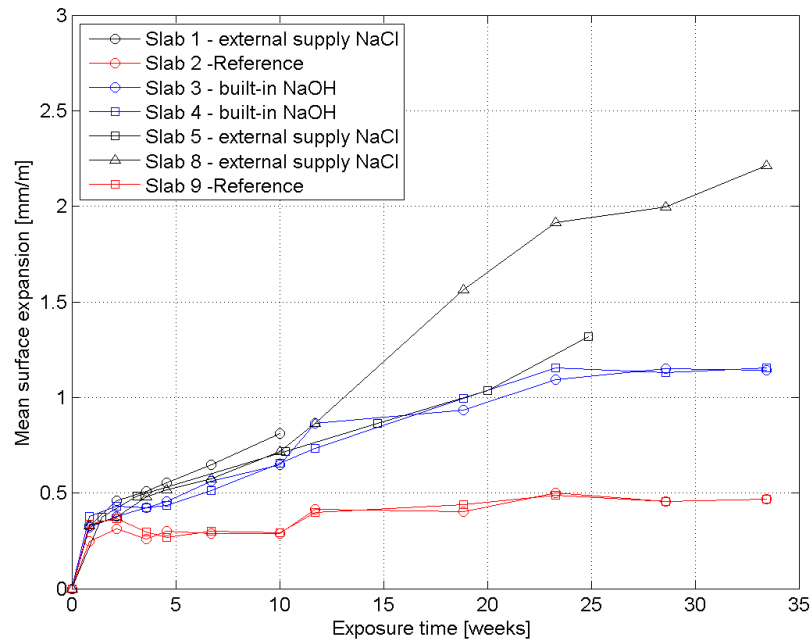
Figure 5.8: Mean surface expansion of slabs.

from $20 \pm 2°C$ to $40 \pm 2°C$. The thermal expansion is calculated to 0.22 mm/m, assuming a thermal expansion coefficient for concrete of $11 \cdot 10^{-6}$ $°C^{-1}$. There is no clear explanation for the contraction in vertical expansion for reference slab 9 seen in Figure 5.7. Increasing vertical expansion due to thermal effects would be expected, but apparently shrinkage compensates for this thermal effect of expansion in the vertical direction.

5.3.4   Correlation between internal vertical expansion and surface expansion

Figure 5.10 shows the correlation between the mean vertical expansion and mean surface expansion for the accelerated slabs. As seen in 5.10, for most slabs except for reference slab 9, the correlation between the vertical expansion and surface expansion can be divided into three phases:

- The first phase is called the *initiation phase*, which varies between each slab. At the initiation phase the surface expansion is larger than the vertical expansion. A portion of the surface expansion in the initiation phase may partially represent thermal effects on the slab surface.

- The second phase is called the *linearity phase*. At the linearity phase, there is a strong linear correlation between surface and vertical expansion. At this phase the vertical expansion increases more than the surface expansion for all slabs. The vertical expansion is approximately 2.4 to 2.7 times larger than the
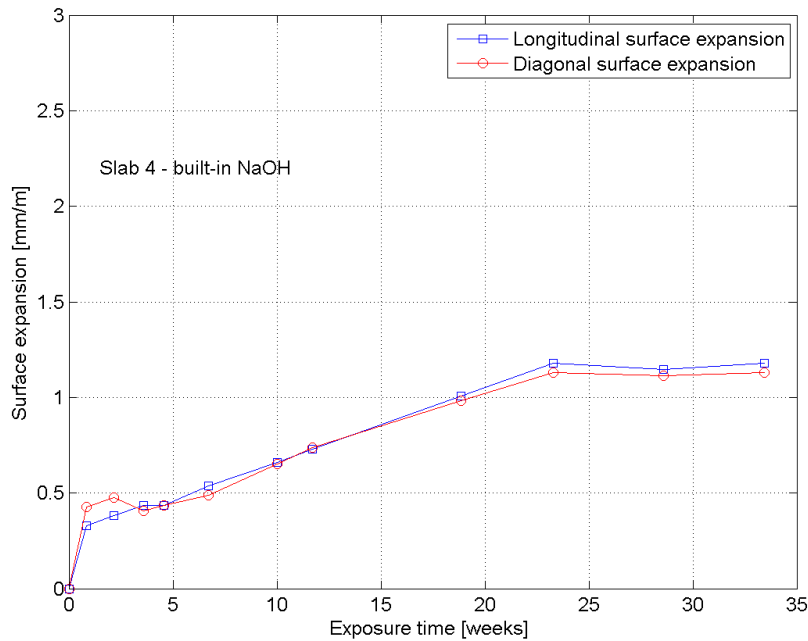
Figure 5.9: Mean longitudinal and diagonal surface expansion of slab 4.

surface expansion. Remarkably, this observation is valid for all slabs, despite differences in ASR crack orientation as shown in section 5.3.7.

- The third phase is called the *surface stabilization or surface stagnation phase*. At this phase the surface expansion stabilizes or stagnates for slabs. The vertical expansion continues linearly to increase for slab 8, exposed to NaCl solution; meanwhile, the surface expansion begins to stagnate. For slabs 3 and 4 with initial high Na_2O eq. content both the vertical expansion and surface expansion stabilizes at the same time.

Assuming the correlation of surface expansion to vertical expansion can be translated to the assessment of bridge slabs in service, we may conclude that surface expansion measurements in the case of an external supply of NaCl is not always a good indicator to the ASR crack extent inside the slab and corresponding vertical expansion. At the third phase, the surface expansion may underestimate the vertical expansion of slabs when exposed to NaCl solution.

When the initial Na_2O eq. content is high in the concrete, apparently the surface expansion can be a good indicator for the vertical expansion. The vertical expansion at the linearity phase is approximately 2.5 times greater than the surface expansion. For bridge slabs in service, this correlation is valid, assuming that the ASR crack orientation inside the structure corresponds to the crack orientation seen in section 5.3.7. It is important to state that the correlation between surface and vertical expansion will depend on the reinforcement ratio and configuration in
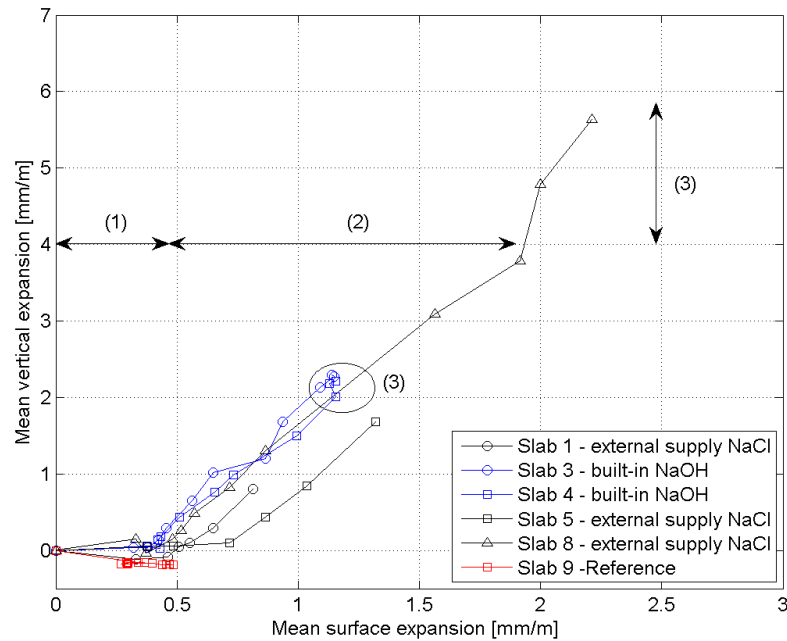
Figure 5.10: Correlation between mean vertical expansion and mean surface expansion for the accelerated reinforced slabs.

the examined structure. Additionally, this correlation may only be valid for fast ASR-reactive sand.

### 5.3.5 Thin-section examinations and diagnosis for ASR

In general, considerably more reactive aggregates in the reinforced slabs with initial high alkali content show signs of reactivity and cracking compared to the slabs exposed to NaCl solution. However, some aggregates in slabs with high alkali content only show signs of dissolution without development of deleterious cracking in the cement paste. As seen in Figure 5.11, two reactive aggregate particles are dissolved without causing cracking in the surrounding cement paste. In the right-hand side of the dissolved aggregates a fine ASR crack is seen in the cement paste which originates from other aggregates.

In slabs with initial high Na_2O eq. content, all the reactive particle sizes show initial sign of reactivity, whereas in the slabs exposed to NaCl solution, it is mostly the smaller potential aggregate particles that are reacting. Figure 5.12 shows a larger reactive aggregate in slab 8 at 10 weeks of exposure causing cracking in the surrounding cement paste. Figure 5.13 shows a large potential reactive aggregate in slab 8 at 23 weeks of exposure without any sign of reactivity. In the lower right-hand side of this large potential reactive aggregate, a small reactive aggregate particle causes cracking in the surrounding cement paste.

Another very important observation achieved from the thin-section examinations
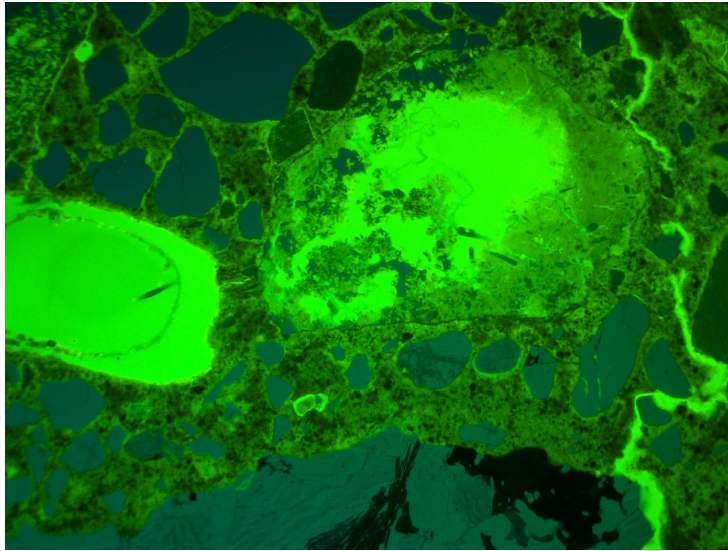
Figure 5.11: Microphotograph taken under fluorescent light. Width of field 4.7 mm. Two dissolved reactive aggregate particles in slab 3 at 10 weeks of exposure.
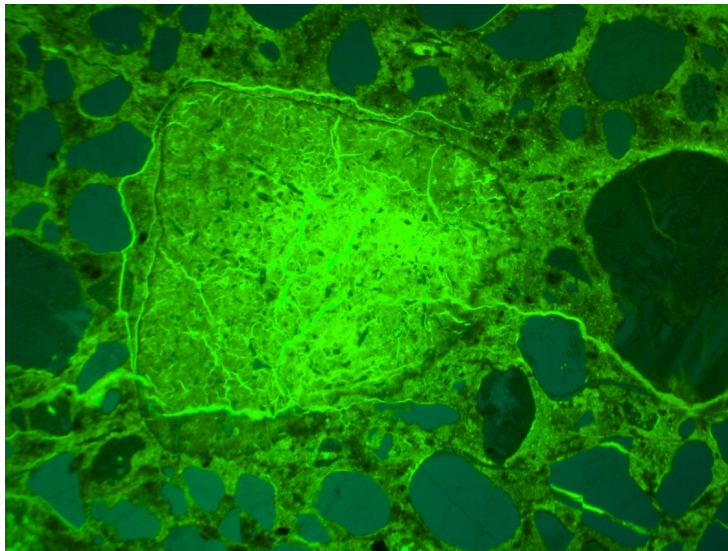
Figure 5.12: Microphotograph taken under fluorescent light. Width of field 4.7 mm. Slab 8 after 10 weeks of exposure. A reactive aggregate particle causes deleterious cracking in the cement paste.

is the detection of concrete carbonation mainly along the already formed ASR cracks. It is well known that the chemical reaction between $Ca(OH)_2$ and other compounds with atmospheric CO_2 lowers the pH in the concrete pore solution (Poulsen *et al.*, 1985). This lowering in pH will affect the future activity of reactive aggregates, assuming that some potential reactive aggregates may be surrounded by carbonated concrete. The solubility of reactive SiO_2 is very dependent on the surrounding pH solution in the concrete and is therefore dependent on the amount of $Ca(OH)_2$ in the pore solution and cement paste (Wigum *et al.*, 2006). When
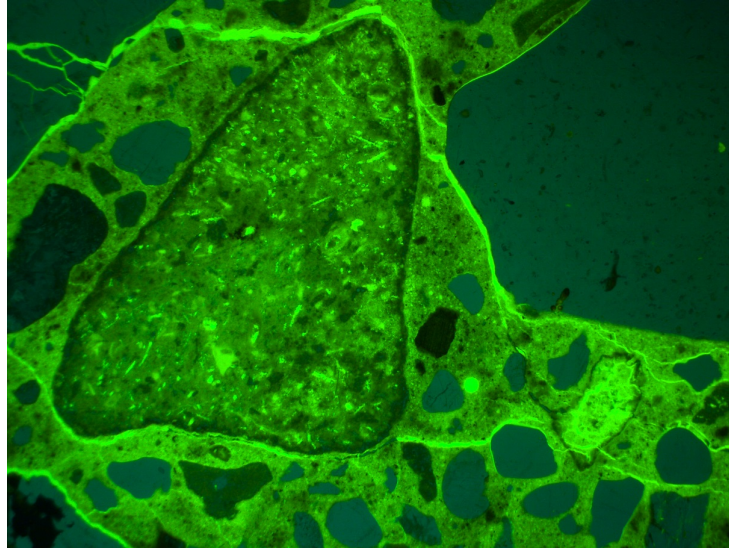
Figure 5.13: Microphotograph taken under fluorescent light. Width of field 4.7 mm. Slab 8 after 23 weeks of exposure. Large potential reactive aggregate particle without significant sign of reactivity.

the relative humidity is higher than 70 % the concrete tends to saturate, and the diffusion of CO_2 through the concrete slows down. However, with a constant high relative humidity, an increase in temperature is reported to significantly accelerate the carbonation rate in concrete (Poulsen *et al.*, 1985).

In general, concrete carbonation was mainly observed on the ASR cracks in the slabs exposed to NaCl solution, where carbonation was observed in the entire ASR crack penetration depth along the already-formed ASR cracks. Presently, there is no observation of reinforcement corrosion on the slabs. However, we may expect future reinforcement corrosion in the slabs due to a combination of concrete carbonation and chloride penetration. This combined action of carbonation and chloride penetration may accelerate the reinforcement corrosion. As reported by Wan *et. al* (Wan *et al.*, 2012), carbonation not only lowers the pH value in the concrete but also releases chemically bound chloride to the pore solution, resulting in a local increase in chloride concentration.

5.3.6 Chloride content in one slab supplied with NaCl solution

The total chloride content profile in one core drilled from slab 8 exposed to saturated NaCl solution at 23 weeks of exposure was determined by potentiometric titration. The sample preparation was identical to the procedure described in NT BUILD 208 (NT BUILD 208, 1996). Figure 5.14 shows the chloride profile for 0-200 mm of the half longitudinal core. The ASR crack penetration depth at this specific core was measured to 70 mm, based on the matching half fluorescence-impregnated part of the core.

Figure 5.14 shows that the chloride content on the surface of the slab is extremely high, which was expected because saturated NaCl solution was periodically poured
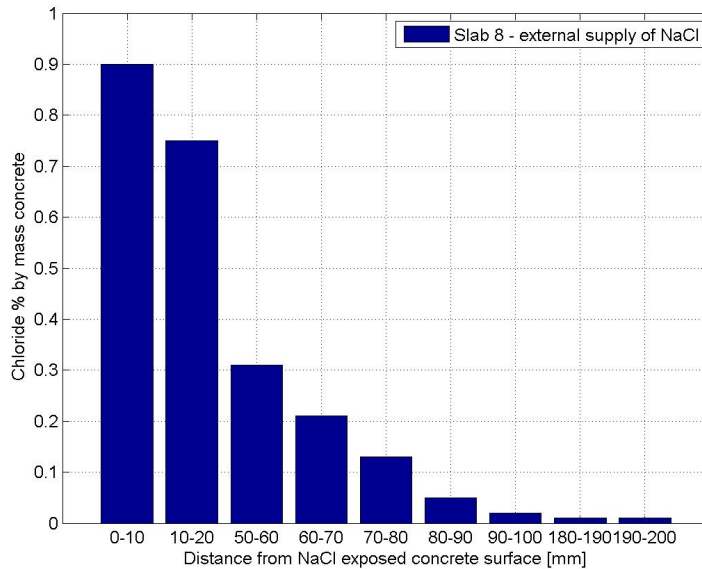
Figure 5.14: Chloride % by mass concrete for a concrete core drilled from slab 8 exposed to NaCl solution.

onto the upper slab surface. At depths around the ASR crack penetration depth, 70 mm, the chloride content decreases considerably to chloride contents of 0.13 to 0.21% by mass concrete. At depths below the ASR crack penetration depth of 70 mm, the chloride content drops to 0.05% by mass concrete, which confirms that NaCl is essential to initiate ASR cracking in the slabs where the alkali content in the cement is assumed to be too low to initiate severe ASR cracking.

The chloride contents inside the slab at the ASR crack penetration depth are similar to the chloride contents reported on a Danish ASR-damaged road bridge slab. Although it is expected that the chloride content will vary significantly between ASR-damaged bridge slabs in service, Nielsen et al. (Nielsen *et al.*, 2004) reported that the chloride content in ASR-damaged areas in one road bridge slab was measured to approximately 0.15 to 0.20% by mass concrete. Consequently, the chloride content near the crack penetration depth is not unrealistic compared to this specific ASR-damaged road bridge slab. As previously stated, due to this extreme chloride concentration and carbonation near the upper reinforcement, corrosion may in the future cause larger crack widths inside the slab, resulting in larger vertical expansions that are not related to ASR cracking. Thus, reinforcement corrosion may disturb the future measurements of vertical and surface expansion of slabs exposed to NaCl solution.

5.3.7   ASR crack orientation in the slabs

The initial Na$_2$O eq. content in the concrete has a significant influence on the orientation of cracking in the slabs. Figure 5.15 shows the ASR-induced crack orientation in three drilled fluorescence impregnated cores. Figure 5.15a shows the

crack orientation in slab 4 with initial high alkali content, and Figure 5.15b shows the crack orientation in slab 8 exposed to NaCl solution. Figure 5.15c shows the typical crack orientation in a core drilled from an ASR-damaged bridge slab in service. The reference slabs show no sign of cracking.
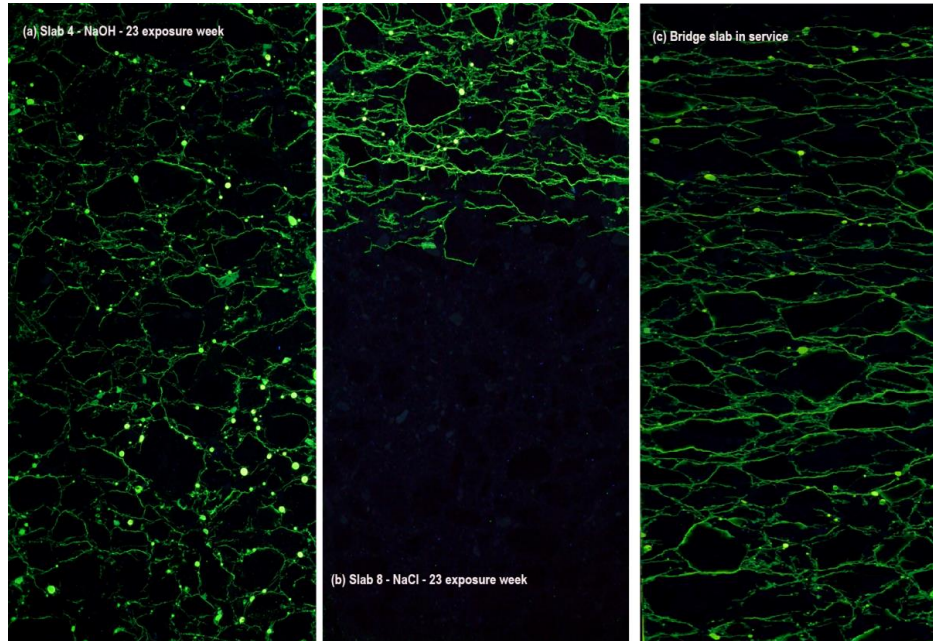
Figure 5.15: ASR crack orientation seen under ultraviolet light in fluorescence-impregnated cores. The height of the cores is 200 mm and not 250 mm as the slab tickness.

Subjectively, it is seen that the ASR cracking in slab 4 with initial high alkali content has a random ASR cracking pattern; see Figure 5.15a, compared to the ASR cracking in slab 8, exposed to NaCl solution; see Figure 5.15b. The total cross section of slab 4 is ASR cracked. Because the water-cement ratio in the concrete is 0.5, there is sufficient free water and alkalis in the concrete pore solution to start the reaction through the entire cross section in slabs 3 and 4.

In Figure 5.15b the orientation of the ASR cracks is similar to the cracks observed in ASR-damaged bridge slabs; see Figure 5.15c, where the cracks are mainly oriented parallel to the main reinforcement direction. However, the distance between the horizontal cracks in Figure 5.15b is smaller than in Figure 5.15c. This circumstance may be explained by the method for impregnating the cores; in Figure 5.15c the whole concrete core was impregnated and afterwards sawn into longitudinal halves, whereas in Figure 5.15b the core was sawn into two longitudinal halves before impregnation. Consequently, all the ASR cracks in the sawn cross sections were impregnated in Figure 5.15b compared to the cracks connected to the core surface of the whole core, as seen in Figure 5.15c.

Obviously, the differences in ASR crack orientation between the slabs are due to the source of alkali to the concrete. As seen in Figure 5.5, increased alkali content in the concrete causes a fast reaction and expansion development when a fast-reactive Danish sand aggregate is used. This rapid reaction may already have caused ASR

cracking in the early age of the concrete. Consequently, the tensile strength of the concrete and anchorage of reinforcement may not be sufficient at that time to restrain the ASR expansion in the longitudinal and transverse directions.

5.3.7.1 Verification of ASR cracking orientation by image analysis

The image analysis program provided by Andreassen *et al.* (Andreassen *et al.*, 2016) is used to verify the subjective evaluation of the ASR crack orientation in the cores and to quantify the orientation of the cracks in the three polished impregnated sections shown in Figure 5.15. Figure 5.16 shows the crack orientation histogram for all the three impregnated polished sections. Remember, crack orientation corresponding to 0 and 180 degrees represents horizontally oriented cracks, whereas 90 degrees represents vertically oriented ASR cracks. The ASR crack orientation in slab 4; see Figure 5.16a, is significantly more random than the crack orientation in slab 8; see Figure 5.16b, and the bridge slab; see Figure 5.16c. The random distribution of cracks in slab 4 is visualized by the proximity of the calculated crack orientation curve (red curve) to the blue horizontal line in the crack-orientation histogram. The horizontal line in the histogram corresponds to the assumption that all cracks (100%) were equally divided into 180 degrees. Consequently, in a core with randomly distributed cracks, 0.56% of cracks will be present in each orientation. It is shown that the shape of the crack orientation in slab 8 corresponds well to the crack orientation observed in a core from a bridge slab, although the impregnation method between the cores was different.

Generally, the image analysis program, as concerns the identification and quantification of the crack orientation, is a useful tool. As reported in Chapter 2, the orientation of the ASR cracks in cores has a significant influence on the compressive and tensile strength of ASR-damaged concrete and must be determined. However, as reported by Andreassen *et al.* the manual selection of a threshold value is a problematic feature in the image analysis program applied in this project. In all the analysis conducted shown in Figure 5.16, a threshold value of 150 was selected as a plausible value. Figure 5.17 shows the influence of threshold selection on the impregnated core seen in Figure 5.15a. It is seen from Figure 5.17 that an increase in threshold value will lead to the removal of ASR cracks which are present in the impregnated concrete core. On the contrary - a decrease in threshold value will lead to more noise to the output results. By selection of a threshold value, the objectiveness of the image analysis may decrease. In addition to the threshold value, also the impregnation method will have a significant influence on the visualization of the cracks and corresponding results of the image analysis program. Differences in green intensity will result in a different selection of threshold value; thus it may be impossible to compare several impregnated concrete cores with each other if the green intensity in the epoxy is not exactly the same. More research on the validation of one specific impregnation method and corresponding results from the image analysis program is needed. A standardized approach to the impregnation method of concrete cores that shall be used for image analysis and also photography of the impregnated cores is essential.

It is important to state that the image analysis shall always be supplemented
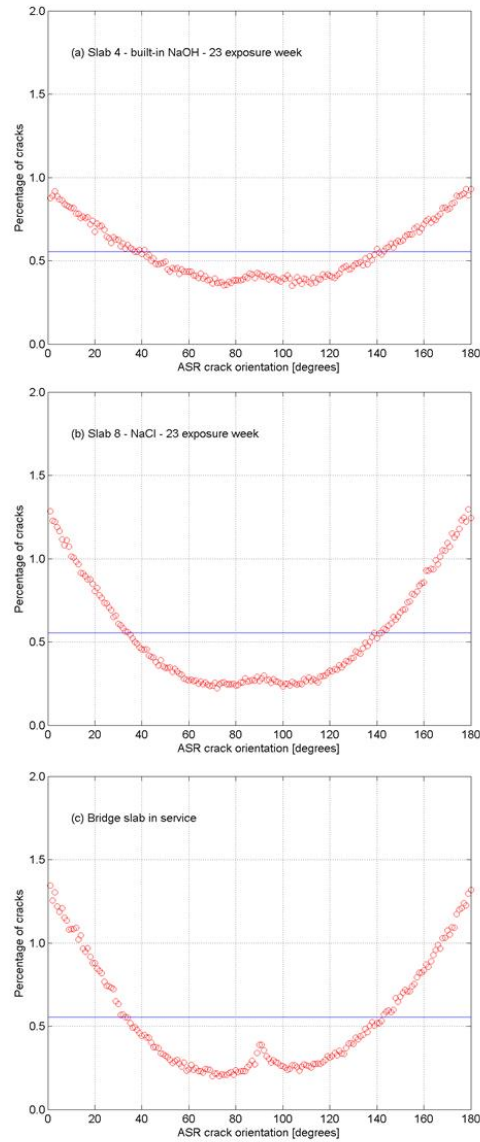
Figure 5.16: Orientation of ASR cracks by image analysis in impregnated polished sections shown in Figure 5.15.

by thin-section examinations, to verify that the impregnated cracks are due to ASR and no other mechanisms.

5.3.8 Crack penetration depth in slabs exposed to NaCl solution

Figure 5.18 shows the gradual downwards development of the ASR cracks in the slabs exposed to NaCl solution. As seen in Figure 5.18, there is an increase in gradual development of the ASR cracks as a function of exposure weeks. The predominant crack orientation corresponding to horizontal cracks is the same for
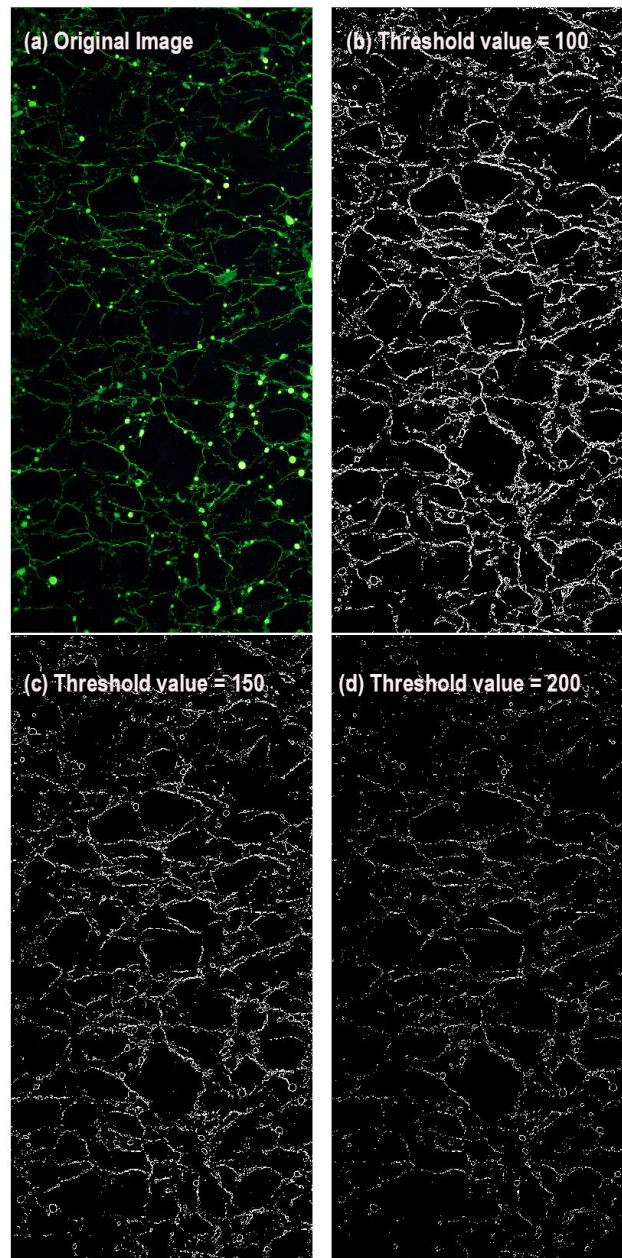
Figure 5.17: Influence of threshold value on the grayscale image applied for quantification of crack orientation. (a) Original input image. (b) Grayscale image threshold value of 100. (c) Grayscale image threshold value of 150. (d) Grayscale image threshold value of 200.

all the slabs. However, as seen in Figure 5.18f, there is a vertical crack in slab 8 at 35 weeks of exposure. In total two cores were impregnated from slab 8 at 35 weeks of exposure, where both cores show identical vertical cracking. Both cores were drilled from the same area in the slab. From the examinations conducted until now, it is not possible to verify if similar vertical cracks exist in other areas in the slabs. One may argue that at a specific crack penetration depth, the horizontal

expansion and corresponding tensile forces in the upper ASR cracked part of the slab will be sufficient to cause local splitting vertical cracks in the lower "intact" part of the slab. Thin-section examinations conducted in the border line between the typical horizontal ASR cracks and the vertical crack confirmed that the vertical crack developed due to ASR and originated from the horizontal cracks. There was no sign of carbonation in the vertical crack in Figure 5.18f. One may expect that there will be ingress of moisture and NaCl trough the vertical crack in Figure 5.18f. In the future, local development of ASR cracks near the vertical crack and not just the gradual development of cracks from the upper slab surface will be expected.

Figure 5.19 shows the mean crack penetration depth as a function of exposure weeks. The crack penetration depth was measured visually on fluorescence-impregnated cores and is based on measurements of two impregnated cores. The crack penetration depth corresponds to the penetration of horizontal ASR cracks. Without fluorescence impregnation, it was difficult to verify the presence of the border between cracked and the noncracked area in the cores, because the crack widths are rather fine. As seen in. Figure 5.19, there was, up to 34 weeks, a strong linear correlation between the crack penetration depth and the exposure time of the slabs. However, it is seen that this linear correlation will be slab dependent. Assuming the current crack penetration rate, it will approximately take 74 weeks for full ASR crack penetration, 250 mm for slab 8 and 100 weeks for slab 5, respectively.

Figure 5.20 shows the correlation between the mean vertical expansion and the mean crack penetration depth. As seen in Figure 5.20, for slab 8 there is currently a linear correlation between the vertical expansion and the crack penetration depth. This linear correlation occurs after an initiation period where the crack penetration depth is higher than the measured vertical expansion. We cannot assume the same linear correlation for slab 5 because there still are not enough results for this verification. However, considering Figure 5.20, one may argue for slab 5 that the vertical expansion underestimates the crack penetration depth compared to slabs 8 and slab 1. This fact may be explained by local differences of crack penetration depth in the slabs. The vertical expansion on slab 5 is based on one vertical measurement. For slab 8, and slab 1 the vertical expansion is based on 4 measurements. Consequently, more local variations are included in the vertical expansion of slabs 8 and slab 1.

Although it is well known that the Danish reactive sand aggregates are fast reactive, it is still a surprise that after only 34 weeks the cracks penetrated an average of 115 mm from the surface of the slabs. This gradual ASR crack development is very fast. For bridge slabs in service, this rapid development should be included in the evaluation of remedial actions. Actions for prevention of moisture and alkali ingress to the concrete should be conducted as soon as possible to prevent further development of ASR into larger areas in the structure. There is no doubt that the high temperature inside the container has a significant influence on the rate of the reaction. As reported by Poole in (Swamy, 1992), the initiation of expansion increases with increased temperature. However, the total expansion decreases with increased temperature. For the Danish reactive sand aggregate, Chatterji and Christensen (Chatterji and Christensen, 1990) have shown the effect of temperature on the total expansion and initiation of expansion of mortar bars. The results of
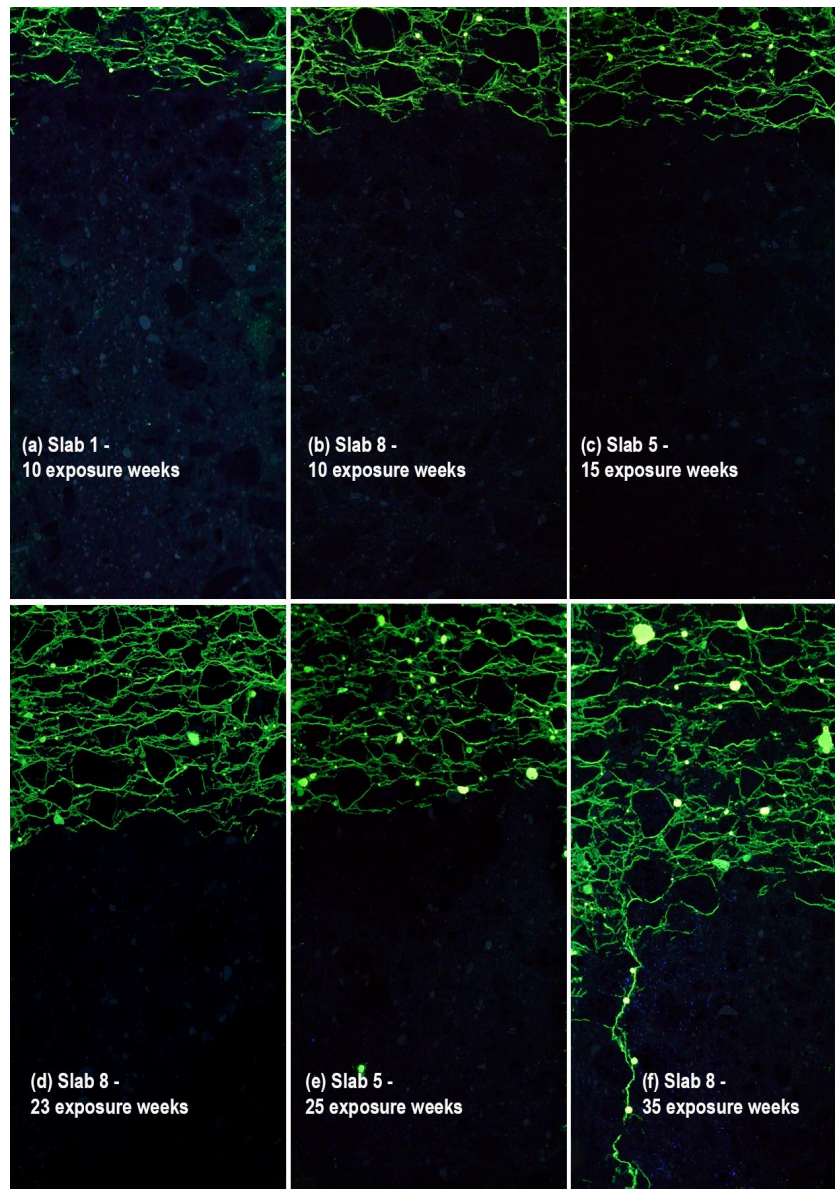
Figure 5.18: Visualization of the crack penetration depth in the slabs exposed to an external supply of saturated NaCl solution. The height of the concrete cores is 200 mm and not 250 mm as the entire slab thickness.

Chatterji and Christensen confirm the results by Poole. Figure 5.21 shows the temperature effects on mortar bar expansion with Danish reactive sand aggregate by Chatterji and Christensen (Chatterji and Christensen, 1990; Wigum *et al.*, 2006).

As seen in Figure 5.21, the initiation time of the expansion increases with increasing temperature. At 20 ºC it takes approximately 10 to 15 weeks longer to initiate the expansion compared to the time it takes at 50 ºC. However, the most interesting results from Figure 5.21 are not the initiation time or the final expansion at different temperatures; but the slope of the expansion curves at
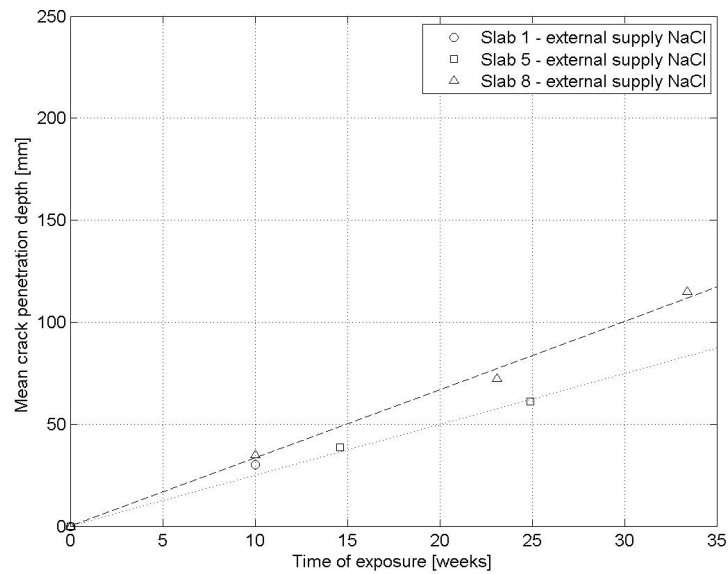
Figure 5.19: Mean crack penetration depth as a function of time of exposure in weeks.

different temperatures. Although the initiation of expansion is prolonged at 20 ^{o}C, the slope of the curve is the same or even more steep at 20 ^{o}C than at higher temperature. One may argue that the expansion rate is not considerably lower at lower temperatures, but primarily the initiation time of the expansion.

By placing the slabs in outdoor temperature conditions, it may be possible to correlate the laboratory-accelerated slabs with similar in-situ exposed slabs within one or two years. However, outdoor temperature vary considerably during a one-year period, and we can only guess the crack penetration rate on the slabs. The correlation between the accelerated slabs and in-situ conditioned slabs will be crucial, in order to validate all the results achieved in this study and to correlate the results with actual bridge slabs in service. For in-situ exposed slabs we may expect increased ASR crack widths compared to the laboratory-accelerated slabs. Most importantly, the ASR crack orientation should be the same for in-situ and laboratory-accelerated slabs.
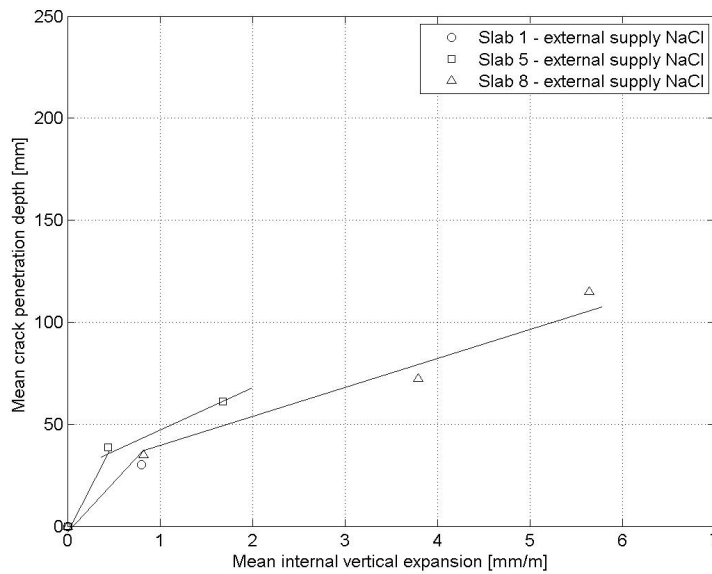
Figure 5.20: Mean crack penetration depth as function of mean internal vertical expansion.
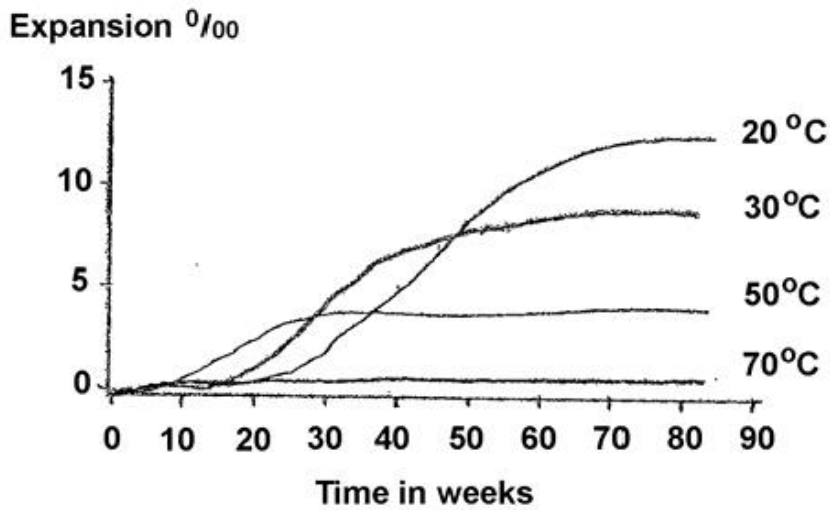
Figure 5.21: Temperature effect on the expansion of mortar bars with Danish reactive sand aggregate. The mortar bars were immersed in 1M NaCl solution. Adapted from (Wigum *et al.*, 2006).

5.3.9 Compressive strength of drilled cores

The strength of cores extracted from slab 4 with a high Na_2O eq. content and random ASR crack pattern is not included in the results seen in Figure 5.22. Unfortunately, the reference cylinders for slabs 3 and 4 were completely ASR cracked at time of testing. The cylinders of slabs 3 and 4 were stored at room temperature and sealed in plastic bags for 30 weeks. Compared to cylinders from

slabs without a high initial $Na_2Oeq.$ content, the strength of cores from slab 4 decreased by approximately 50% at 23 weeks of exposure; however this comparison may not be valid. Shayan and Ivanusec (Shayan and Ivanusec, 1989) reported that due to an increased addition of NaOH to mortar bars, the strength decreases, although no sign of ASR was detected. Shayan and Ivanusec reported that the increasing addition of NaOH weakens the cement paste matrix.
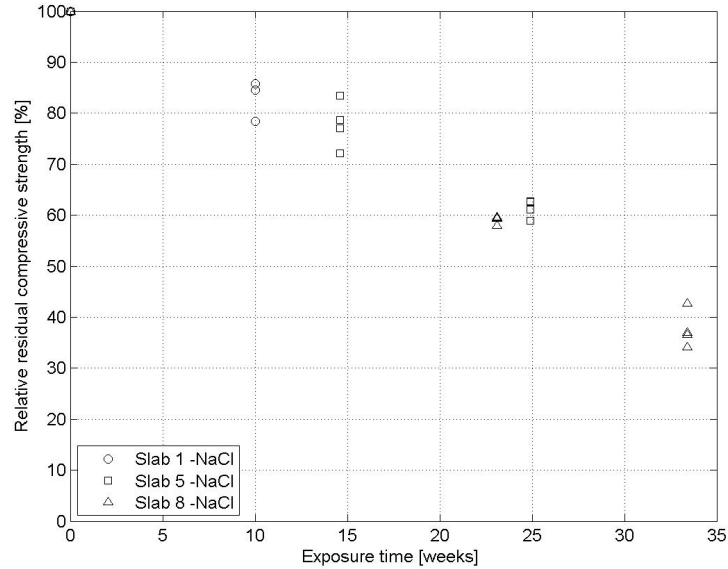
Figure 5.22: Relative residual compressive strength of cores as a function of exposure time.

Figure 5.22 shows the relative residual strength of cores extracted from the slabs exposed to NaCl solution as a function of exposure weeks. As seen in Figure 5.22 the strength of cores decreases significantly as function of exposure time. At 33 weeks of exposure the strength have in average decreased by 62%. The relative residual strength is determined as the ratio between the core strength with the reference cylinder strength. The cylinders were sealed in plastic bags and stored at room temperature for 30 weeks before testing. From slab 2 and 9, it is measured that the cylinder strength is 3-4% higher than the core strength. The cores from slab 2 and 9 were drilled at 23 weeks of exposure. As seen in Figure 5.23 the decrease in strength is unquestionably influenced by the gradual penetration of the ASR cracks inside the slabs. There is a strong linear correlation between the residual strength and the crack penetration depth for the slabs exposed to NaCl solution. For cores vertically drilled from ASR-damaged bridge slabs in service, see Chapter 2, it is proposed that the residual strength will stabilize at a certain level in the ASR-deterioration progress, despite that further cracks may develop in the concrete. For the cores from the slabs we expect that the residual strength of cores will also stabilize at a certain level of ASR crack penetration depth. The strength will not propagate towards zero, although the ASR cracks continues to penetrate the slabs and corresponding cores.
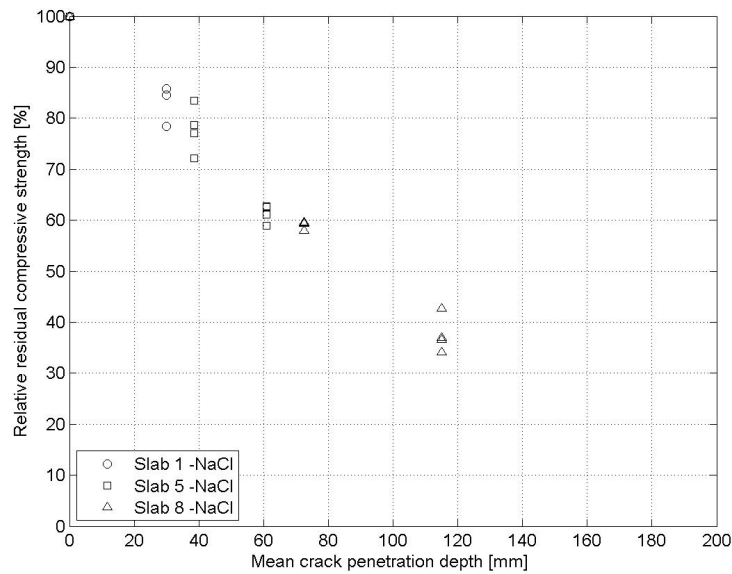
Figure 5.23: Relative residual compressive strength of cores as a function of mean crack penetration depth.

As seen in Figure 5.20, the vertical expansion apparently underestimates the crack penetration depth for slab 5. Despite this fact, as seen in Figure 5.24, the strength decreases as a function of increasing expansion. Comparing Figure 5.24 with Figure 5.23 one may argue that the crack penetration depth better illustrates the decrease in strength than the vertical expansion.

5.3.9.1 Observed failure mechanism of cores after compression

The observed failure mechanism between the cores drilled from slabs exposed to NaCl solution and cores drilled from reference slabs varies considerably. As seen in Figure 5.25a, the failure mechanism of cores with horizontal ASR cracks located in the upper part of the core (red square) is governed by the closure of ASR cracks. As a consequence of this closure, vertical splitting tensile cracks are introduced in the concrete, resulting in lateral deformations in ASR-cracked part. One may argue that, as a consequence of ASR cracks in the upper part of the concrete, shear forces near the upper steel loading platen do not restrain the lateral deformation of the core in the upper end faces. The splitting tensile stresses introduced in the upper ASR-cracked volume results in vertical splitting tensile cracks (red arrows) in the "intact" lower part of the core. The larger the "intact" volume in the core, the more load is needed to develop vertical splitting tensile cracks in the "intact" concrete part. As seen in 5.25b, the load-induced cracks in a core drilled from reference slab 9 mainly develop in the middle part of the core, as expected for normal, uncracked concrete. Here we expect triaxial compressive stress near the steel loading platens at the concrete ends, which prevents lateral deformations near the top and bottom ends of the concrete core.
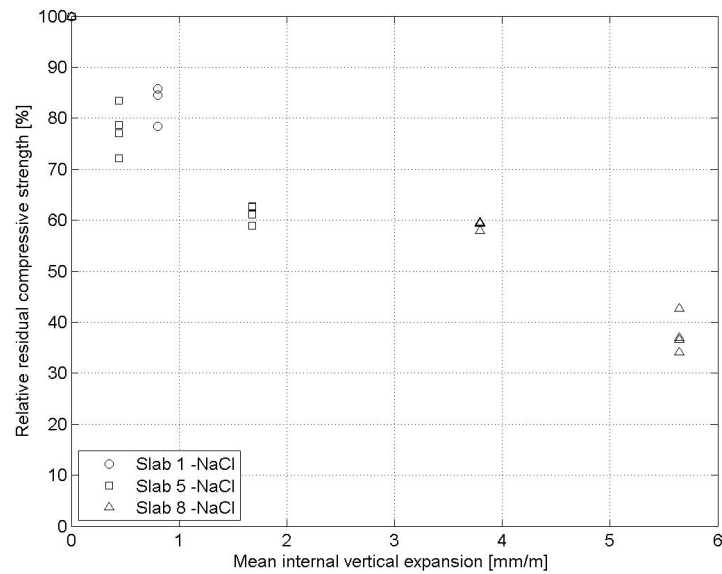
Figure 5.24: Relative residual compressive strength of cores as a function of mean internal vertical expansion.

The development of splitting cracks has also been observed in ASR-damaged cores drilled vertically from slabs in service, as seen in Chapter 2. It is, however, important to state and acknowledge that the proposed failure mechanism presented in this study is simplified and may be significantly more complex than described. From these strength results we may argue that the strength of vertically drilled cores is not a good indicator of ASR-deterioration. Only small proportions of ASR cracks at specific parts on the cores have a significant negative impact on the strength. Consequently, the strength of vertically drilled cores overestimates the "real" ASR-deterioration of the slabs as a function of exposure time. This argument does not match the general view regarding ASR-deterioration and compressive strength of accelerated cylinders under free expansion. Here it is argued that low ASR expansion does not cause a significant decrease in strength of the accelerated cylinders (Fournier and Bérubé, 2000).
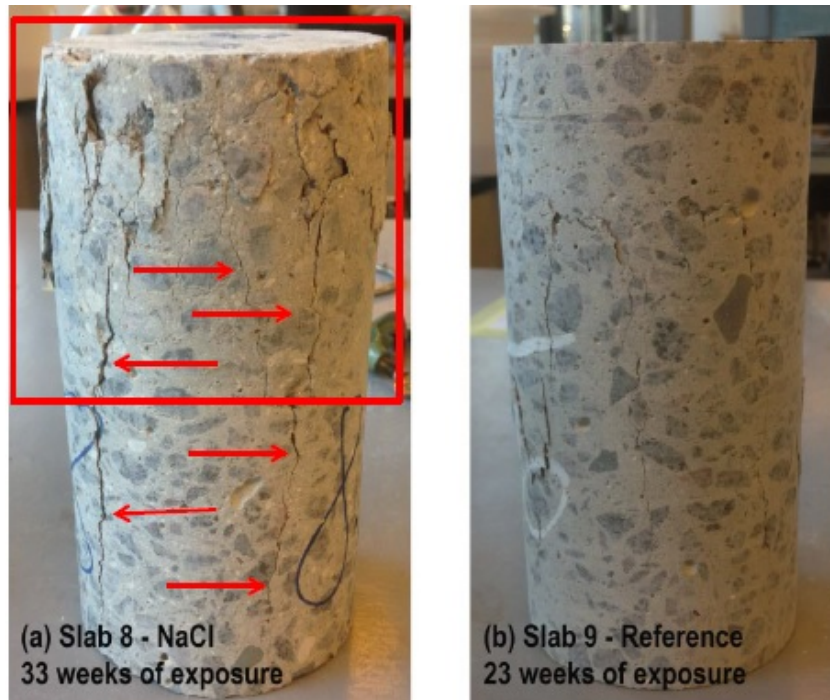
Figure 5.25: Cores after compressive loading. (a) Core drilled from slab 8 at 33 weeks of exposure. Red square indicates part in the core where closure and lateral deformation are introduced. Red arrows represent vertical splitting tensile cracks. (b) Core drilled from reference slab 9.

5.3.10 Ultrasonic pulse velocity of drilled cores

Figure 5.26 shows the measured ultrasonic pulse velocity as a function of the compressive strength of drilled cores and cylinders. The results of every core and cylinder are included in Figure 5.26. As seen in Figure 5.26, a linear correlation between strength and ultrasonic pulse velocity is observed from the reference strength until approximately 30 MPa. Below 30 MPa, a continuous drop in strength is measured without any remarkable decrease in pulse velocity. The correlation between pulse velocity and strength may be interpreted as a rapid linear decrease phase and corresponding stabilization phase of the pulse velocity.

From Figure 5.26 it can be argued that the pulse velocity can, with some boundaries, be applied to roughly estimate the decrease in strength due to ASR cracking. Especially if one assumes that the strength of cores will stabilize at strengths corresponding to 10-15 MPa. There is no expectation that the strength of cores will decrease towards 0 MPa, despite increasing crack penetration depth.

As seen in Figure 5.27, the pulse velocity cannot be applied to estimate the crack penetration depth in the slabs and corresponding vertical expansion. In Figure 5.27, after only 60 mm of crack penetration the pulse velocity seems to stabilize. Consequently, an increase in crack penetration depth may not result in a further decrease in pulse velocity. However, before 60 mm of crack penetration there is a correlation between pulse velocity and crack penetration depth. Swamy (Swamy, 1992) reported that on reinforced beams the pulse velocity can quantify
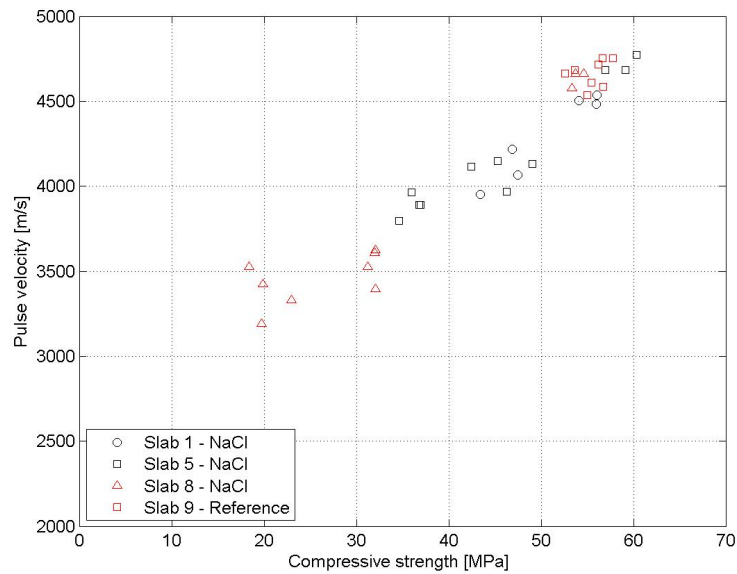
Figure 5.26: Ultrasonic pulse velocity as a function of compressive strength of cores and reference cylinders.

the deterioration in reinforced beams, which may not be consistent with the results presented in Figure 5.27. In this context, one may ask which parameters are interpreted as deterioration. The author agrees with Swamy, that there is no unique relationship between ASR expansion and ultrasonic pulse velocity. Giannini (Giannini, 2012) reported that based on measurements of exposure blocks and reinforced beams, the ultrasonic pulse velocity does not correlate well with an expansion in a particular direction, which is of more interest for reinforced structures and the slabs.

Despite of the correlation between pulse velocity and compressive strength seems interesting, there are some challenges with estimations of strength based on pulse velocity and application of the pulse velocity measurements in bridge slabs in service. For a rough estimation of the residual strength based on pulse velocity, one must be able to estimate the original pulse velocity of uncracked concrete, which is not always possible for ASR-damaged bridge slabs in service. As an alternative, pulse velocity measurement on cores with cracks parallel to the direct pulse velocity direction could be applied as a lower-bound original pulse velocity. For that approach, horizontal core drilling must be conducted in-situ, which has been evaluated to be too expensive and unrealistic when compared to the relevance of such testing to real-life ASR-damaged structures. Although the correlation between pulse velocity and residual strength may seem interesting, the applicability of the ultrasonic pulse velocity in-situ is also highly restricted. Direct pulse velocity measurements are crucial to evaluate the pulse velocity through slabs. In-situ it is impossible to obtain satisfactory alignment of the transducer and receiver across large areas. In Denmark, an asphalt pavement on top of the
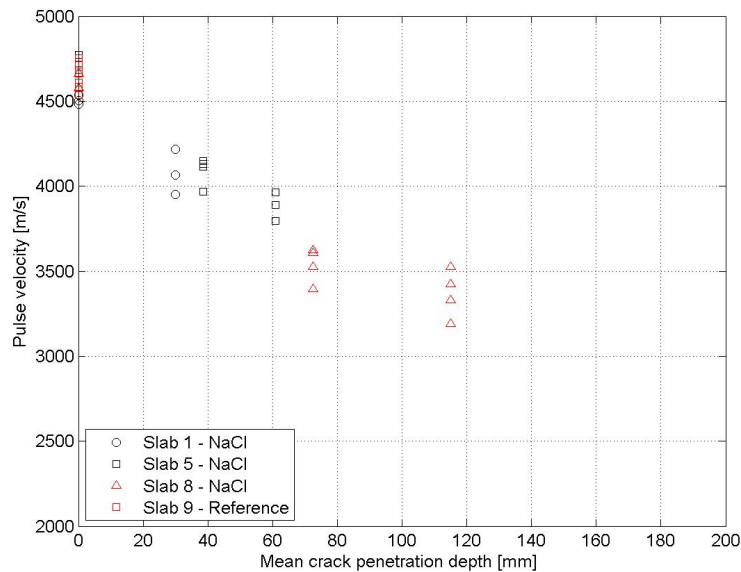
Figure 5.27: Ultrasonic pulse velocity as a function of mean crack penetration depth for cores and reference cylinders.

bridge deck is normally used and must be removed before pulse velocity testing, which once again is not realistic. If evaluated on drilled cores, it may be better to test the compressive strength of the cores from the slabs rather than roughly estimate the residual strength based on pulse velocity measurements. Consequently, pulse velocity measurements may be a suitable nondestructive test method for laboratory purposes but not an applicable in-situ nondestructive method. Generally, concerning nondestructive test methods it can be argued that the vast majority of the nondestructive test methods can be applied to evaluate both good and deteriorated areas. However, the nondestructive methods may not be suitable to distinguish between different deterioration degrees, crack-penetration depths, and expansion rates in specific areas of the structure.

5.4 Conclusions

In this study, the time-dependent influence of ASR on the physical and mechanical properties of large laboratory-accelerated reinforced slabs was investigated. The main findings of the study are:

- The free expansion of cylinders immersed in NaCl solution was considerably higher than cylinders with high Na_2O eq. content. The results from the free expansion of cylinders was similar to the results by Chatterji *et al.*, based on expansion of mortar bars.

- The internal vertical expansion of the slabs is strongly related to the initial alkali content in the concrete. Slabs exposed to NaCl solution have a higher

vertical expansion than slabs with high initial Na_2O eq. content.

- The correlation between vertical expansion and surface expansion can be divided into three phases. As a consequence of these phases, the surface expansion cannot be correlated to the vertical expansion or deterioration of slabs exposed to NaCl solution. However, for slabs with initial high Na_2O eq. content there is a very good correlation between surface expansion and vertical expansion.

- The sources of alkali to the concrete have also a significant influence on the ASR crack pattern inside the slabs. Initial high Na_2O eq. content in the concrete leads to random cracking patterns that cannot be related to Danish ASR-damaged bridge slabs in service. Supply of NaCl solution is essential in order to correlate the ASR crack orientation observed in bridge slabs in service and laboratory-accelerated slabs.

- The MatLab program used to quantify the crack orientation in cores is evaluated as a very useful program. The selection of a threshold value, however, is challenging and is a weakness in the program.

- Thin-section examinations verified that ASR only caused the cracking in the slabs. However, carbonation in cracks may prevent the future development of ASR in carbonated areas.

- For slabs exposed to NaCl solution, reinforcement corrosion is expected in the future. The chloride content is, as expected, extremely high in the upper surface of the slabs. However, the chloride content close to the crack penetration front can be similar to ASR-damaged bridge slabs in service.

- When exposed to NaCl solution from the upper slab surface, the ASR crack penetration is very fast. These accelerated tests provide a better understanding of the rate of the reaction in slabs. The rate of the reaction should be accounted for in remedial actions. Apparently, there is a strong linear correlation between ASR crack penetration depth and time of exposure.

- ASR crack penetration has a significant influence on the compressive strength of cores. ASR crack penetration of only 115 mm resulted in a 62% decrease in strength. Until approximately 115 mm penetration, there is a strong linear correlation between residual strength and ASR crack penetration depth.

- The failure mechanism in compression for the cores could be correlated to the failure mechanism of cores drilled from ASR-damaged bridge slabs in service.

- Ultrasonic pulse velocity measurements showed promising results in determination of strength. However, the ultrasonic pulse velocity is not sensitive enough to detect the crack penetration depth and corresponding vertical expansion of the slabs. The applicability of pulse velocity measurements in-situ is, as discussed, highly limited.

CHAPTER 6

Conclusions

6.1 Novelty and major contributions

This study investigated the mechanical properties of alkali-silica reaction (ASR) damaged drilled concrete cores and the residual load-carrying capacity of reinforced beams sawn from a severely ASR-damaged flat slab bridge without shear reinforcement. I also investigated the time-dependent influence of ASR on the physical and mechanical properties of large laboratory-casted and laboratory-accelerated reinforced slabs. The main contributions and findings of this study are summarized below:

Influence of ASR and crack orientation on the uniaxial compressive strength of drilled concrete cores from slab bridges (Paper I)

- ASR has a significant negative influence on the uniaxial compressive strength of drilled concrete cores from all three examined ASR-damaged slab bridges in service. The decrease in compressive strength is governed by the orientation and by the amount of ASR cracks in the cores.

- The strength in the direction perpendicular to ASR cracks is significantly smaller than the strength in the direction parallel to ASR cracks. Consequently, evaluation of compressive strength based on vertically drilled concrete cores (ASR cracks oriented perpendicular to the load direction) can be rather conservative. Strength reduction of up to 64 percent has been found for vertically drilled cores, and up to 52 percent for horizontally drilled cores.

- ASR cracks oriented perpendicular to the load direction have a more rapidly negative impact on the compressive strength than cracks oriented parallel to the load direction. It is argued that the strength in direction parallel to ASR cracks is more representative for the amount of ASR cracks and corresponding ASR-deterioration in the concrete.

- Apparently, an increase in ASR cracks in the cores results in decrease in strength. However, a lower limit of strength will be reached for cores with ASR cracks oriented perpendicular to the load direction. This is the case despite further development of ASR cracks in the concrete. It seems that the difference in strength for the two crack orientations (perpendicular or parallel to the load direction) will decrease as the amount of ASR cracks in the concrete increases.

- The differences in strength for the two crack orientations may be explained by the differences in failure mechanisms. The failure in cores with cracks perpendicular to the load direction is governed by eccentric closure of horizontal cracks perpendicular to the load direction and the formation of load-induced vertical tensile splitting cracks in the concrete. In cores with cracks parallel to the load direction, the failure is governed by opening of the parallel ASR cracks. Due to this opening the parallel cracks will fail due to bending, buckling or crushing.

- Closure of uneven distributed perpendicular cracks results in large eccentric deformations and possible local stress concentrations in the core. This eccentric behaviour will result in a more rapid and negatively impact on strength than cores having ASR cracks parallel to compression.

- The static Young's modulus is also significantly influenced by the ASR crack orientation within the cores. As a consequence of the closure of horizontal cracks perpendicular to the load direction, the static Young's modulus decreases by up to 90 percent, on average, compared to uncracked concrete. For cores with cracks parallel to the load direction, the average Young's modulus is reduced by 41 percent.

Influence of ASR and crack orientation on the tensile strength of specimens from slab bridges (Paper II)

- The direct and indirect tensile strength of ASR-damaged specimens are both negatively influenced by the ASR cracks. As for the compressive strength, both the direct and indirect measured tensile strengths are strongly influenced by the orientation of the cracks in the specimens.

- Both the direct and indirect tensile strength test methods present disadvantages when testing ASR-cracked specimens. Three tensile strength test methods are tested: the uniaxial tensile strength test, the Brazilian split test, and the wedge splitting test.

- The Brazilian split test is less sensitive for the effect of ASR cracks than the other tensile strength methods. The conversion factor that is normally used to predict the uniaxial tensile strength from the splitting tensile strength is not applicable for ASR-cracked cores. The conversion factor should be significantly lower.

- The wedge splitting test is rather simple, but concrete cubes must be tested, which challenges the size of specimens to be sawn or drilled from bridge slabs in service. The inverse analysis based on the implementation of the crack hinge model to WST geometry does not completely fit the experiments. This may be explained by the opening of existing ASR cracks and corresponding different failure mechanisms than the theoretical failure mechanism given by the crack hinge model. Despite this, the crack hinge model fits with the experiments surprisingly well.

- The uniaxial tensile strength test is definitely more negatively affected by the ASR cracks than the other test methods. The presence of ASR cracks makes it impossible to maintain a centric loading during testing.

- The formula that is used for normal uncracked concrete to predict the uniaxial tensile strength from the compressive strength is not applicable for ASR-cracked concrete. The measured tensile strengths are significantly lower than the tensile strength predictions.

- In practical terms, when testing vertically drilled cores from ASR-damaged flat slab bridges in service, the Brazilian split test will provide the highest and the uniaxial tensile test will provide the lowest tensile strength results.

Residual shear strength of reinforced beams sawn from a severely ASR-damaged flat slab bridge (Paper III)

- The elastic restraint of ASR expansion by the longitudinal reinforcement results in significant tensile strains and stresses (pre-stress effect) in the reinforcing bars. The measured tensile strains are not proportional to the visual amount of cracks in the sawn beam surfaces or the compressive strength of drilled cores. Measurements of the tensile strains by strain gauges are rather simple and have proven to be applicable in-situ.

- The bending test setup has a significant influence on the failure mechanism of the beams. Most of the beams tested in the three-point bending setup suffered ductile rotational failure in diagonal cracks (bending type of failure). Most of the beams tested in the asymmetrical four-point bending setup suffered ductile shear failure. The propagation of load-induced cracks varied from beam to beam and was strongly influenced by the ASR cracks in the beams.

- The measured load-carrying capacities in the three-point bending setup express the moment capacity of the beams and not their shear strength.

- When based on the compressive strength of drilled cores, the calculated sectional moment capacity is in most cases lower than the maximum moment carried by the beams. However, the type of failure on individual beams and larger crack widths due to the combined effect of ASR and corrosion may result in calculated sectional moment capacity higher than the measured maximum moment.

- For beams tested in the four-point bending setup, the shear span-to-effective-depth (a/d) ratio significantly influences the shear strength of the ASR-damaged beams. An increase in a/d-ratios results in a decrease in shear strengths.

- When based on the compressive strength of drilled cores there is a poor correlation between shear strength calculations by Eurocode 2 and measured shear strengths. In most cases, the shear strength calculations are conservative. However, the conservatism of the calculations decreases with increasing a/d-ratios. The benefit in applying the strength of horizontally drilled cores (strength in the direction parallel to ASR cracks) is negligible compared to vertically drilled cores (strength in the direction perpendicular to ASR cracks).

- The calculated shear strength based on the compressive strength of vertically drilled cores where the ASR-induced pre-stress effect has been accounted for are in better agreement with measured shear strengths at a/d-ratios between 2.8 and 3.5. However, the calculated shear strengths at a/d-ratios above 3.5 are up to 19 percent higher than the measured shear strengths. At an a/d-ratio of 2.2 the pre-stress effect alone can not explain the enhancement in measured shear strengths.

- The test results indicate that the ASR-induced pre-stress effect has a positive effect on the shear strength of ASR-damaged beams.

Time-dependent influence of ASR on the physical and mechanical properties of laboratory-casted and laboratory-accelerated reinforced slabs (Chapter 5)

- The sources of alkalis to the concrete, either within the mix water or externally supplied as saturated NaCl solution, result in different influence on the physical and mechanical properties of the reinforced slabs and drilled cores.

- The internal vertical expansion and the surface expansion of the slabs are strongly related to the sources of alkalis to the concrete. When externally exposed to saturated NaCl solution from the upper slab surface the vertical expansion and surface expansion of the slabs are considerably higher than for slabs having initial alkali, Na_2O eq., content of 7 kg/m^3 primarily from NaOH added to the mix water. This difference in vertical expansion can be explained by (a) the differences in observed ASR cracks in the slabs; (b) the possibility that, in slabs with high intial alkali content, some ASR cracks have developed before the beginning of measurements; and (c) the possible differences on the influence of NaCl and NaOH on the expansive reaction.

- When exposed to NaCl solution, the surface expansion cannot be correlated to the vertical expansion of the slabs, because the correlation between surface expansion and vertical expansion is divided into three different phases. However, for slabs with high initial alkali content, the surface expansion can fairly be correlated to the vertical expansion. For the slabs with high initial alkali

content the stabilization of the surface expansion results in stabilization of the vertical expansion.

- When exposed to NaCl solution, the orientation of ASR cracks inside the accelerated slabs is comparable to the ASR cracks observed on actual ASR-damaged bridge slabs. In slabs with high intial alkali content, however, the ASR cracks in the slabs are seen as random map-cracks.

- The crack edge detection image analysis MatLab program is evaluated as a useful (that is, more objective than visual observations) tool with which to analyze the orientation of ASR cracks in fluorescent-impregnated cores.

- When exposed to NaCl solution the gradual development of ASR cracks through the slabs is very fast. Although the reaction is accelerated by the high temperature and high RH, this fast rate downwards development of ASR cracks provides significant knowledge that should be accounted for in remedial actions for ASR potential slabs in service.

- There is a strong linear correlation between the compressive strength in the direction perpendicular to ASR cracks and the ASR crack penetration depth. However, this linear correlation may only be valid until a certain crack penetration depth. Although the ASR cracks have only penetrated 115 mm of the 200 mm core, the strength has decreased by an average of up to 62 percent. It is expected that the decrease in strength will reach a lower stable limit, despite continuous increase in crack penetration in the cores.

References

Ahmed T, Burley E, Rigden S. The Static and Fatigue Strength of Reinforced Concrete Beams Affected by Alkali-Silica Reaction. ACI Mater J, 1999;95(4): 376-388.

Ahmed T, Burley E, Rigden S, Abu-Tair AI. The effect of alkali reactivity on the mechanical properties of concrete. Constr Build Mater. 2003;17:123-144.

Allard A, Bilodeau S, Pissot F, Fournier B, Bastien J, Bissonnette B. Performance evaluation of thick concrete slabs affected by alkali-silica reaction (ASR) - Part I: Materials aspects, In: Proceedings of the 15th International Conference on Alkali-Aggregate Reaction in Concrete; 2016 Jul 03-07; São Paulo.

Andreassen EN, Elbrønd AB, Hasholt MT. The use of image analysis to quantify the orientation of cracks in concrete. In: Proceedings of the International RILEM Conference Materials, Systems and Structures in Civil Engineering 2016: Segment on Frost Action in Concrete; 2016 Aug 22-23; Copenhagen. p. 55-57.

Bach F, Thorsen TS, Nielsen MP. Load-carrying capacity of structural members subjected to ASR. Constr Build Mater. 1993;7(2):109-115.

Barbosa RA, Hansen SG, Hansen KK, Hoang LC, Grelk B. Influence of alkali-silica reaction and crack orientation on the uniaxial compressive strength of concrete cores from slab bridges. Submitted to Cem Concr Res; 2017.

Batic OR, Giaccio G, Zerbino R. On effect of ASR cracking on the mechanical behaviour of concrete in tension and compression. In: Proceedings of 12th International Conference on Alkali-Aggregate Reaction in Concrete; 2004 Oct 15-19; Beijing. p. 1136-1141.

Bilodeau S, Allard A, Bastien J, Pissot F, Fournier B, Mitchell D, Bissonnette B. Performance Evaluation of Thick Concrete Slabs Affected by Alkali-Silica Reaction (ASR) - Part II: Structural Aspects. In: Proceedings of the 15th International Conference on Alkali-Aggregate Reaction in Concrete; 2016 Jul 03-07; São Paulo.

Brühwiler E, Wittmann FH. The Wedge Splitting Test, a New Method of Performing Stable Fracture Mechanics Tests. Eng. Fract. Mech. 1990;35(1/3):117-125.

Byggestyrelsen. Basic Concrete Specifications for Bulding Constructions. Copenhagen: Byggestyrelsen; 1987. Danish.

Chana PS, Korobokis GA. Structural performance of reinforced concrete affected by alkali-silica reaction: Phase I. Contractor Report 267, Crowthorne, Transport and Road Research Laboratory; 1991.

Chatterji S, Thaulow N, Jensen AD. Studies of alkali-silica reaction. Part 4. Effect of different alkali salt solutions on expansion. Cem Concr Res, 1987;17(5):777-783.

Chatterji S, Thaulow N, Jensen AD. Studies of alkali-silica reaction. Part 6. Practical Implications of a proposed reaction mechanism. Cem Concr Res. 1998;18(3):363-366.

Chatterji S, Thaulow N, Jensen AD. Studies of alkali-silica reaction. Part 7. Modelling of expansion. Cem Concr Res. 1990;20(2):285-290.

Clark LA. Critical Review of the Structural implications of the alkali-silica reaction in concrete. PhD thesis; Department of Civil Engineering University of Birmingham, UK; 1989.

Clayton N, Currie RJ, Moss RM. The effects of alkali-silica reaction on strength of prestressed concrete beams. Struct. Eng. 1990;68(15):287-292.

Danish Road Directorate. Load carrying capacity of structural members subjected to alcali-silica reactions. Ministry of Transport - Denmark; The Road Directorate; 1990.

Danish Road Directorate. Inspection of structures. Road regulation council; The Danish Road Directorate; 1994. Danish.

Danish Road Directorate. Guide in loading- and basic calculations. Road regulation council; The Danish Road Directorate; 2010. Danish.

Deschenes, DJ, Bayrak O, Folliard, K. Shear Capacity of Large-Scale Bridge Bent Specimens Subject to Alkali-Silica Reaction and Delayed Ettringite Formation. In: Proceedings of the 2009 Structures Congress - Dont't Mess with Structural Engineers:Expanding Our Role; 2009 Apr-Aug 30-02; Texas. p. 1049-1057.

Duchesne J, Bérubé MA. Effect of the cement chemistry and the sample size on ASR expansion of concrete exposed to salt. Cem Concr Res. 2003;33:629-634.

Fan A, Hanson JM. Effect of Alkali Silica Reaction Expansion and Cracking on Structural Behavior of Reinforced Concrete Beams. ACI Struct. J. 1998;95(5):498-505.

Fournier B, Bérubé MA. Alkali-aggregate reaction in concrete: a review of basic concepts and engineering implications. Can J Civ Eng. 2000;27:167-191.

Fujii M, Kobayashi K, Kojima T, Maehara H. The static and dynamic behaviours of reinforced concrete beams with cracking due to alkali-silica reaction. In: Proceedings of the 7th International Conference on Alkali Aggregate Reactions. 1986 Jun 11-16; Ottawa. p.126-130.

Geseltshaft für Optische Messtechnik. ARAMIS v 5.3.0 - User Manual. 2004.

Giaccio G, Zerbino R, Ponce JM, Batic OR. Mechanical behavior of concretes damaged by alkali-silica reaction. Cem. Concr. Res. 2008;38:993-1004.

Giaccio G, Torrijos MC, Tobes JM, Batic OR, Zerbino R. Development of Alkali-Silica Reaction under Compressive Loading and Its Effects on Concrete Behavior. ACI Mater. J. 2009;106(3):223-230.

Giannini ER. Evaluation of Concrete Structures Affected by Alkali-Silica Reaction and Delayed Ettringite Formation. PhD thesis; University of Texas at Austin; 2012.

Giebson C, Seyfarth K, Ludwig HM. Influence of sodium chloride on ASR in highway pavement concrete. In: Proceedings of the 15th International Conference on Alkali-Aggregate Reaction in Concrete; 2016 Jul 03-07; São Paulo.

Grelk B. Alkali-Silica Reactions. In: The Concrete Handbook. Copenhagen: Dansk Betonforening; 2014. p. 19.1-14. Danish.

Hansen SG, Barbosa RA, Hoang LC. Prestressing of reinforcing bars in concrete slabs due to concrete expansion induced by alkali-silica reaction. In: Proceedings of fib Symposium 2016: Performance-based approaches for concrete structures; 2016 Nov 21-23; Cape Town.

Hansen SG, Barbosa RA, Hoang LC. Shear capacity of ASR damaged structures - In-depth analysis of some in-situ shear tests on bridge slabs. In: Proceedings of the 15th International Conference on Alkali-Aggregate Reaction in Concrete; 2016 Jul 03-07; São Paulo.

Herholdt AD, Justesen CFP, Nepper-Christensen P, Nielsen A. The Concrete Book. Aalborg Portland. 1985. Danish.

Hillerborg A, Modé er M, Peterson PE. Analysis of Crack Formation and Crack Growth in Concrete by means of Fracture Mechanics and Finite Elements. Cem Concr Res. 1976;6(6):773-782.

Hiroi T, Yamamoto T, Toda Y, Manabe H, Miyagawa T. Experimental and analytical studies on flexural behavior of post-tensioned concrete beam specimen deteriorated by alkali-silica reaction (ASR). In: Proceedings of the 15th International Conference on Alkali-Aggregate Reaction in Concrete; 2016 Jul 03-07; São Paulo.

Hobbs DW. Alkali-silica reaction in concrete. London: American Society of Civil Engineers, Thomas Telford; 1988.

Idorn GM. Durability of Concrete Structures in Denmark. PhD thesis; Technical University of Denmark, Denmark; 1967.

Inoue S, Fujii M, Kobayashi K, Nakano K. Structural behaviors of reinforced concrete beams affected by alkali-silica reaction. In: Proceedings of the 8th International Conference on Alkali-Aggregate Reaction; 1989 Jul 17-20; Kyoto, Japan. pp. 727-732.

Jones AEK, Clark LA, Amasaki S. The suitability of cores in predicting the behaviour of structural members suffering from ASR. Mag. Concr. Res. 1994;46(167):145-150.

Jones AEK. Cracking, expansion and strength of concrete subjected to restrained alkali silica reaction. PhD thesis; The University of Birmingham UK; 1994.

Kobayashi K. Load carrying behaviours of concrete structures and members affected by alkali-aggregate reactions. Concr. J. 1986;24:70-78.

Koyanagi W, Rokugo K, Ishida H. Failure Behavior of Reinforced Concrete Beams Deteriorated by Alkali-Silica Reactions. In: Proceedings of the 7th International Conference on Alkali Aggregate Reactions. 1986 Jun 11-16; Ottawa. p. 141-145.

Larsen JB. Road history. The Danish Road Directorate; 2014. Danish.

Lindgård J. Alkali-silica reaction (ASR) - Performance testing. PhD thesis; Norwegian University of Science and Technology, Norway; 2013.

Lindgård J, Andiç-Çakir Ö, Fernandes I, Rønning TF, Thomas MDA. Alkali-silica reactions (ASR): Literature review on parameters influencing laboratory performance testing. Cem Concr Res. 2012; 42:223-243.

Linsbauer HN, Tschegg EK. Fracture energy determination of concrete with cube shaped specimens. Zement Und Bet. 1986;31:38-40. German.

Majlesi Y. A laboratory investigation into the structural performance and mechanical properties of plain and reinforced concrete elements affected by alkali silica reaction. PhD thesis; Queen Mary and Westfield Collage University of London; 1994.

Marzouk H, Langdon S. The effect of alkali-aggregate reactivity on the mechanical properties of high and normal strength concrete. Cem Concr Compos 2003;25:549-556.

McLeish A. Structural implications of the alkali silica reaction in concrete. Report 177. Transport and Road Research Laboratory.1990.

Mørup H, von Scholten C, Wegan V. Have ASR damaged bridges sufficient strength?. Trafik & Veje. March 2013; 23-26. Danish.

Nerenst P. Study of concrete technology in U.S.A; Copenhagen: Udenrigsministeriets Foranstaltning; 1952. Danish.

Nerenst P. Alkali Reactions in Concrete - General. Copenhagen: The Danish Institute of Building Research and the Academy of Technical Sciences; 1957. Danish.

Nielsen HO, Grelk B, Nymand KK. ASR - Alkali-silica reaction. Dansk Vejtidsskrift. 2004; p. 10-13. Danish.

Nielsen MP, Hoang LC. Limit Analysis and Concrete Plasticity, 3rd edition. Taylor and Francis Group. 2011.

Okada K, Tezuka M, Yoshikawa MH, Komada M. Alkali Aggregate Reaction: An investigation on its causes and strength evaluations of materials subjected to its effects. In: Proceedings of the 8th International Conference on Alkali-Aggregate Reaction; 1989 Jul 17-20; Kyoto. p. 609-615.

Olesen JF. Fictitious crack propagation in fibre-reinforced concrete beams. J Eng Mech. 2001;127(3):272-280.

Paulsen RR, Moeslund TB. Introduction to Medical Image Analysis. Kongens Lyngby: DTU Compute - Department of Applied Mathematics and Computer Science. 2015.

Pereira EB, Fischer G, Barros JAO. Image-based detection and analysis of crack propagation in cementitious composites. In: International RILEM Conference on Advances in Construction Materials Trough Science and Engineering. 2011 Sept 5-7; Hong Kong. p. 343-350.

Plum NM, PE, Idorn GM. Preliminary overview of Alkali Reactions in Concrete in Denmark. Copenhagen: The Danish National Institute of Building Research. Danish.

Plum NM. Temporary guide in prevention of damaging alkali-silica reaction in concrete. Copenhagen: The Danish National Institute of Building Research. 1961. Danish.

Poulsen A. Durability of Concrete. Copenhagen: Ingeniøren; 31. 1914. Danish.

Poulsen E et. al. Concrete 4: 13 concrete diseases. Hørsholm, Denmark: Danish Building Research Institute (SBi); 1985. Danish.

Reinhardt HW, Mielich O. Effects of mechanical properties of ASR damaged concrete on structural design, In: Proceedings of International Symposium on Brittle Matrix Composites 10; 2012 Oct 15-17; Warsaw. p. 1-9.

Rigden SR, Salam JM, Burley E. The influence of stress intensity and orientation upon the mechanical properties of ASR affected concrete, In: Proceedings of the 9th International Conference on Alkali-Aggregate Reaction in Concrete, 1992 Jul 27-31; London. p. 865-876.

Rivard P, Bérubé MA, Ollivier JP, Ballivy G. Decrease of pore solution alkalinity in concrete tested for alkali-silica reaction. Mater Struct. 2007;40(9):909-921.

Schmidt JW, Hansen SG, Barbosa RA, Henriksen A. Novel shear capacity testing of ASR damaged full scale concrete bridge. Eng Struct. 2014;79:365.-374.

Shayan A, Ivanusec I. Influence of NaOH on mechanical properties of cement paste and mortar with and without reactive aggregate. In: Proceedings of the 8th International Conference on Alkali-Aggregate Reaction; 1989 Jul 17-20; Kyoto, Japan. pp. 715-720.

Siemens T, Visser J. Low tensile strength in older concrete structures with alkali-silica reaction. In: Proceedings of the 11th International Conference on Alkali-Aggregate Reaction in Concrete, 2000 Jun 11-16; Québec. p. 1029-1038.

Siemens T, Han N, Visser J. Unexpectedly low tensile strength in concrete structures. HERON. 2002; 47(2):111-124.

Skoček J, Stang H. Inverse analysis of the wedge-splitting test. Eng. Fract. Mech. 2008;75:3173-3188.

Skoček J. Fracture propagation in cementitious materials - Multi-scale approach: measurements and modeling. PhD thesis; Technical University of Denmark, Denmark; 2010.

Smaoui N, Bissonnette B, Bérubé MA, Fournier B, Durand B. Mechanical Properties of ASR-Affected Concrete Containing Fine or Coarse Reactive Aggregates. J ASTM Int. 2006;3(3):1-16.

Stoltzner E, Wegan V, Henriksen C. The Danish Road Directorate's strategy for waterproofing of concrete bridges. Dansk Vejtidsskrift. Febr 2005; p. 40-41. Danish.

Swamy RN, Al-Asali MM. Engineering Properties of Concrete Affected by Alkali-Silica Reaction. ACI Mater. J. 1988;85:367-374.

Swamy RN. Alkali-Silica Reaction in Concrete. Glasgow and London: Blackie and Son Ltd. 1992.

Thaulow N, Jensen AD, Chatterji S, Christensen P, Gudmundsson H. Estimation of the compressive strength of concrete samples by means of fluorescence microscopy. Nord. Betong. 1982;51:2-4.

The Institution of Structural Engineers. Structural effects of alkali-silica reaction - Technical guidance on the appraisal of existing structures. The Institution of Structural Engineers, 1992.

Thomas M, Fournier B, Folliard K, Ideker J, Shehata M. Test methods for evaluating preventive measures for controlling expansion due to alkali-silica reaction in concrete. Cem Concr Res. 2006;36:1842-1856.

Uijl JA, Kaptijn N, Walraven JC. Shear resistance of flat slab bridges affected by ASR. In: Proceedings of the 11th International Conference on Alkali-Aggregate Reaction in Concrete, 2000 Jun 11-16; Québec. p. 1129-1138.

Uijl JA, Kaptijn N. Shear Tests on Beams Cut from ASR-Affected Bridge Decks. ACI Special Publication. 2004;115-133.

Vonk RA. Softening of concrete loaded in compression. PhD Thesis; Technical University of Eindhoven, Netherlands; 1992.

Wan X, Zhao T, Wittmann FH. Influence of carbonation on the chloride in the pore solution of concrete. In: Proceedings of the 3rd International Conference on Concrete Repair, Rehabilitation and Retrofitting (ICCRRR); 2012 Sep 3-5; Cape Town. p. 138-139.

Wegan V. Surfacing of concrete bridges. Danish Road Institute Report 106. Road Directorate; 2000.

Wigum BJ, Pedersen LT, Grelk B, Lindgård J. State of the art report: Key Parameters influencing the alkali aggregate reaction. SINTEF Building and Infrastructure; 2006.

Østergaard L. Early-Age Fracture Mechanics And Cracking of Concrete. PhD thesis; Technical University of Denmark, Denmark; 2003.

Østergaard N. Aggressive concrete disease attack 600 danish bridges. Ingeniøren: Aug 2012. Available at: https://ing.dk/artikel/aggressiv-betonsygdom-angriber-600-danske-broer-131714.

Standards

CRD-C 164-92. Standard Test Method for Direct Tensile Strength of Cylindrical Concrete or Mortar Specimens. U.S. Army Engineering Research and Development Center (ERDC), Vicksburg; 1992.

DS Standard 12390-6. Testing of hardened concrete - Part 6: Tensile splitting strength of test specimens. Copenhagen: Danish Standards; 2000.

DS Standard 12390-3. Testing hardened concrete - Part 3: Compressive strength of test specimens. Copenhagen: Danish Standards; 2009.

DS Standard 2426. Concrete - Materials - Rules for application of EN 206-1 in Denmark. Copenhagen: Danish Standards; 2011.

DS Standard 1992-1-1. Eurocode 2 - Design of concrete structures - Part 1-1: General rules and rules for buildings. Copenhagen: Danish Standards; 2008.

DS Standard 1992-1-1 DK NA:2013. The Danish National Annex for Design of concrete structures - Part 1-1: General rules and rules for buildings. Copenhagen: Danish Standards; 2013.

NT BUILD 208. Concrete, hardened: Chloride content by Volhard titration. Edition 3. Finland:Nordtest; 1996.

TI-B 51. Test method: Alkali-silica reactivity of sand. Denmark: Danish Technological Institute; 1985.

Cracking in concrete structures due to alkali-silica reaction (ASR) has been obser-
ved worldwide. During the last few decades, an increasing number of bridges in
Denmark have been severely damaged due to ASR. This PhD thesis is a collection
of papers that investigate the influence of ASR on the physical, mechanical and
structural behaviour of reinforced concrete. The reinforced concrete originated
from ASR-damaged flat slab bridges in service, and from laboratory-casted and
laboratory-accelerated reinforced slabs.